ETH
Swiss Federal Institute of Technology Zurich

Finite-frequency effects in global seismology: forward modeling and implications on tomographic imaging

Ph.D. defense
Daniel Peter

Motivation

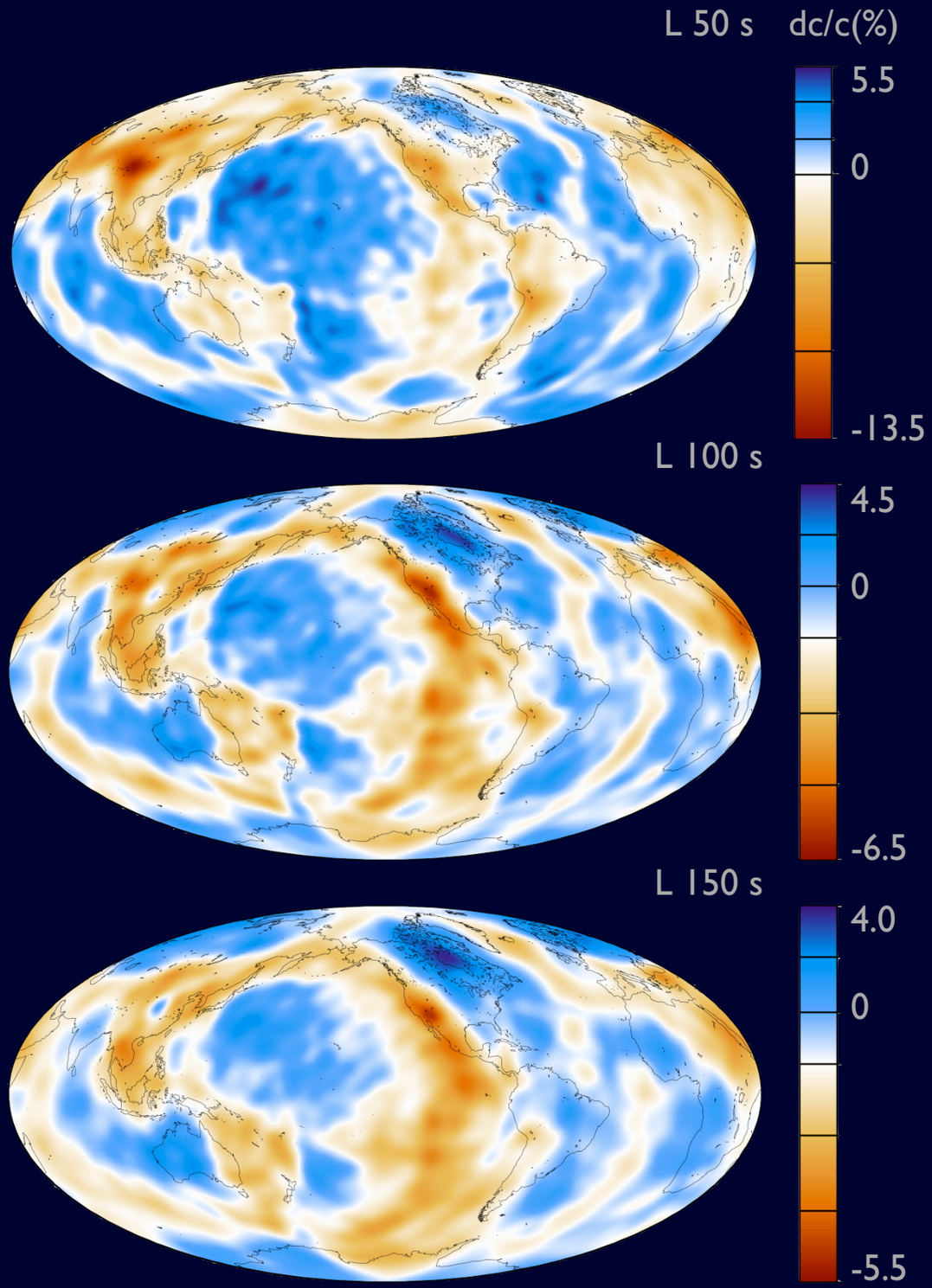

Ekström et al. (1997)

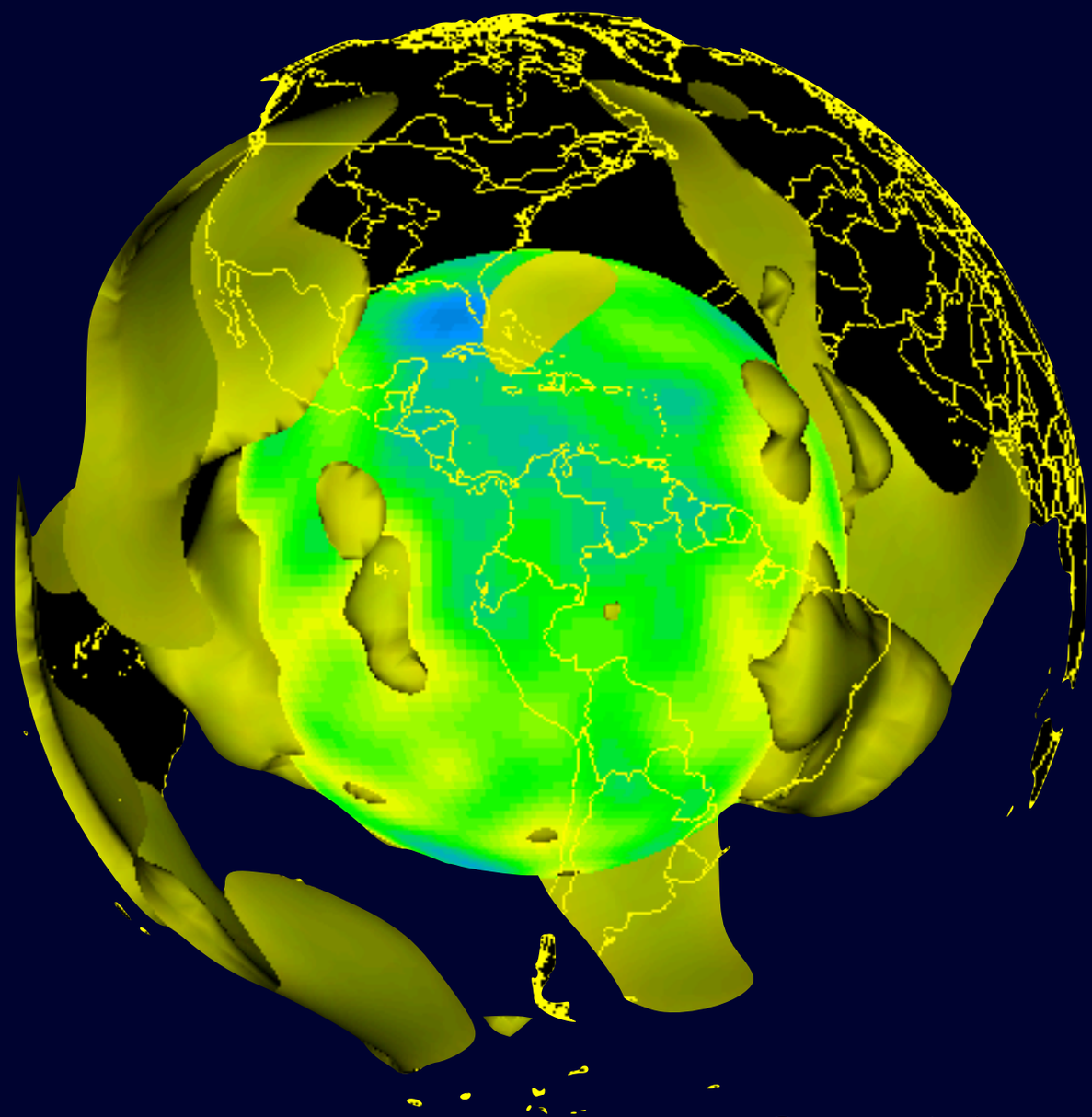

Gu et al. (1999)

Improving tomographic resolution

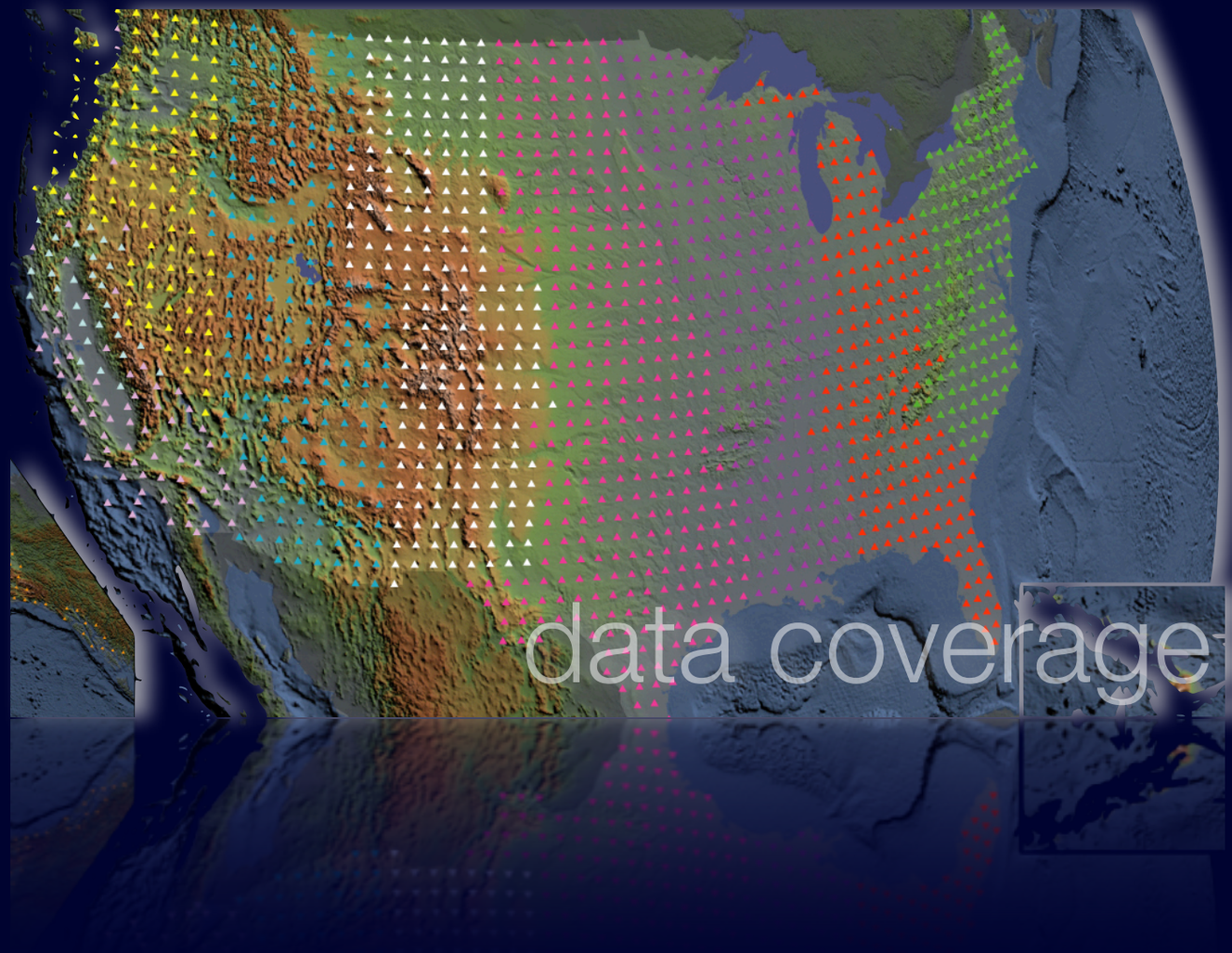

Improving tomographic resolution

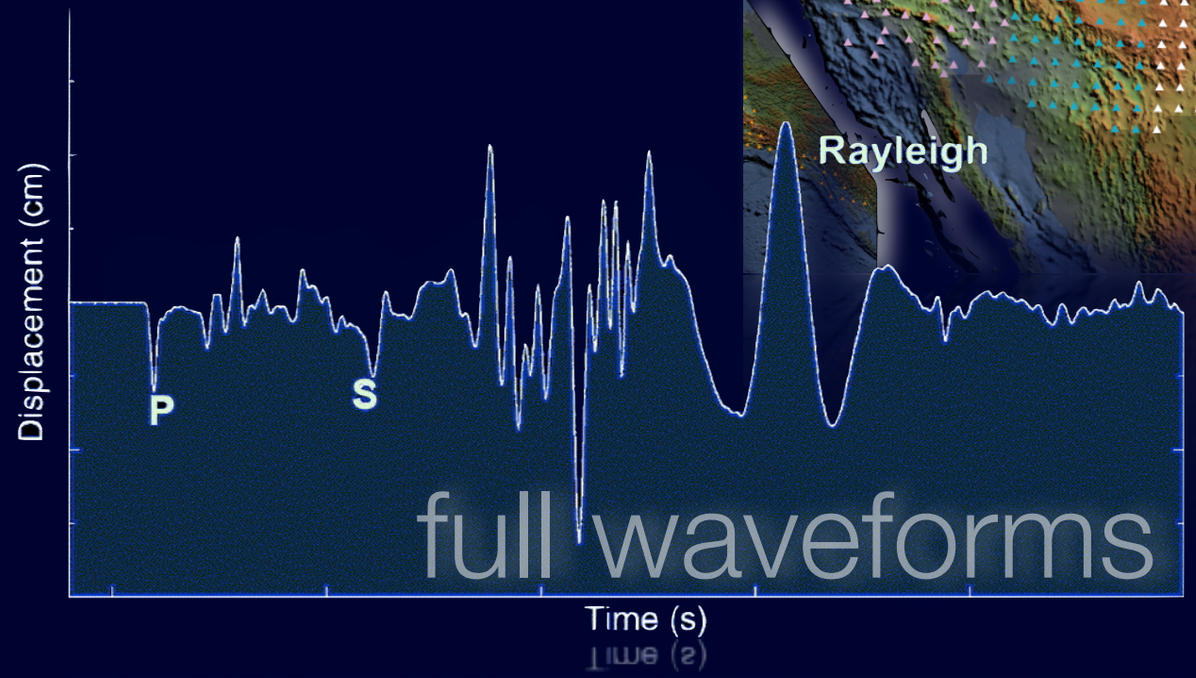

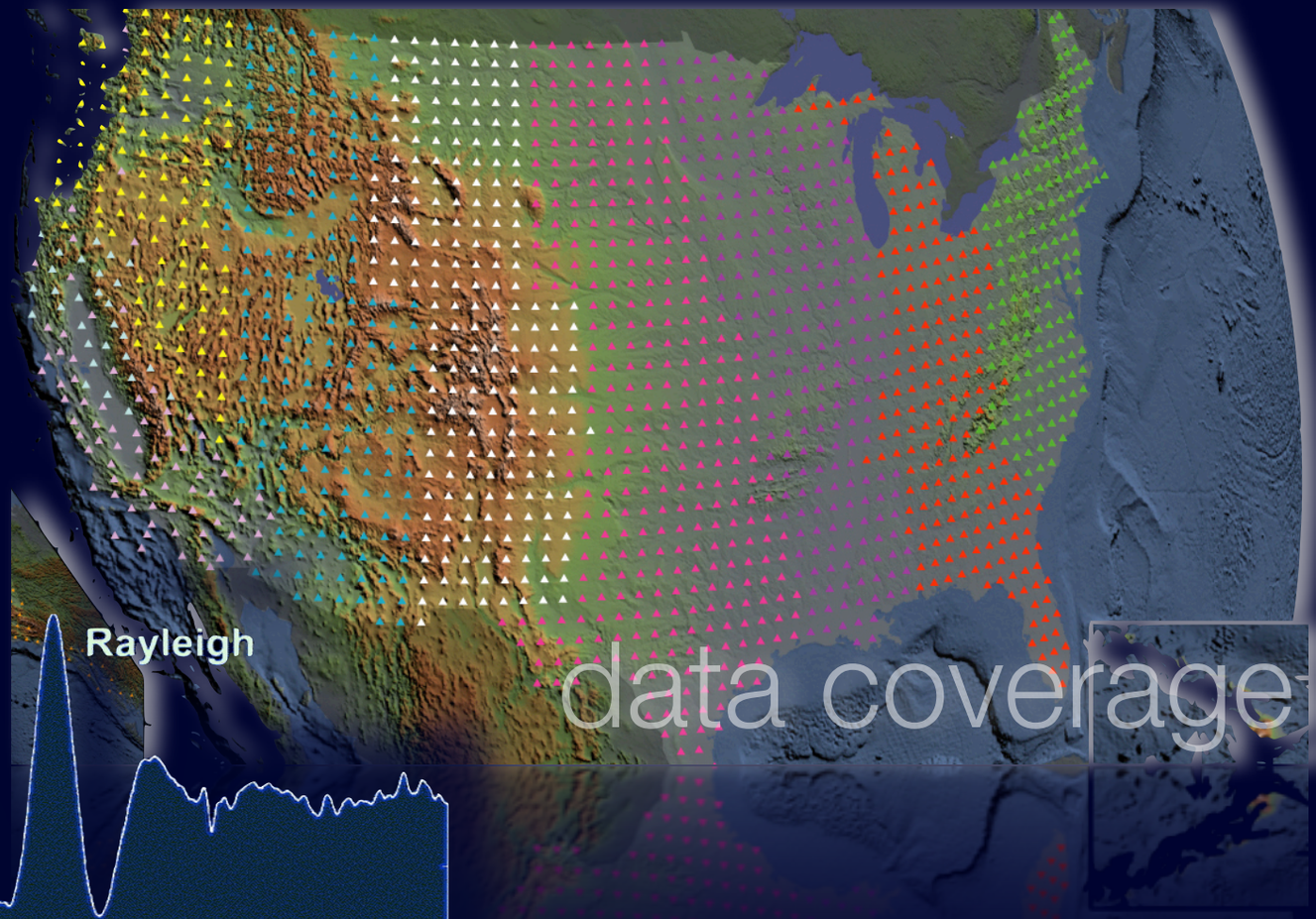

Improving tomographic resolution

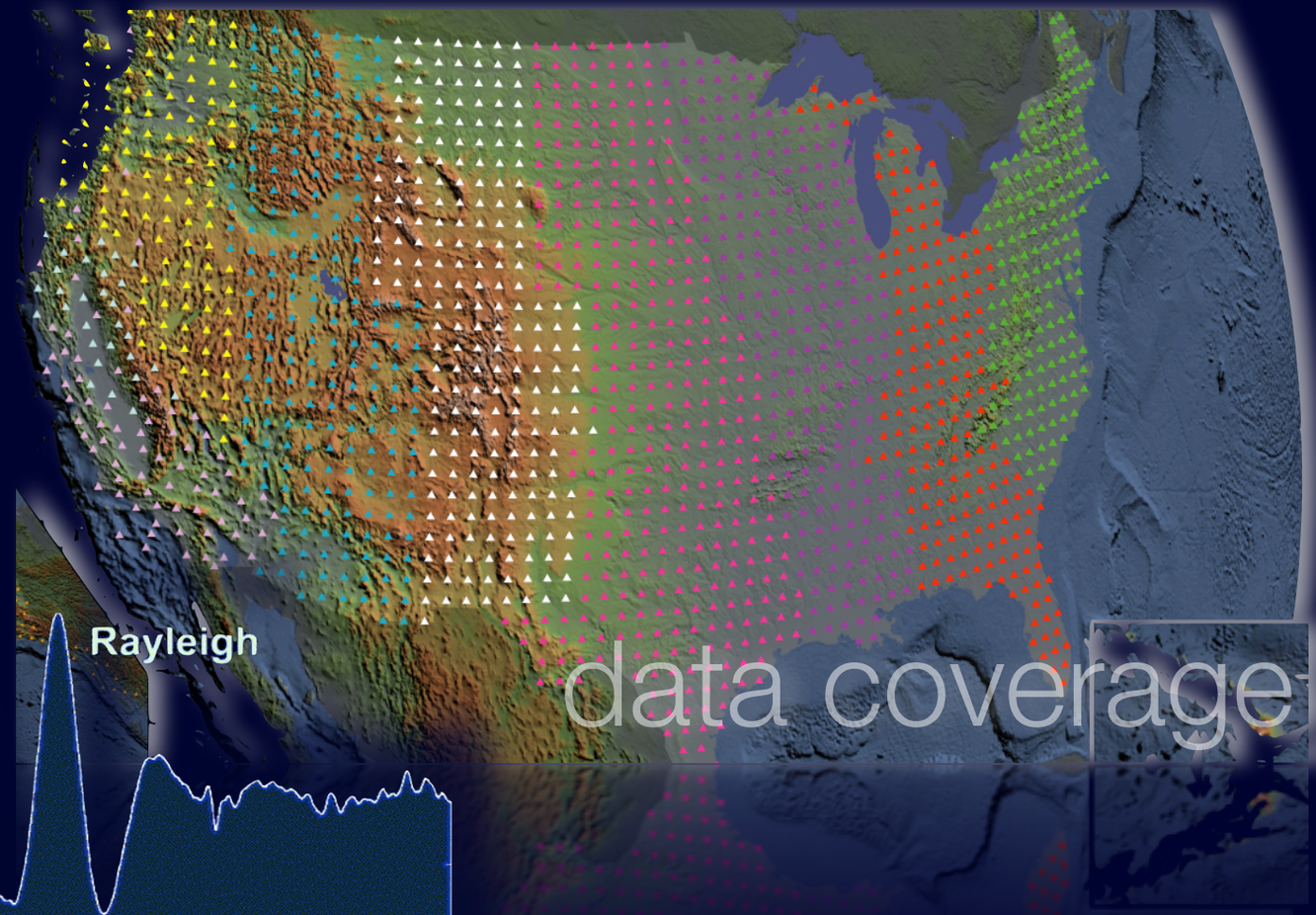

data coverage

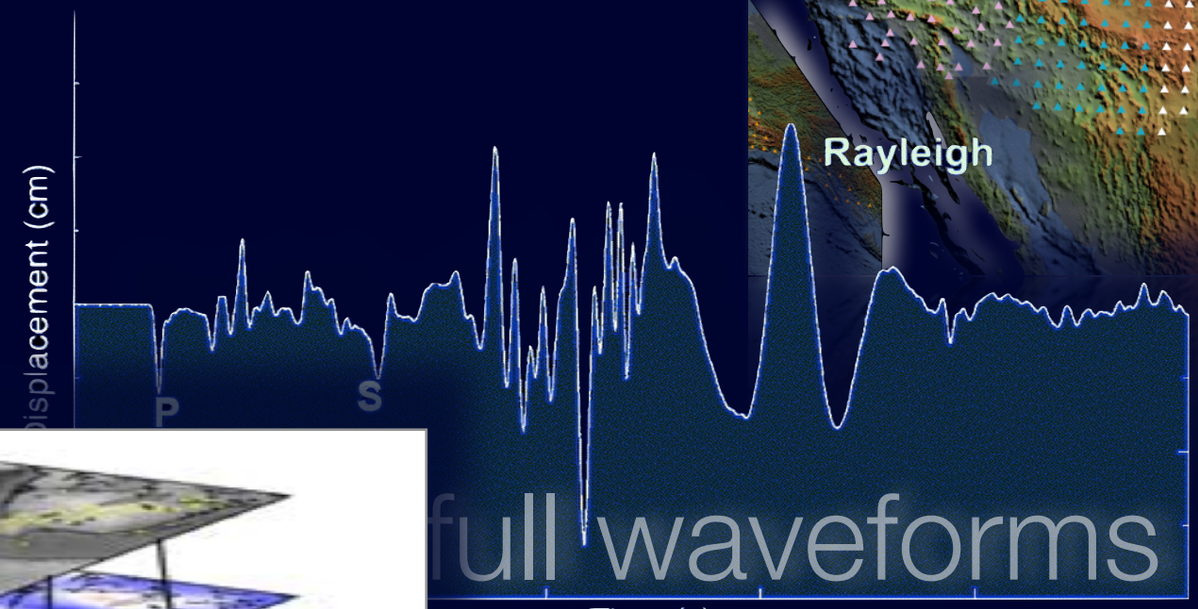

full waveforms

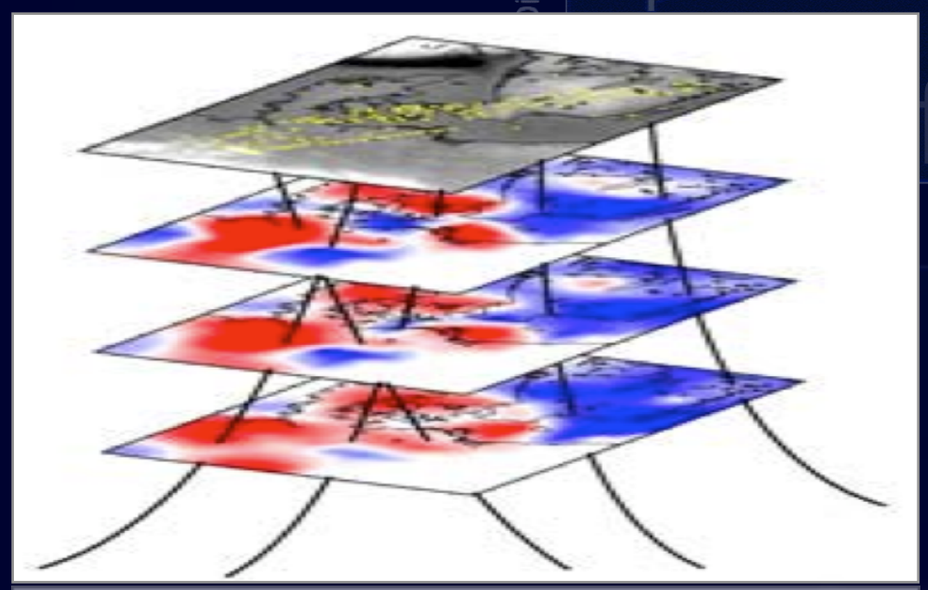

wave representations

Daniel Peter | ETH Zurich

Improving tomographic resolution

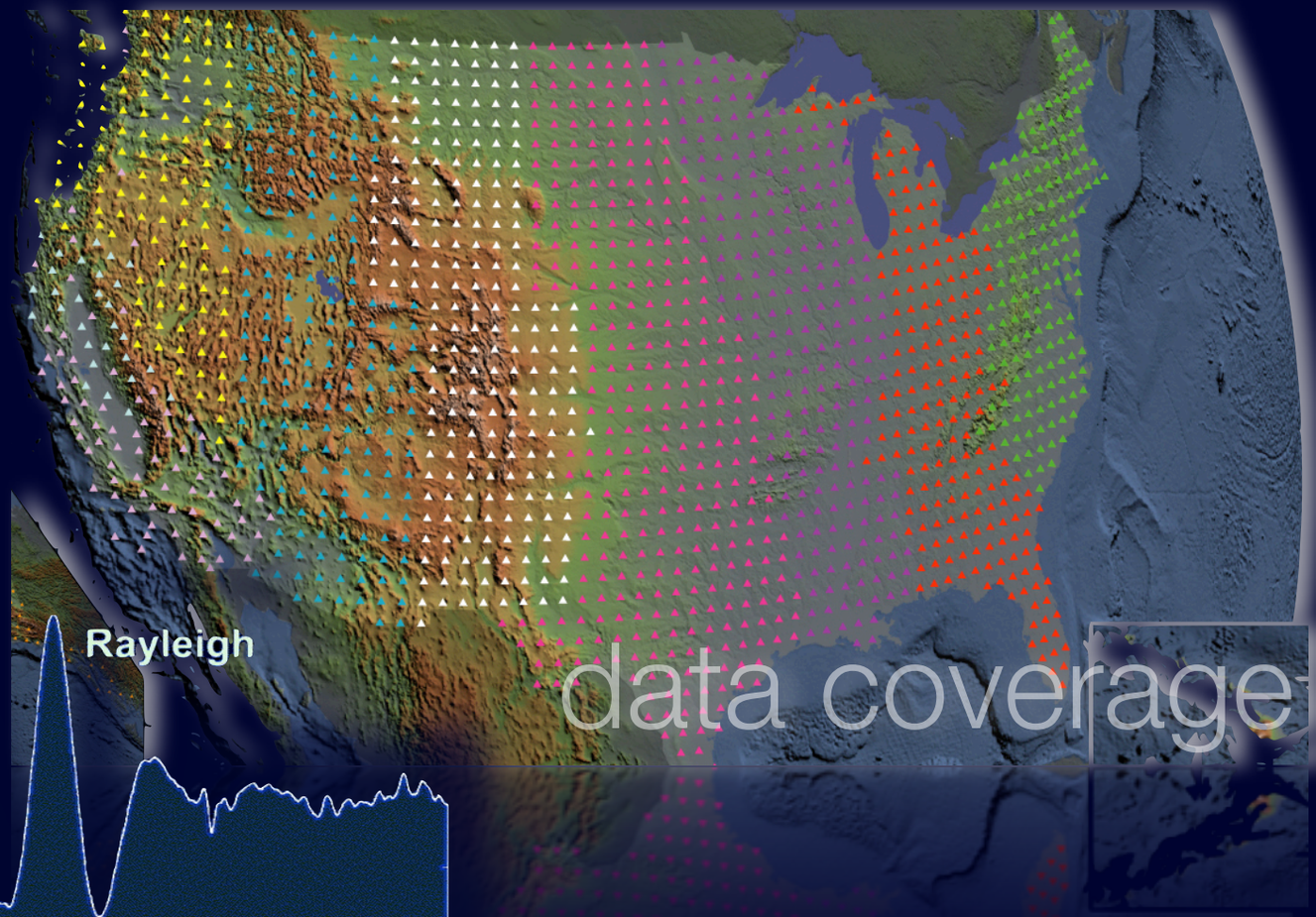

data coverage

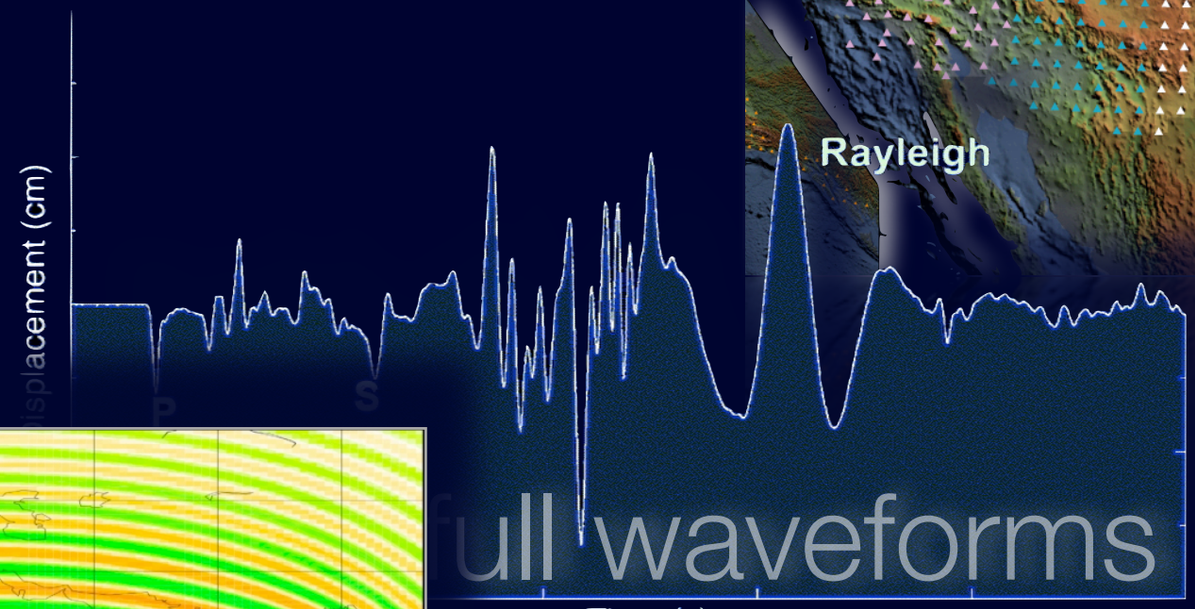

full waveforms

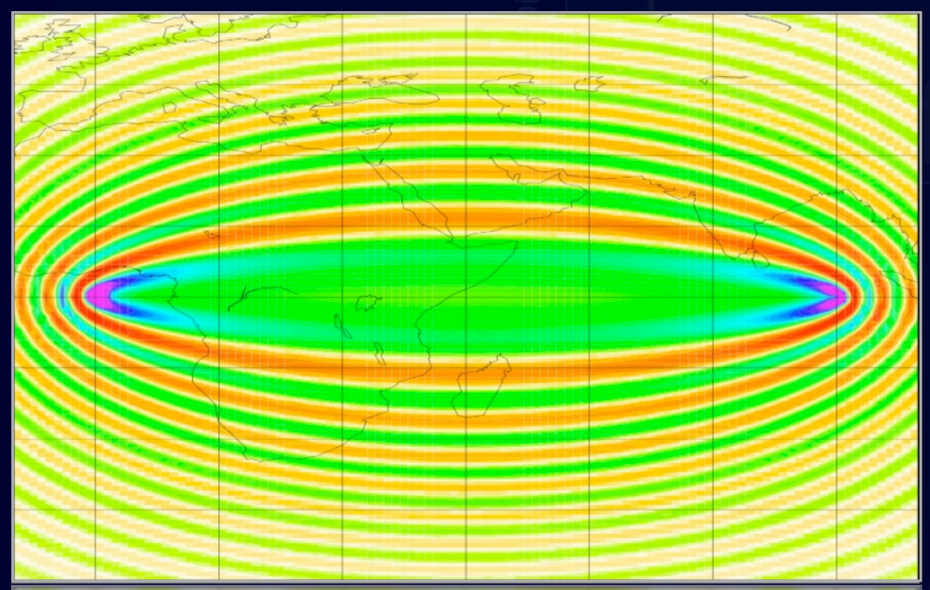

wave representations

Daniel Peter | ETH Zurich

Outline

Outline

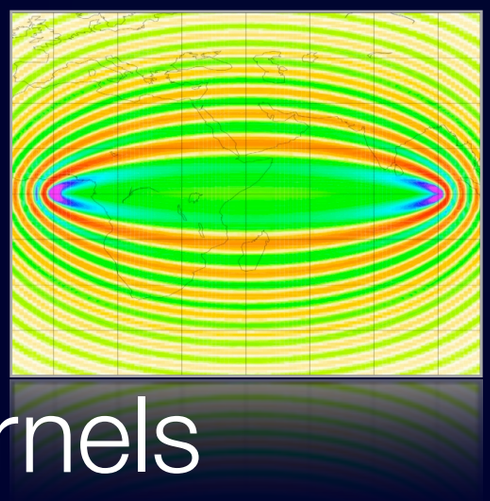

- Forward modeling:

  Membrane waves and sensitivity kernels

Outline

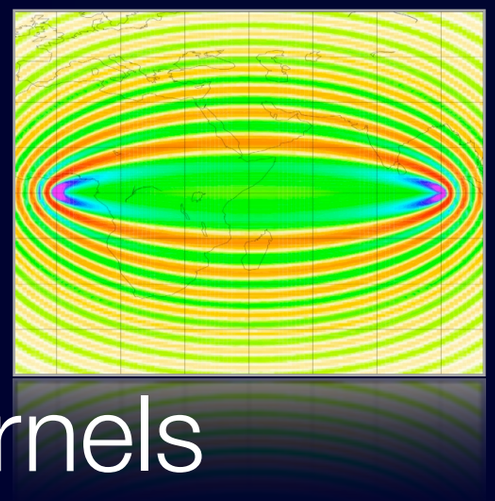

- Forward modeling:

  Membrane waves and sensitivity kernels

- Implications on tomography:

  Resolution benchmark

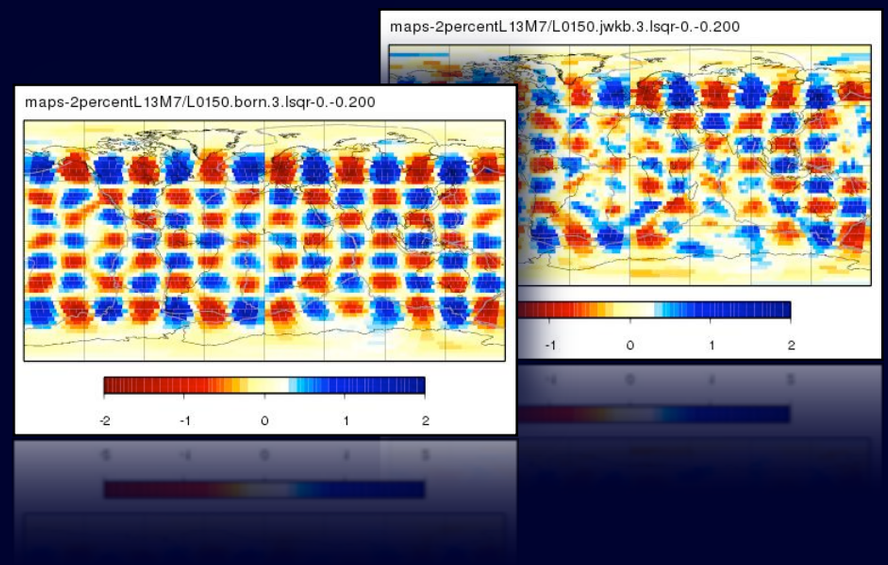

Outline

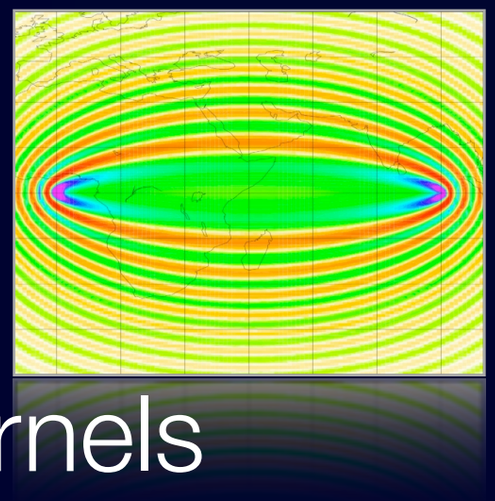

- Forward modeling:
  Membrane waves and sensitivity kernels

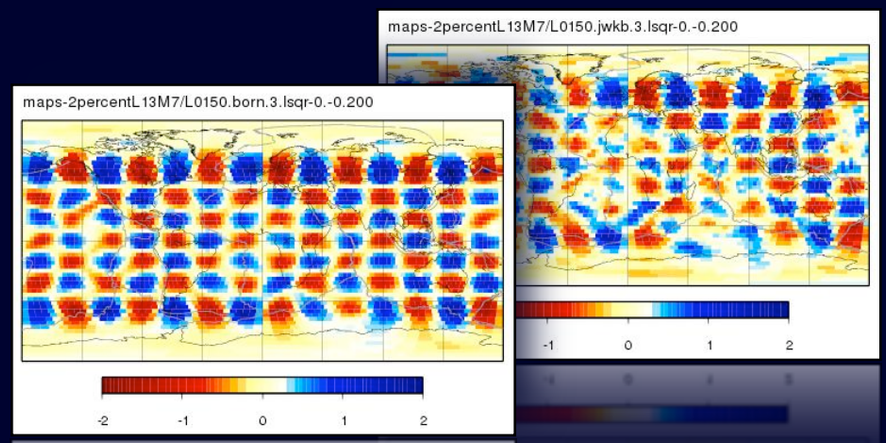

- Implications on tomography:
  Resolution benchmark

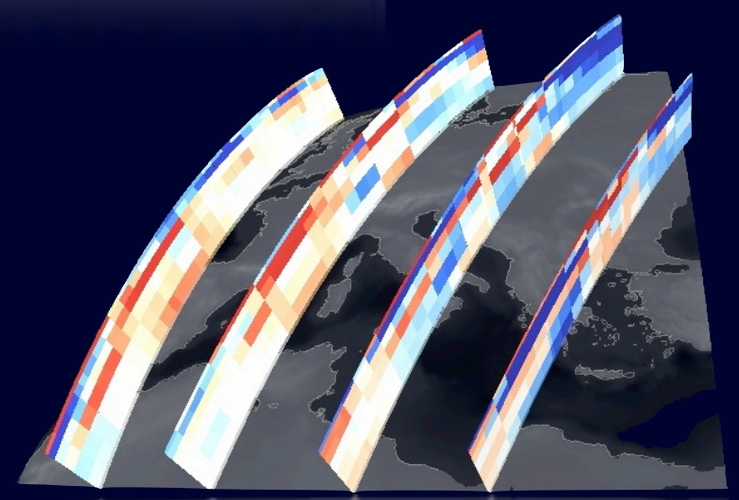

- Application to 3-D seismology:
  Mediterranean tomography

Wave representations

Wave representations

Ray

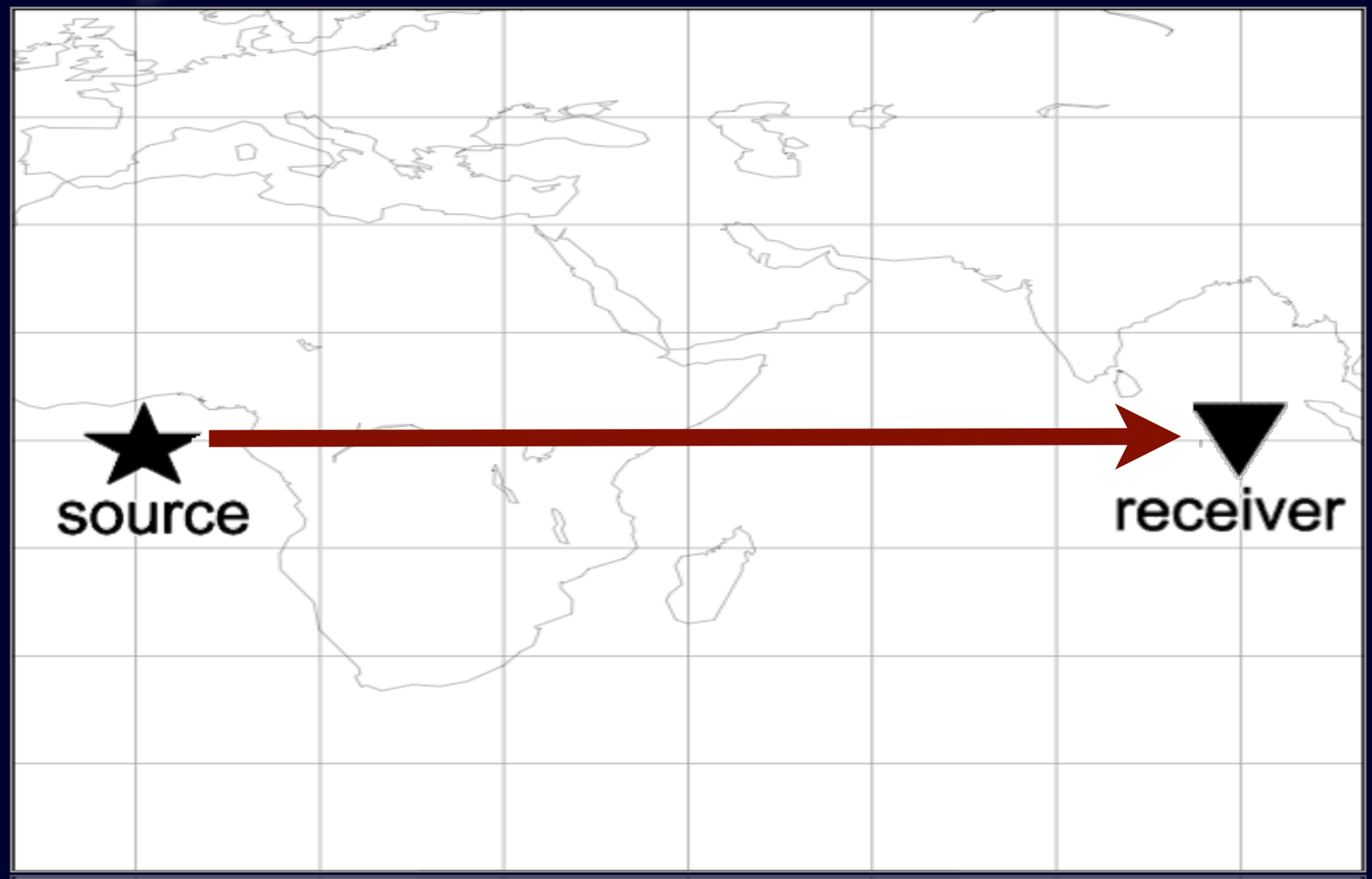

Wave representations

Ray

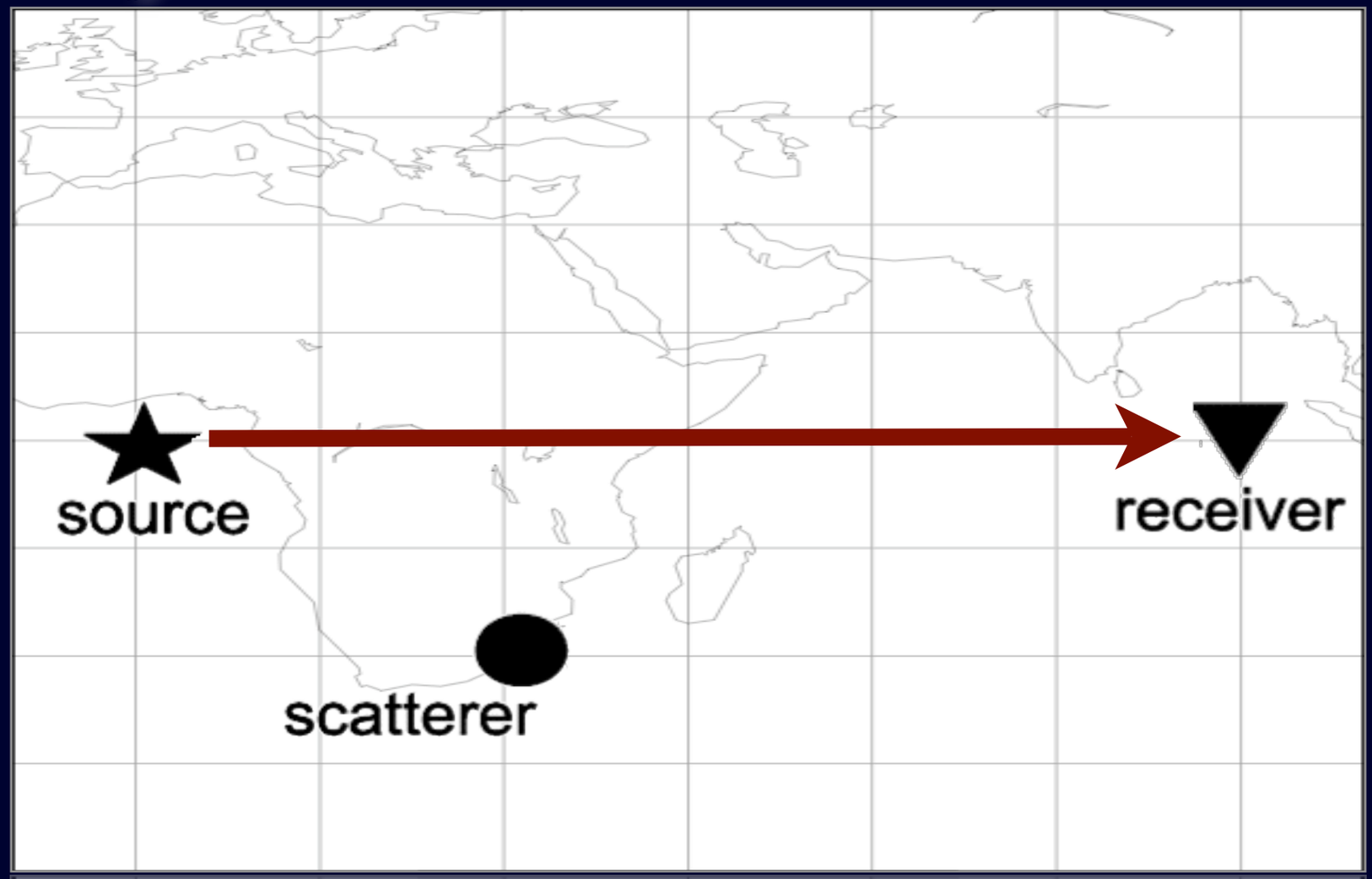

Wave representations

Ray

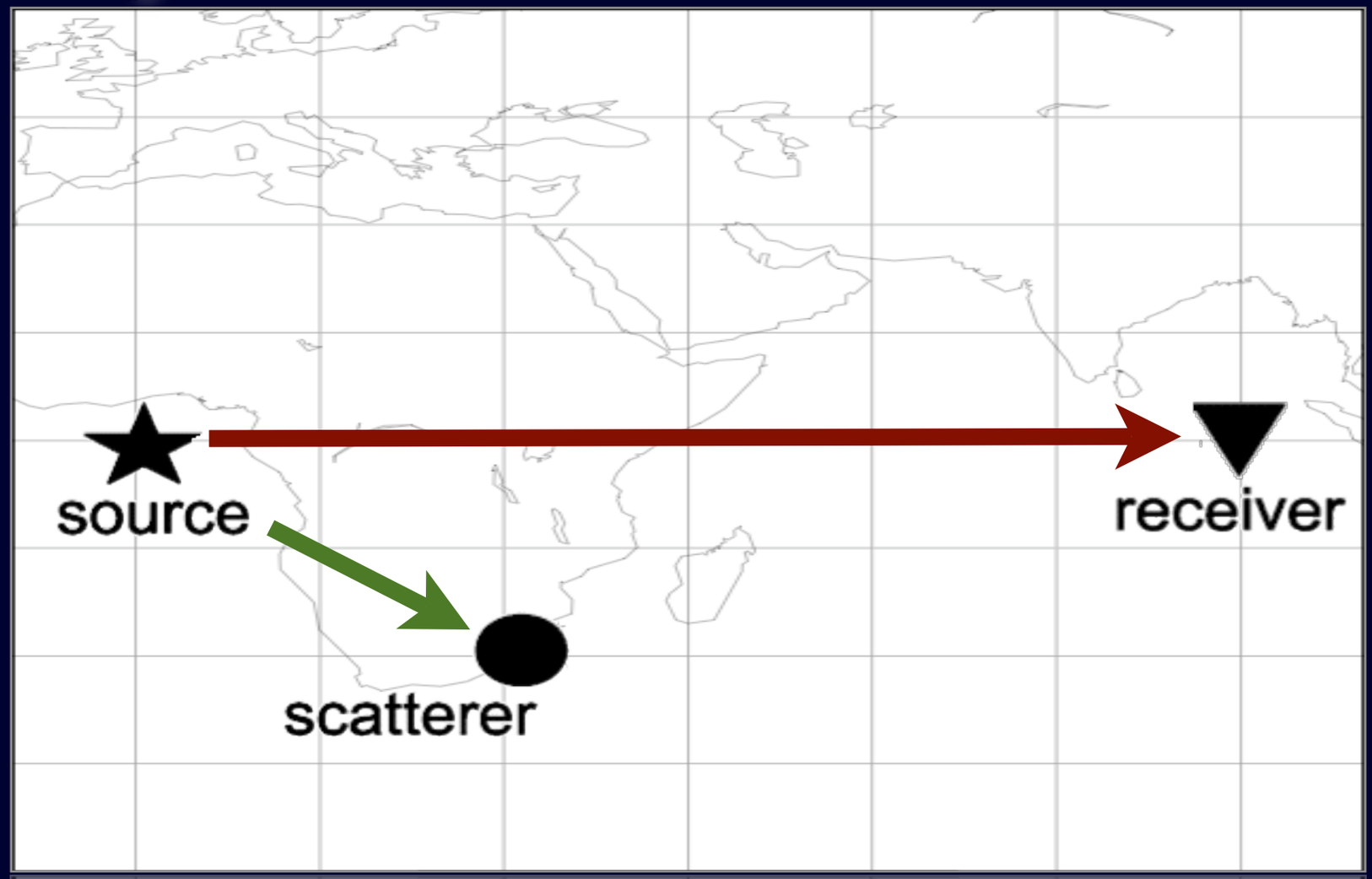

Wave representations

Ray

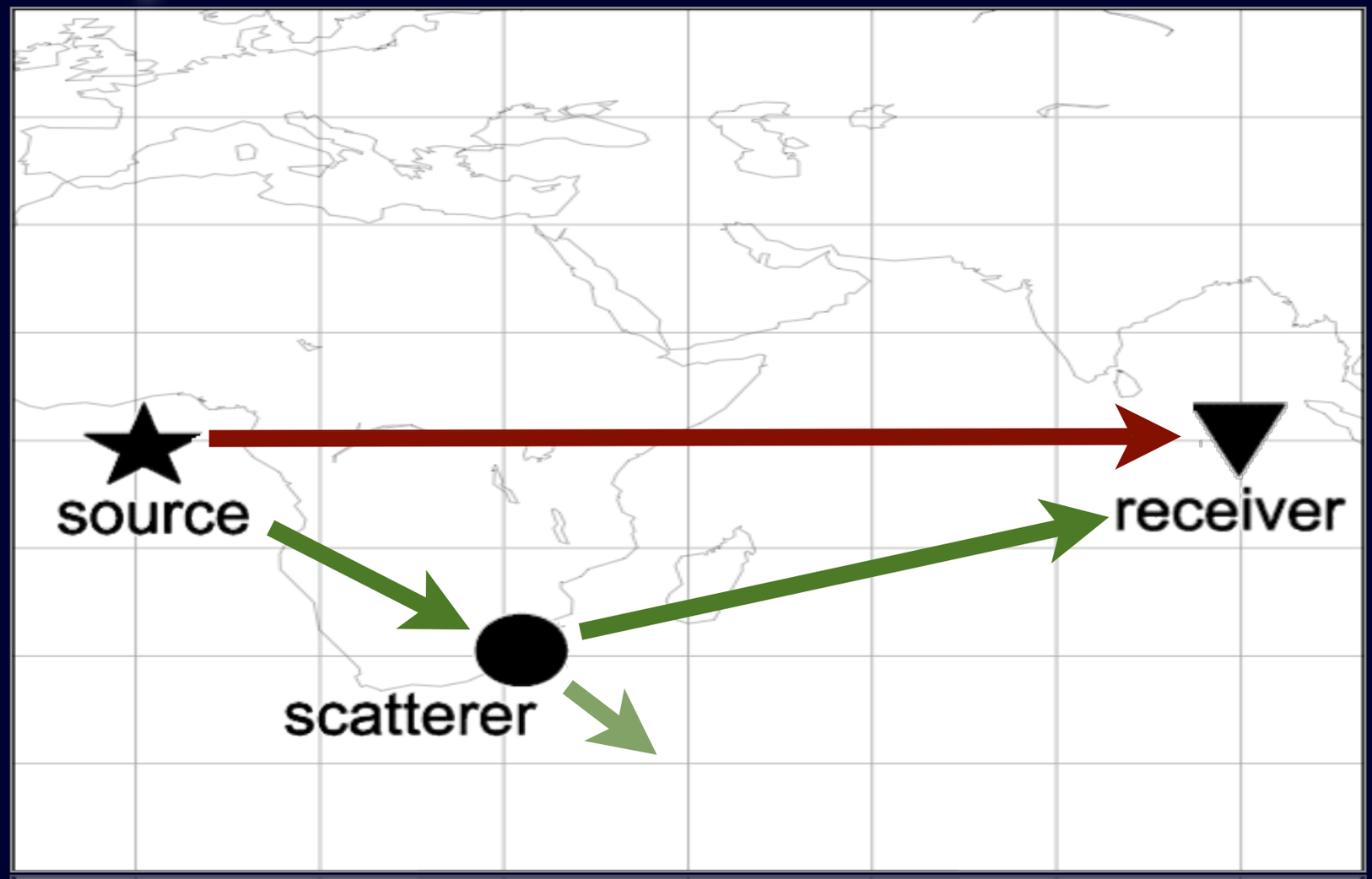

Wave representations

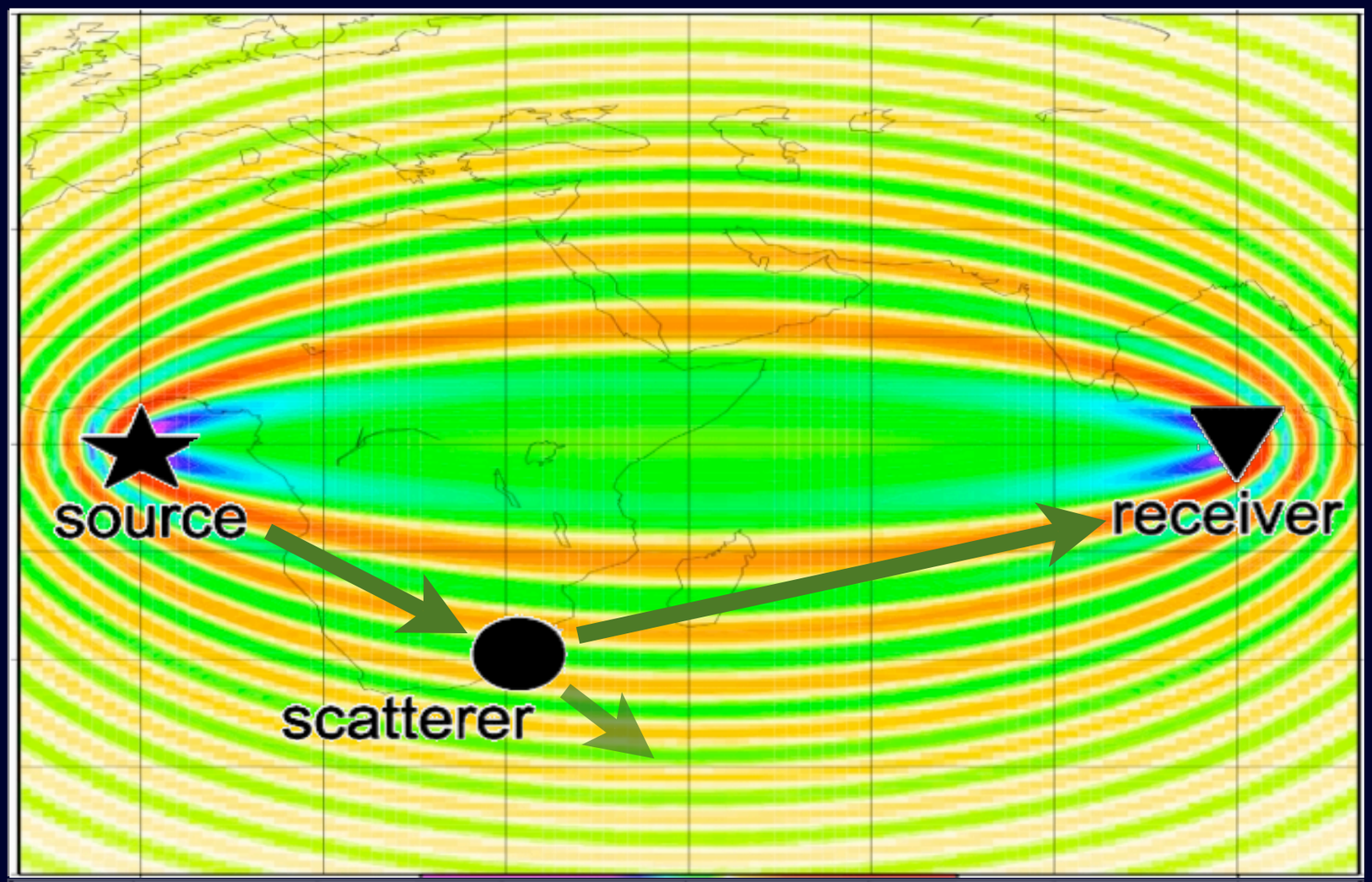

Finite-frequency

Membrane waves

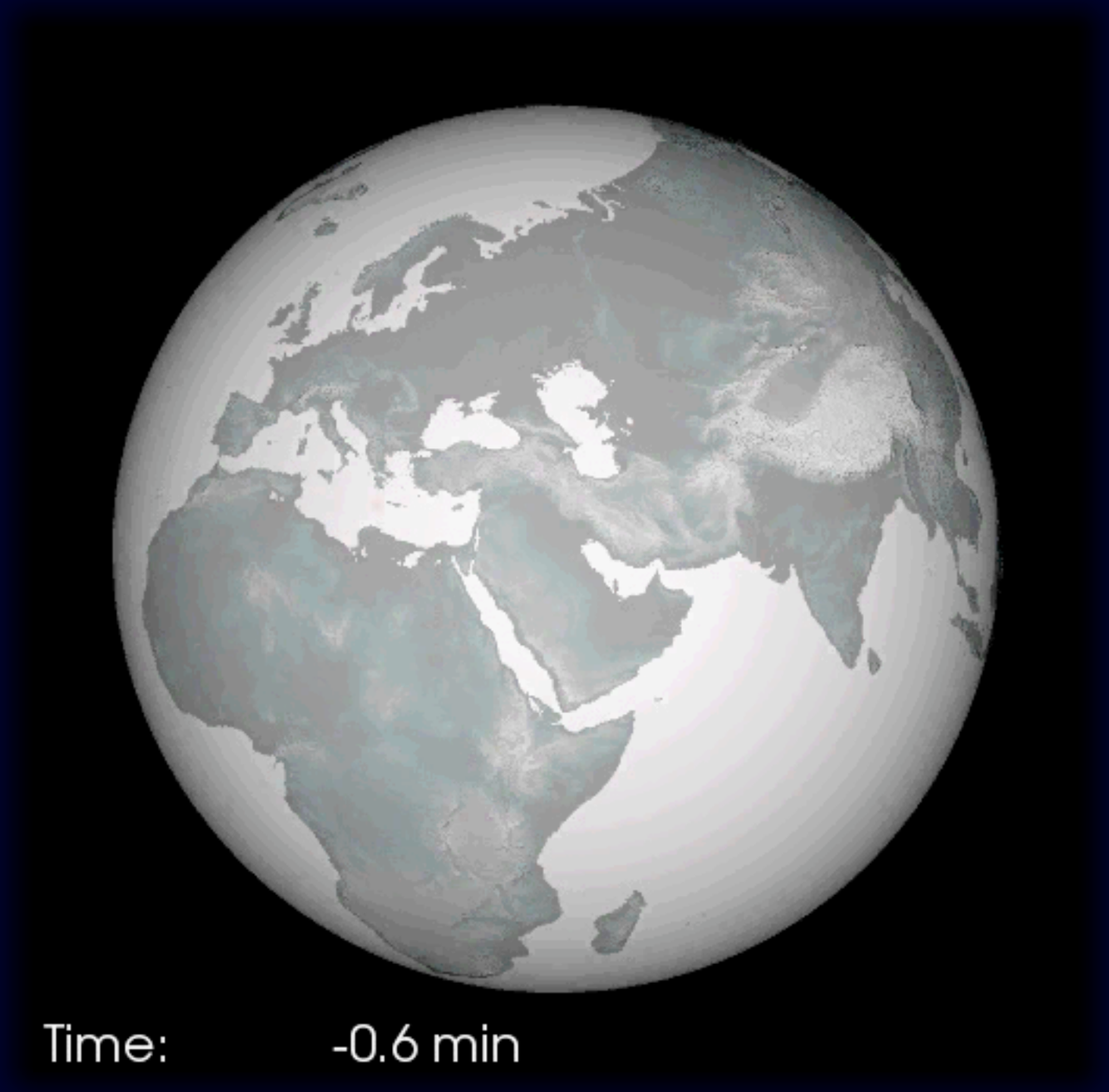

Equations of motion

$$\rho\,\ddot{\mathbf{u}} = \mathbf{f} + \nabla\cdot\tau$$

with a Love wave ansatz

$$\mathbf{u}_L = W(r)(-\hat{\mathbf{r}}\times\nabla_1)\mathbf{s}(\vartheta,\varphi)$$

lead to a 2-D wave equation (Tanimoto 1990)

$$\left[\frac{1}{c^2(\mathbf{x})}\partial_t^2 - \nabla_1^2\right] s(\mathbf{x},\mathbf{t}) = \mathbf{f}(\mathbf{x_s},\mathbf{t})$$

Sensitivity kernels

Phase-shift $\delta\Phi$ related to phase-velocity perturbation δc :

$$\delta\Phi = \int_\Omega K(\theta,\phi)\ \delta c(\theta,\phi)\, d\Omega$$

direct approach

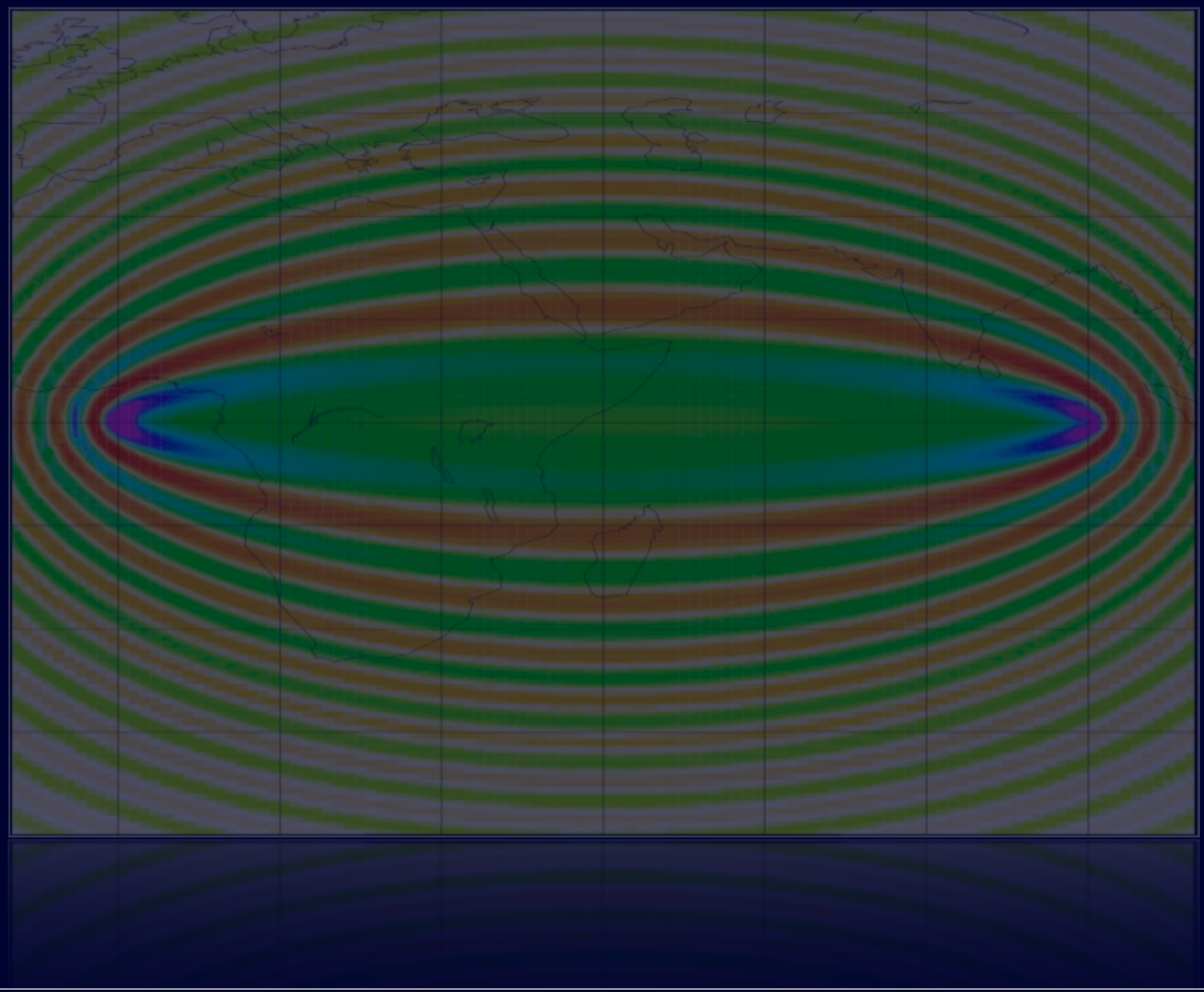

Tape (2003)

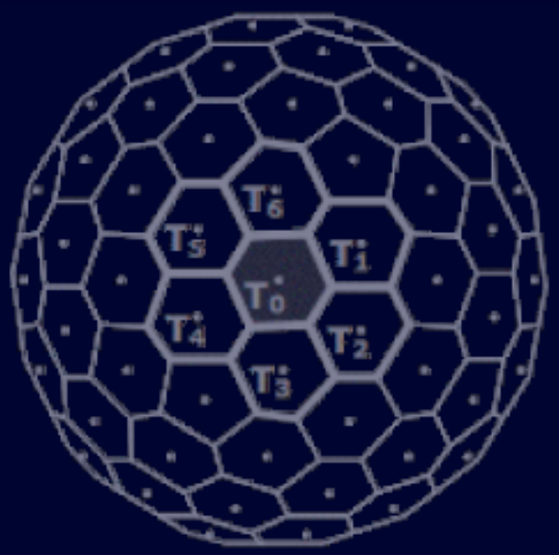

Sensitivity kernels

Phase-shift $\delta\Phi$ related to phase-velocity perturbation δc :

$$\delta\Phi = \int_\Omega K(\theta,\phi)\ \delta c(\theta,\phi)\, d\Omega$$

direct approach

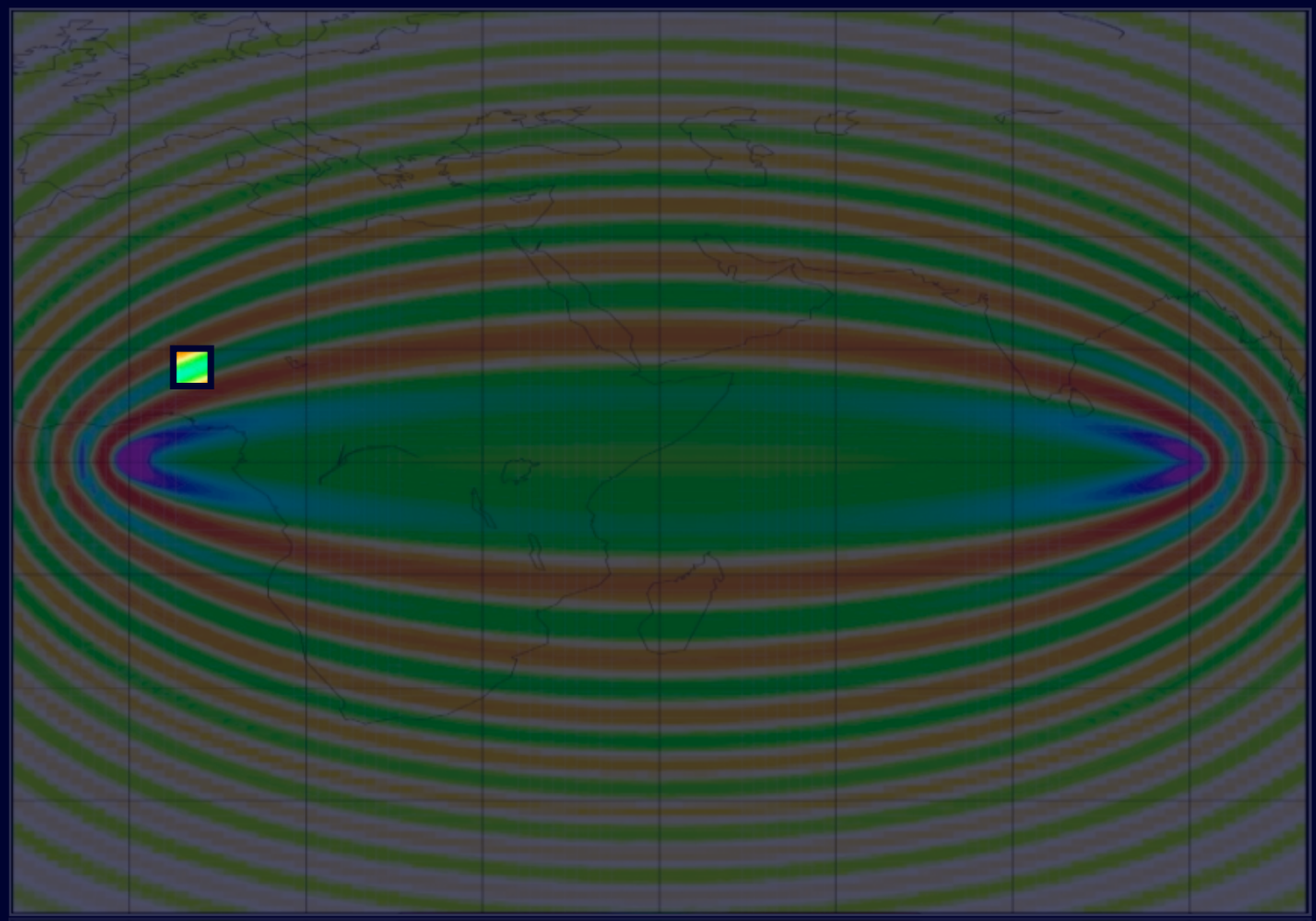

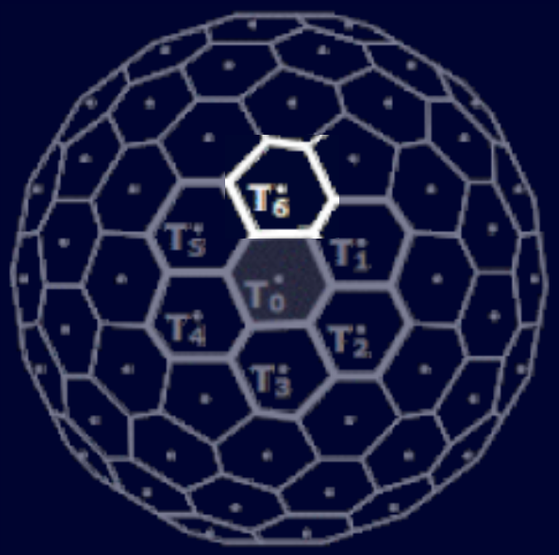

Tape (2003)

Sensitivity kernels

Phase-shift $\delta\Phi$ related to phase-velocity perturbation δc :

$$\delta\Phi = \int_\Omega K(\theta,\phi)\ \delta c(\theta,\phi)\, d\Omega$$

direct approach

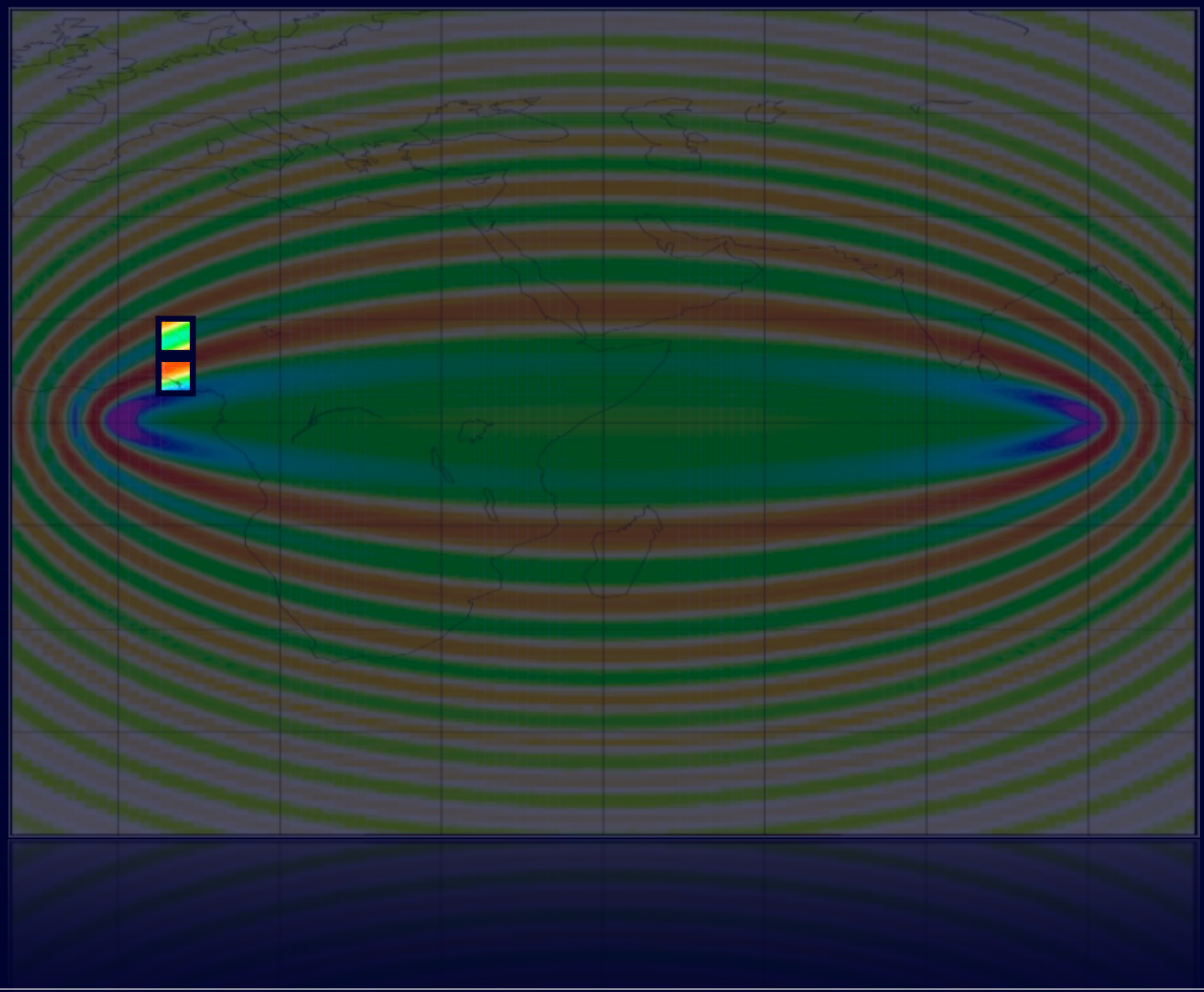

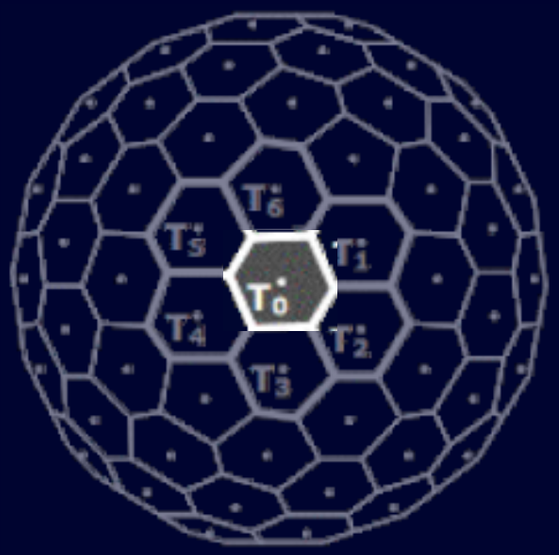

Tape (2003)

Sensitivity kernels

Phase-shift $\delta\Phi$ related to phase-velocity perturbation δc :

$$\delta\Phi = \int_\Omega K(\theta,\phi)\ \delta c(\theta,\phi)\, d\Omega$$

direct approach

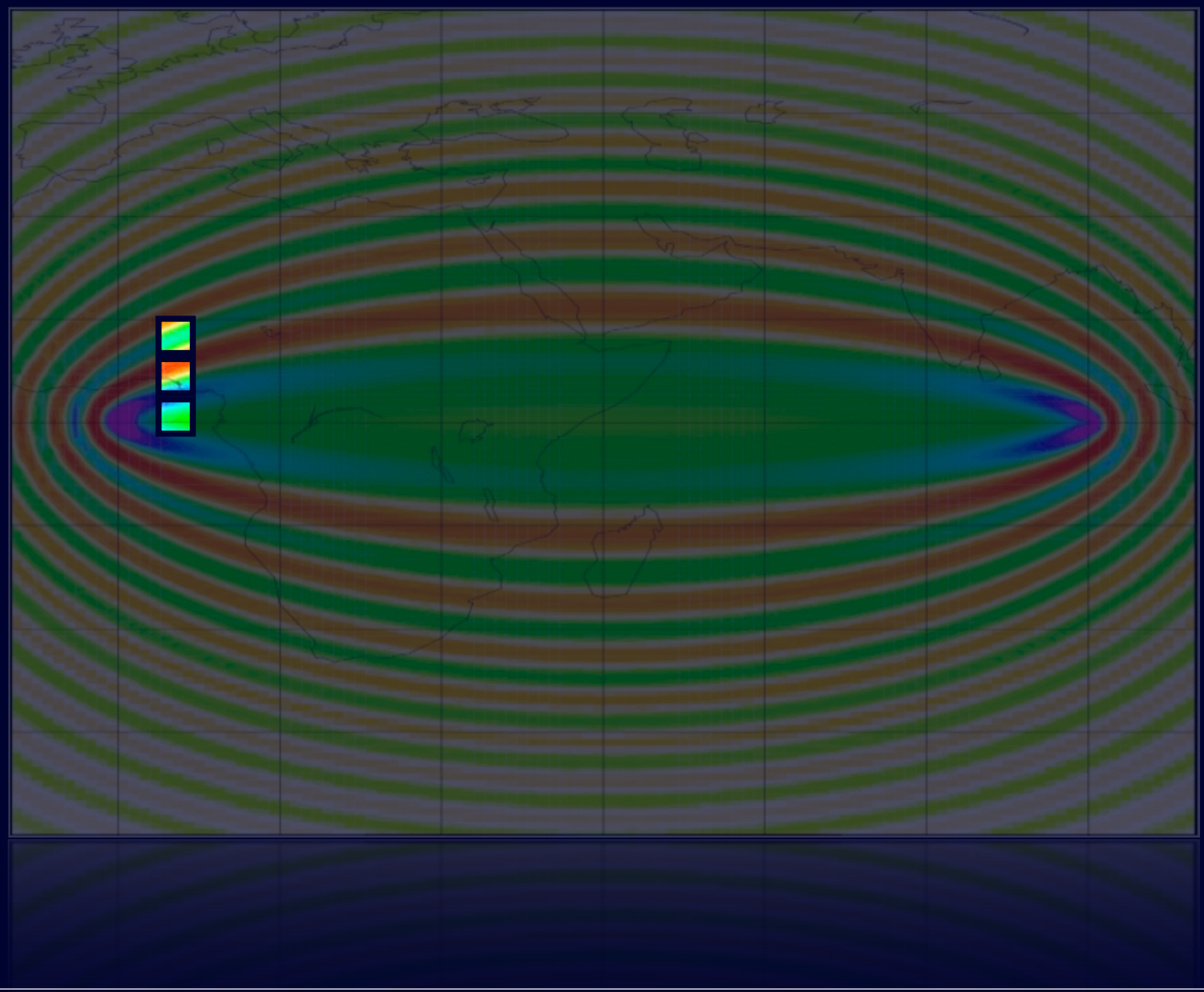

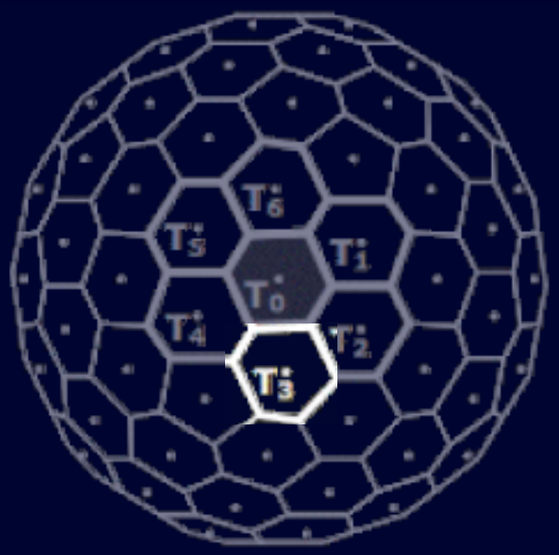

Tape (2003)

Sensitivity kernels

Phase-shift $\delta\Phi$ related to phase-velocity perturbation δc :

$$\delta\Phi = \int_\Omega K(\theta,\phi)\ \delta c(\theta,\phi)\, d\Omega$$

adjoint method

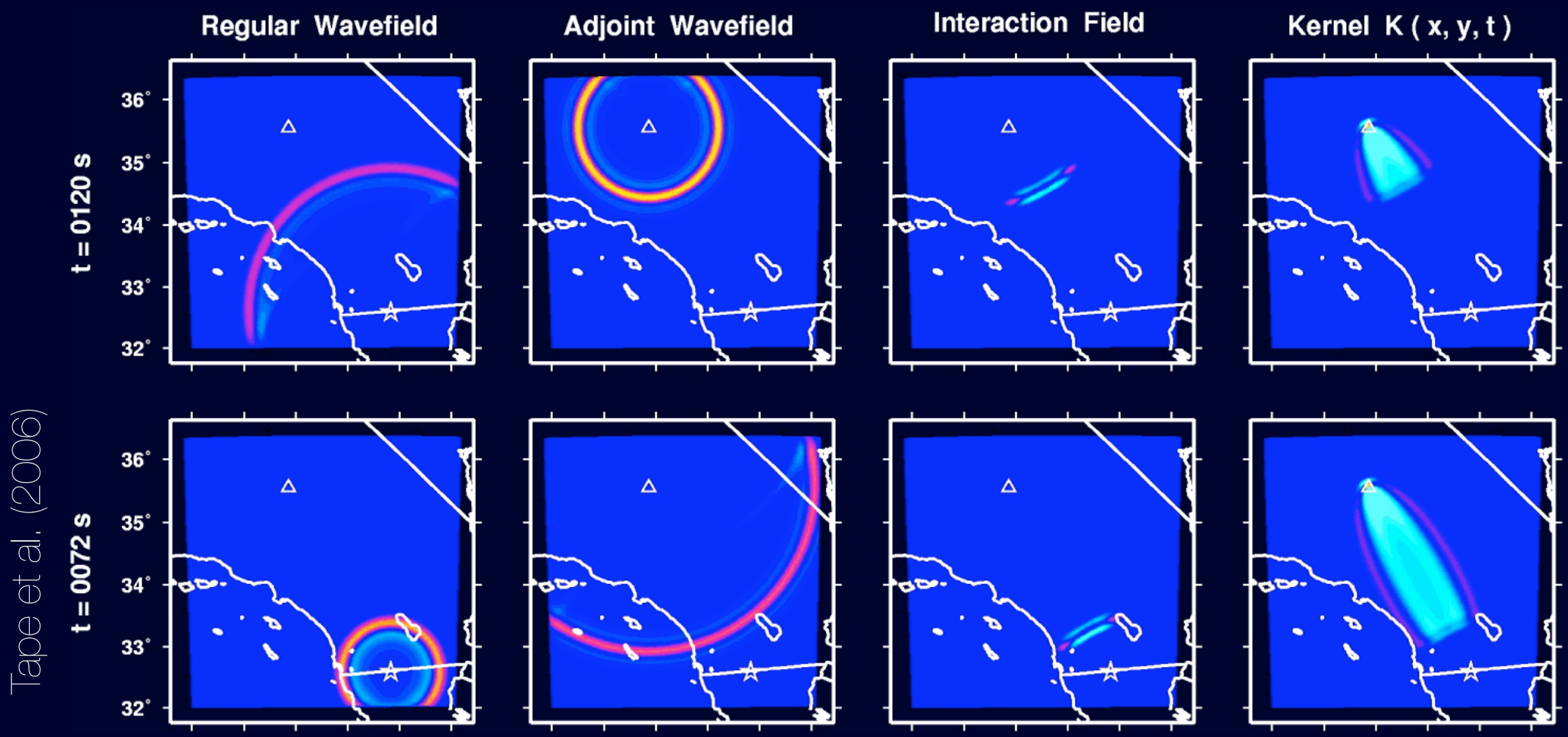

Tape et al. (2006)

Sensitivity kernels

Phase-shift $\delta\Phi$ related to phase-velocity perturbation δc :

$$\delta\Phi = \int_\Omega K(\theta,\phi)\ \delta c(\theta,\phi)\, d\Omega$$

adjoint method

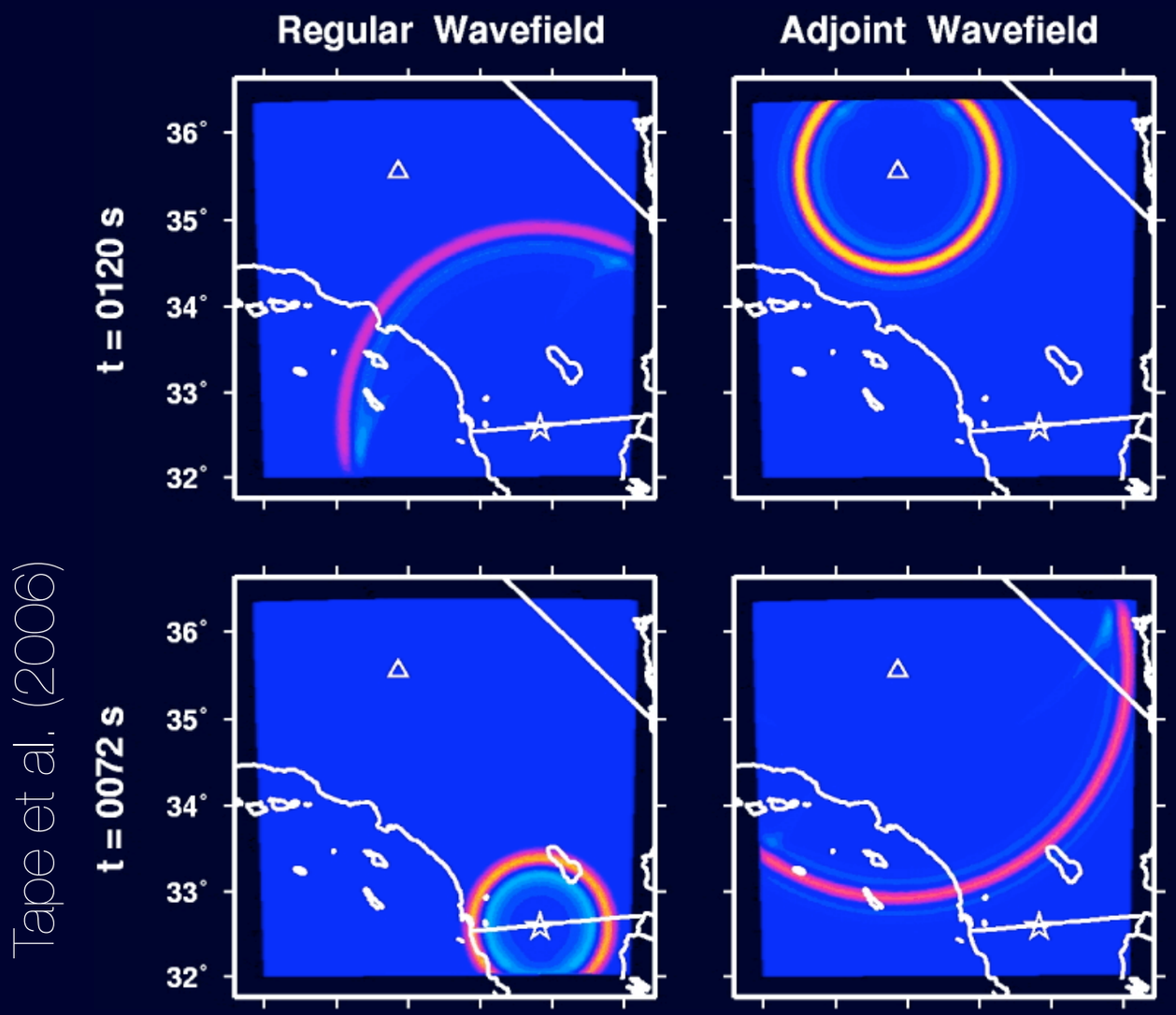

Tape et al. (2006)

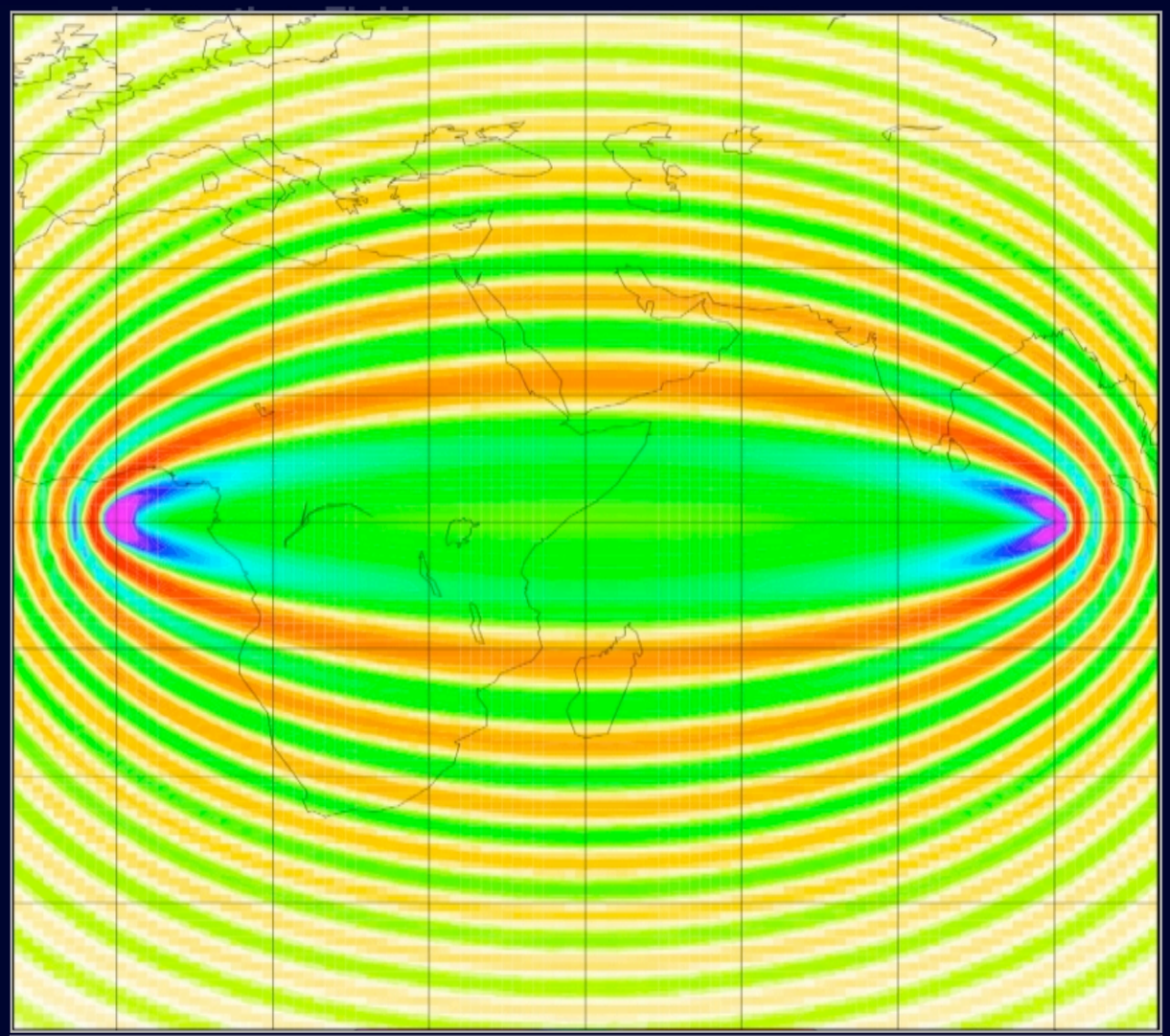

Sensitivity kernels

Inverse problem

$$\mathbf{A} \cdot \mathbf{x} = \mathbf{d}$$

uses sensitivity kernels

$$A_{ij} = \int_{j^{th}\ pixel} K_{i^{th}\ datum}(\omega, \theta, \phi)\ d\Omega$$

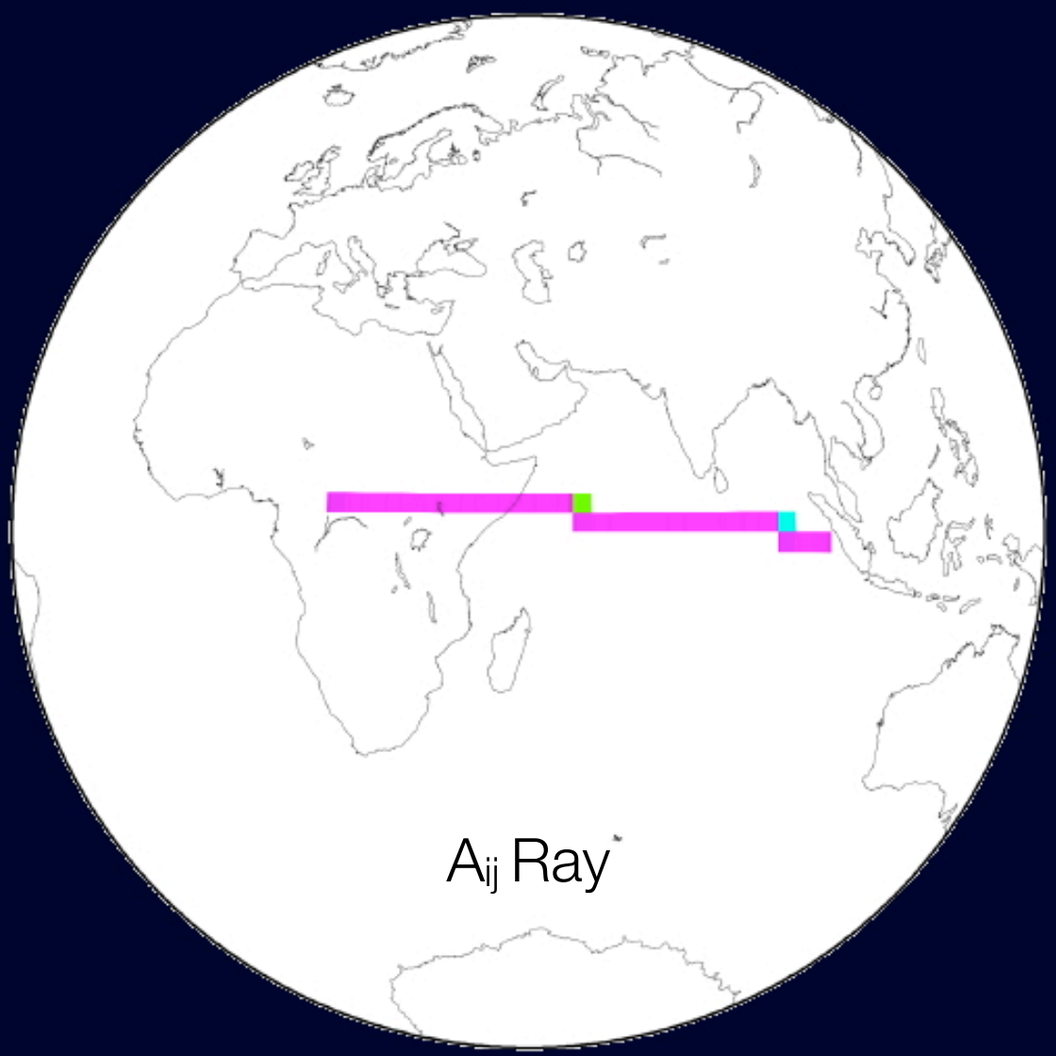

A_{ij} Ray

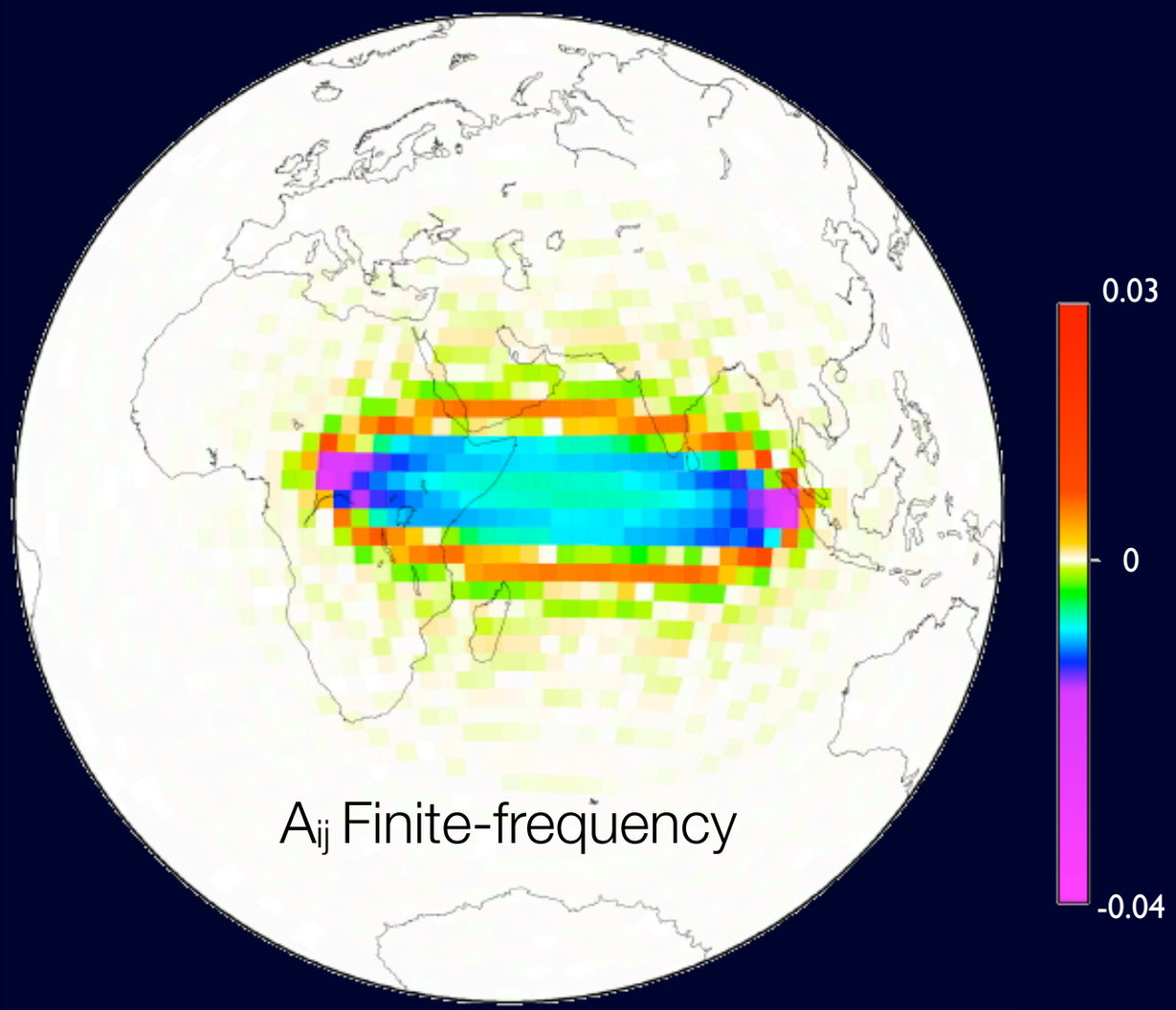

A_{ij} Finite-frequency

Sensitivity kernels

Inverse problem

$$\mathbf{A} \cdot \mathbf{x} = \mathbf{d}$$

uses sensitivity kernels

$$A_{ij} = \int_{j^{th}\ pixel} K_{i^{th}\ datum}\left(\omega, \theta, \phi\right)\ d\Omega$$

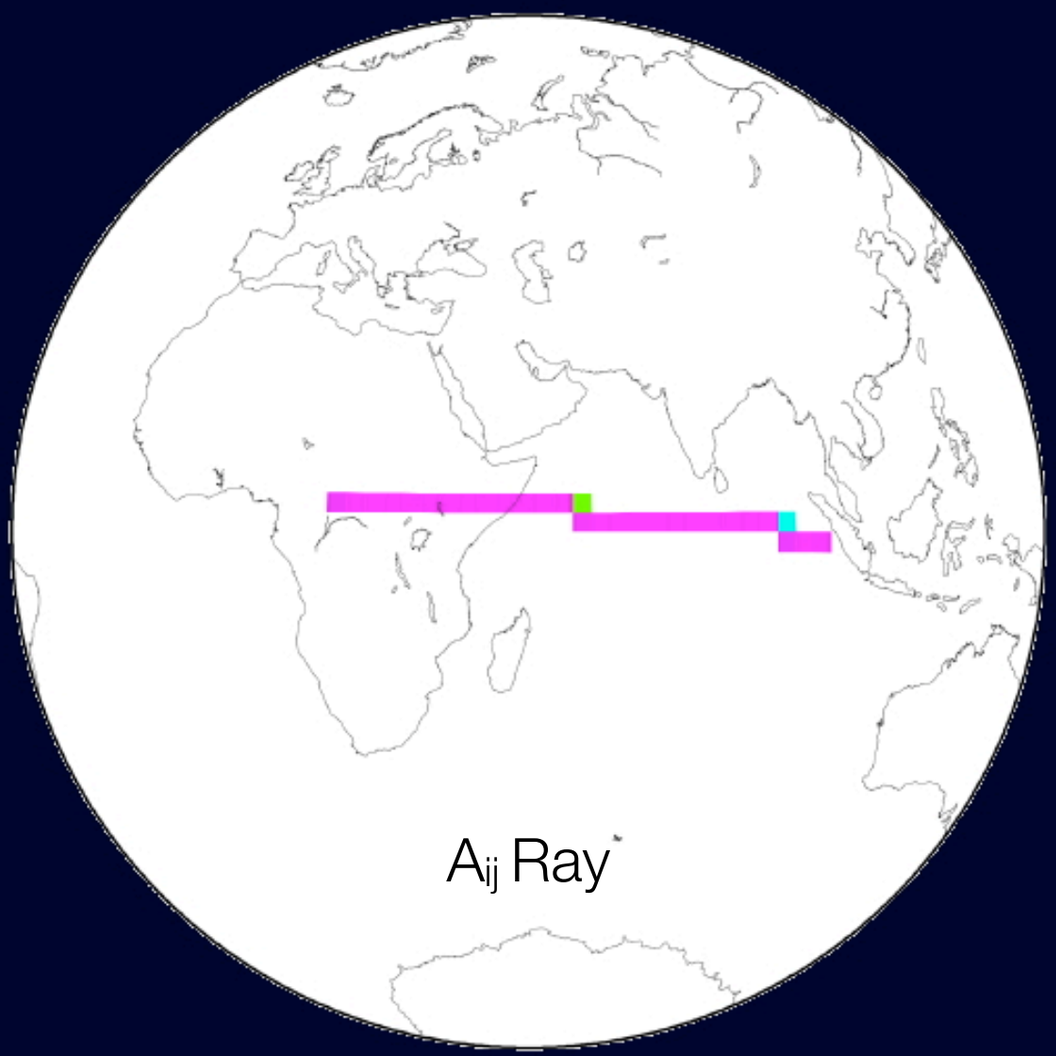

A_{ij} Ray

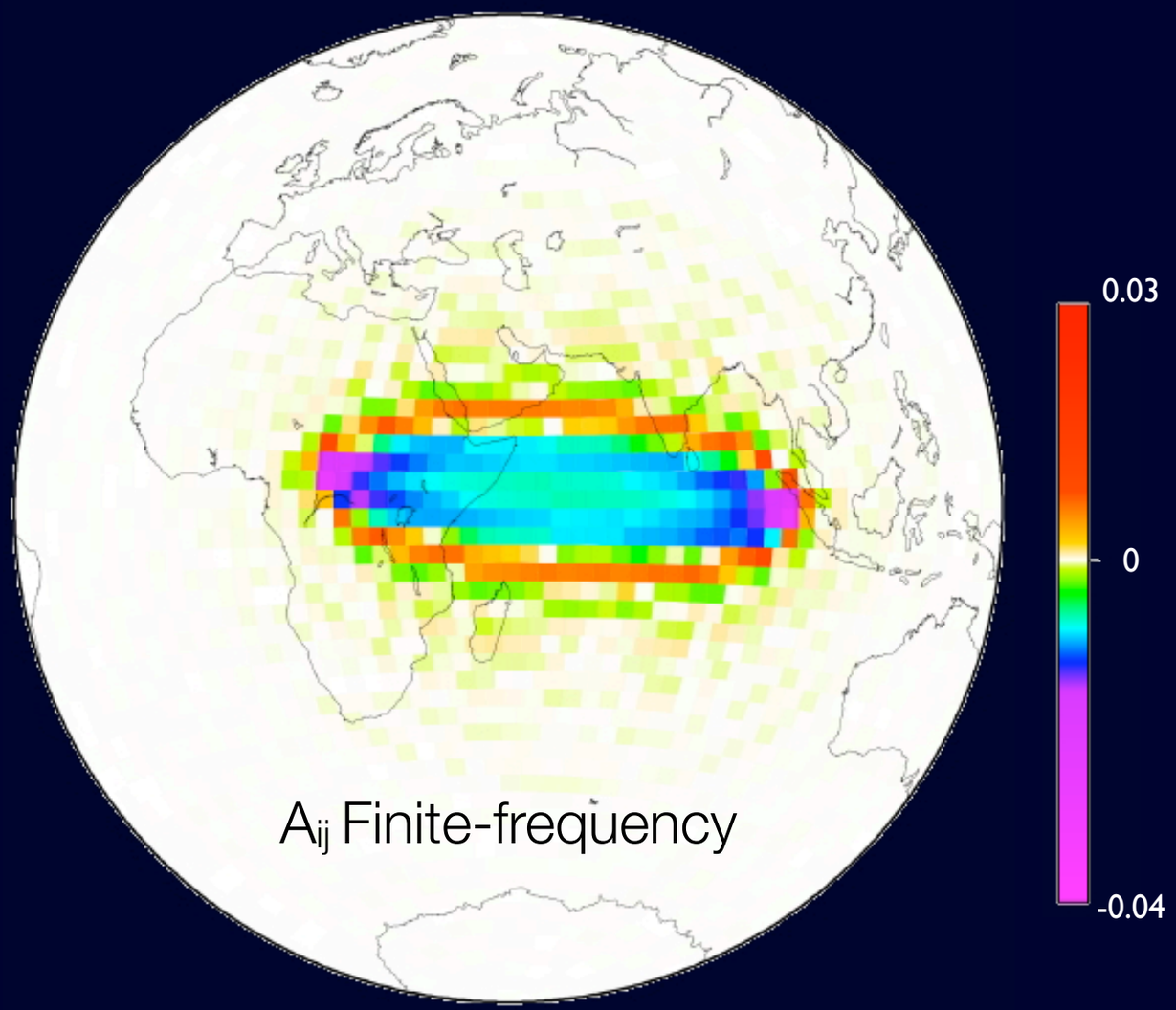

A_{ij} Finite-frequency

Phase velocity maps

Rays

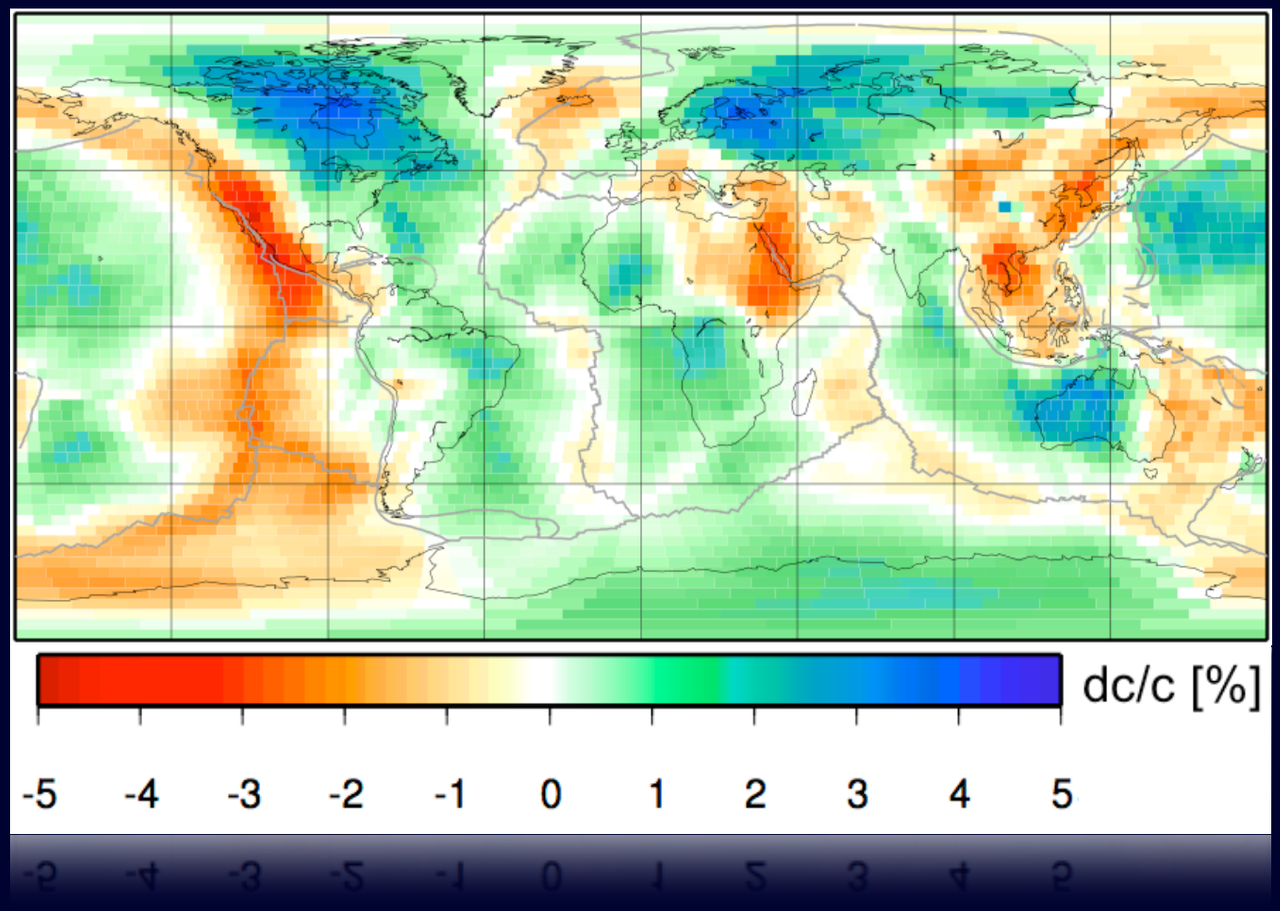

Finite-frequency

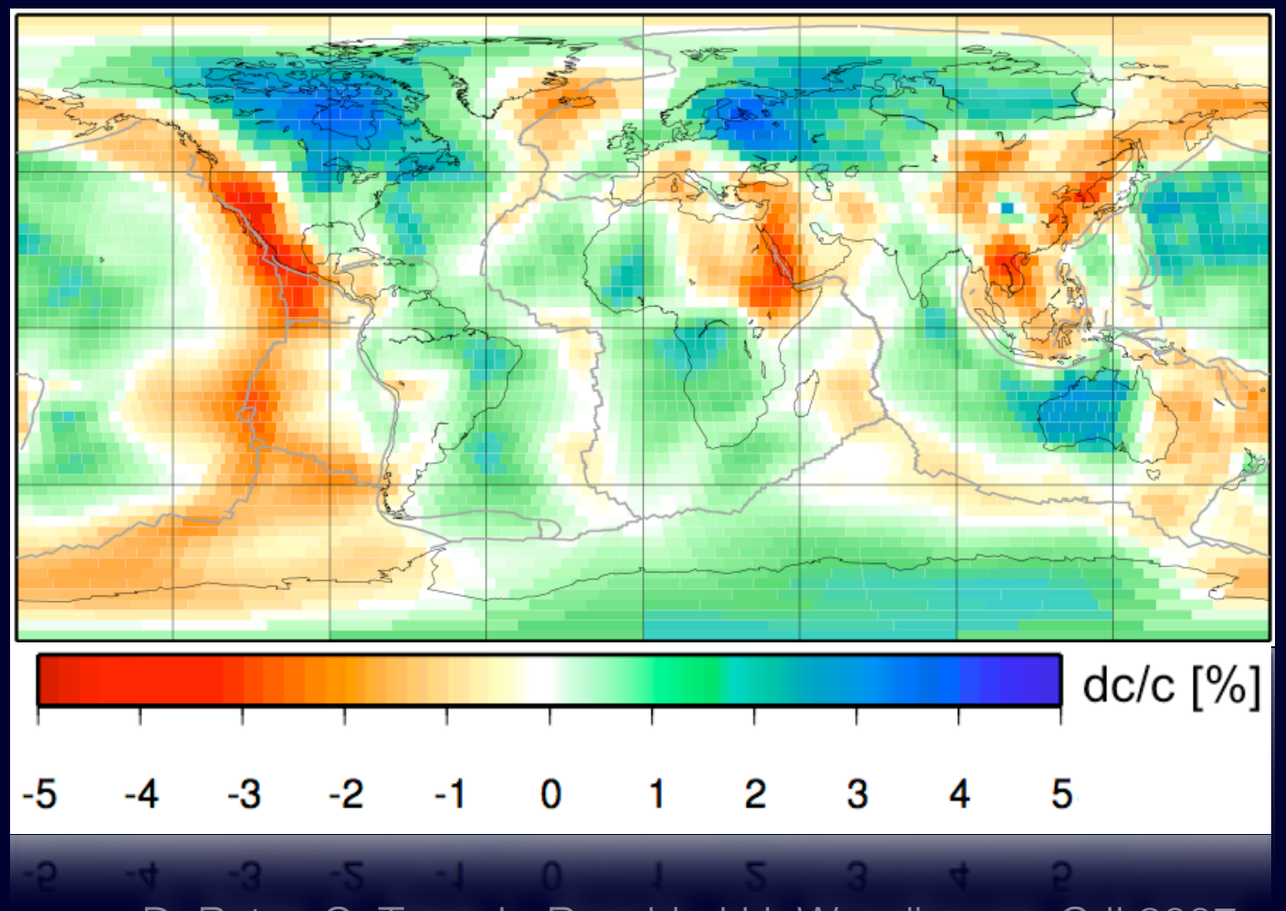

D. Peter, C. Tape, L. Boschi, J.H. Woodhouse, GJI 2007

Phase velocity maps

Rays

Finite-frequency

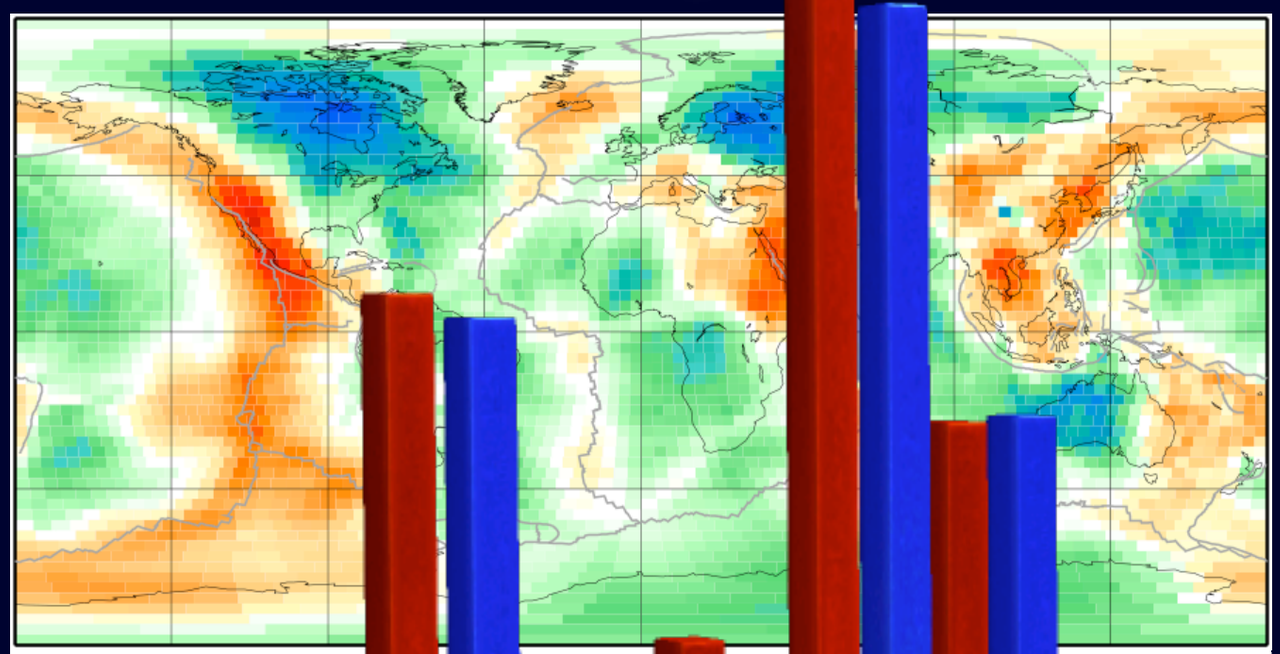

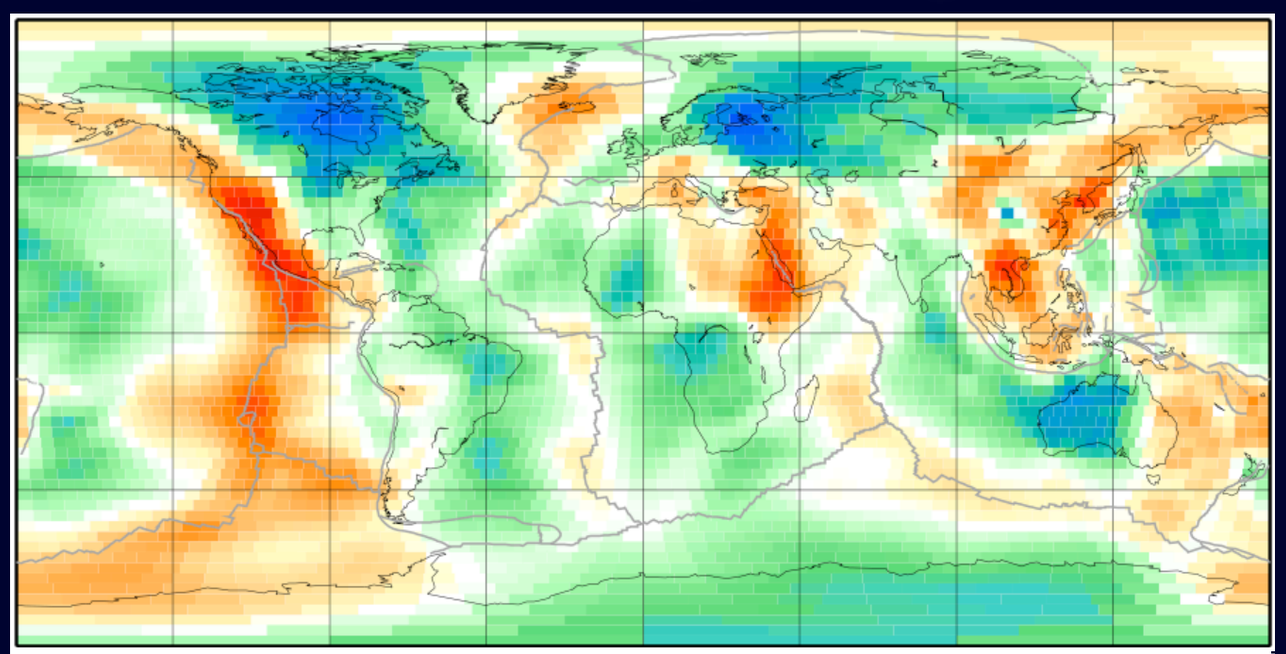

D. Peter, C. Tape, L. Boschi, J.H. Woodhouse, GJI 2007

Outline

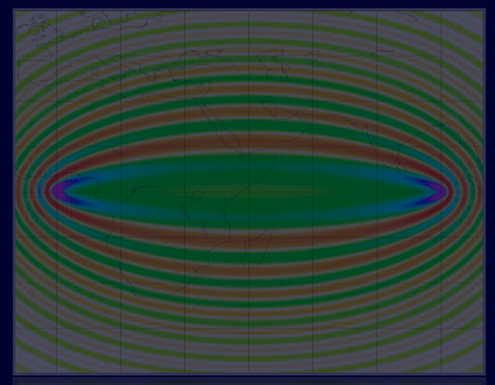

- Forward modeling:
  Membrane waves and sensitivity kernels

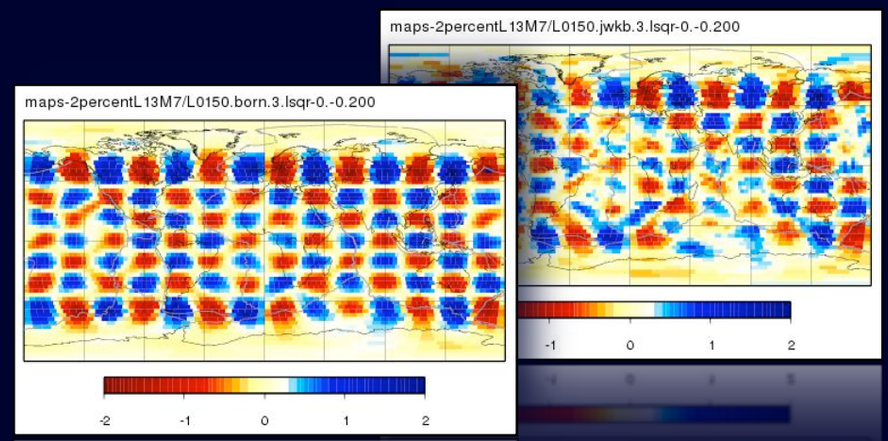

- Implications on tomography:
  Resolution benchmark

- Application to 3-D seismology:
  Mediterranean tomography

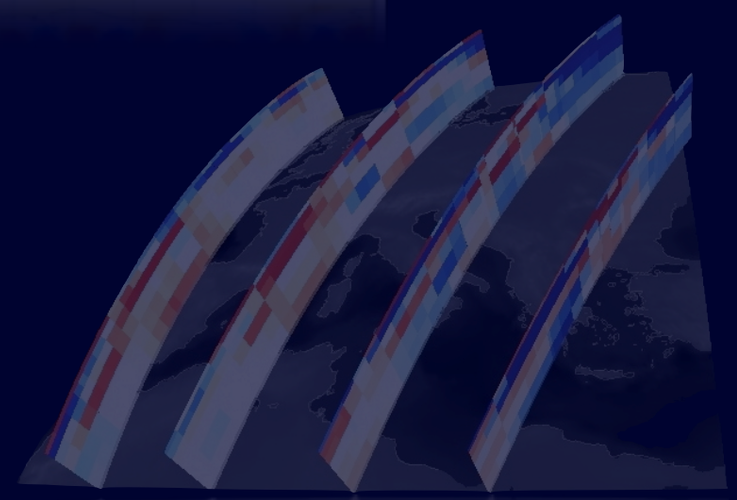

Synthetic benchmark

Data coverage

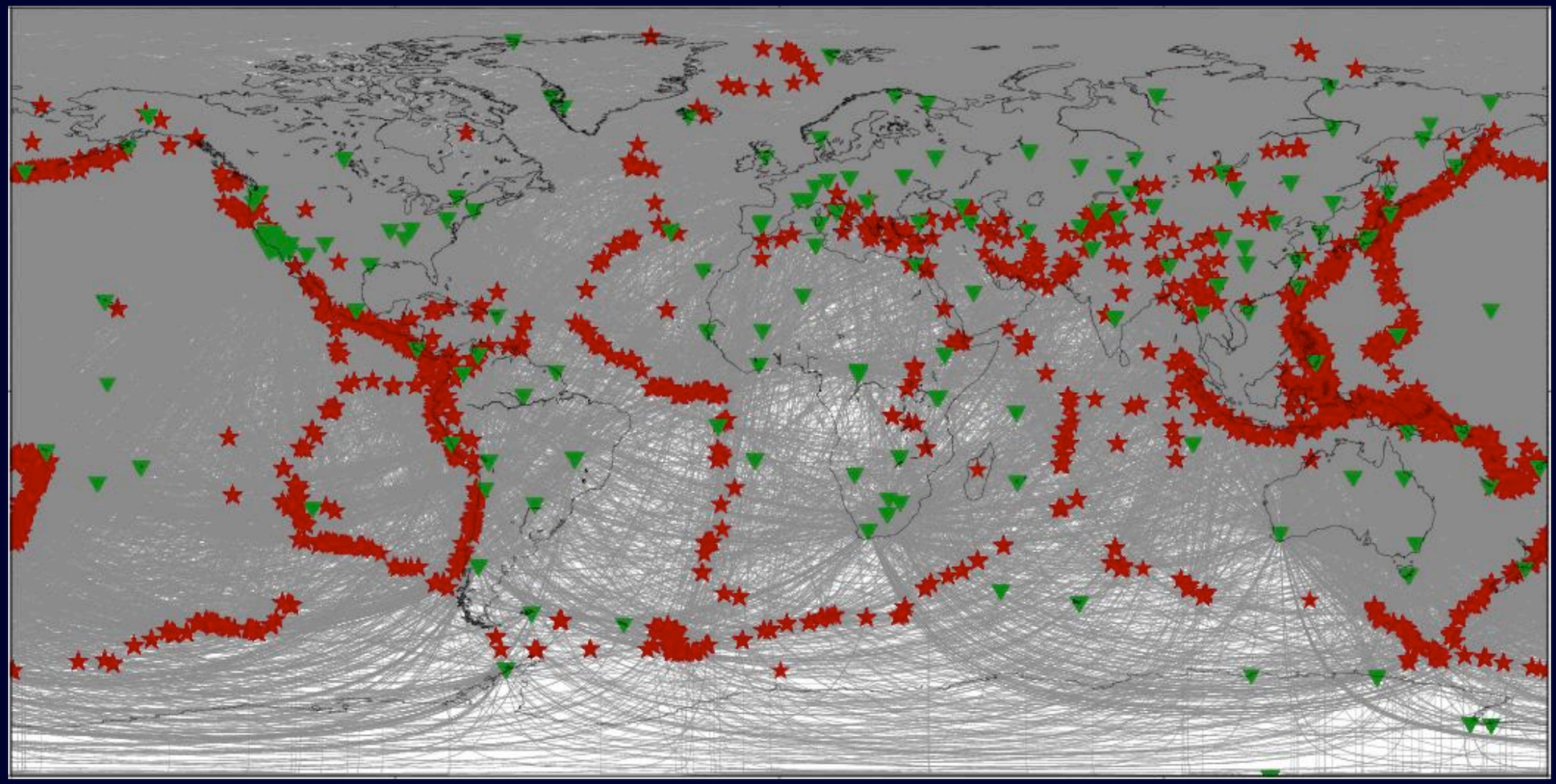

Synthetic benchmark

Data coverage

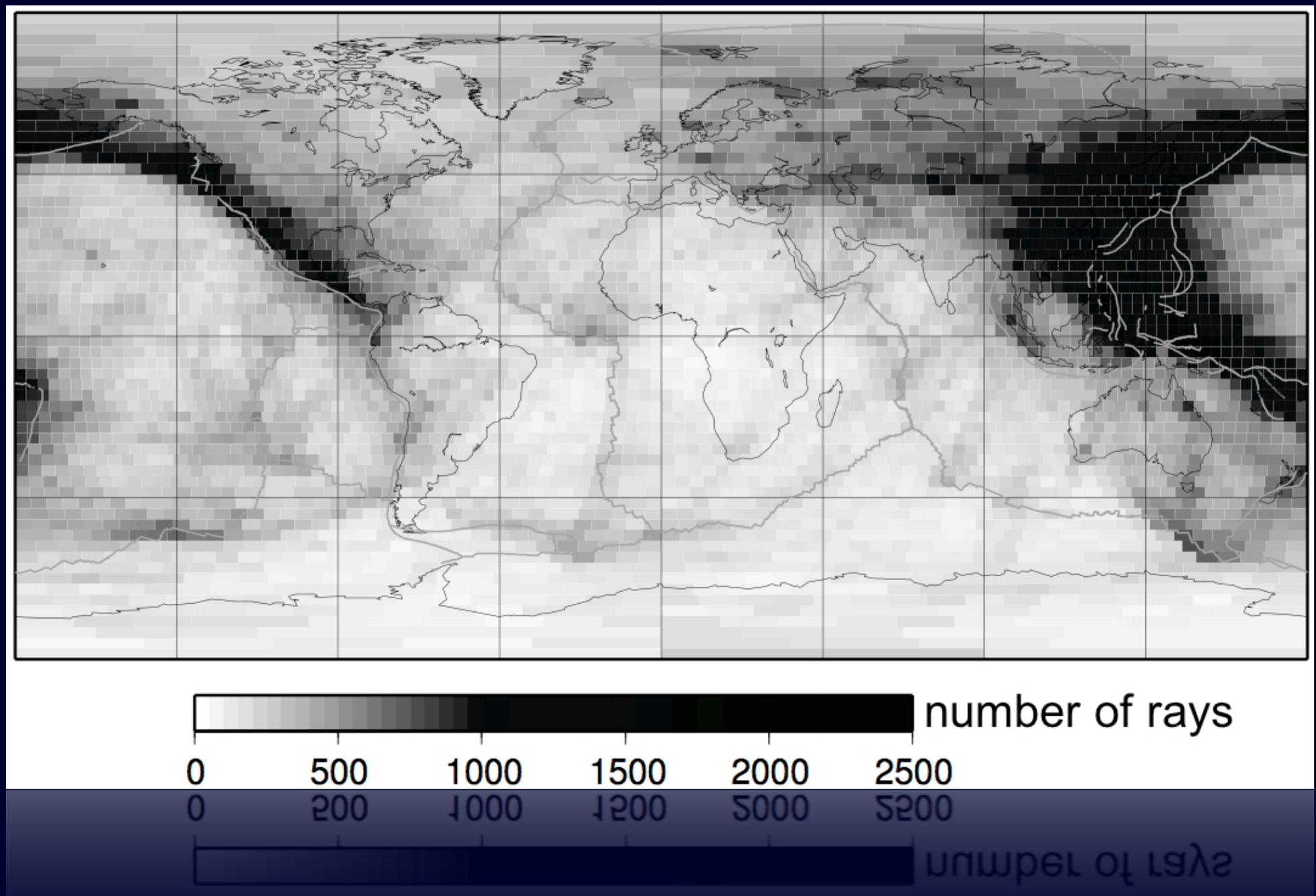

Synthetic benchmark

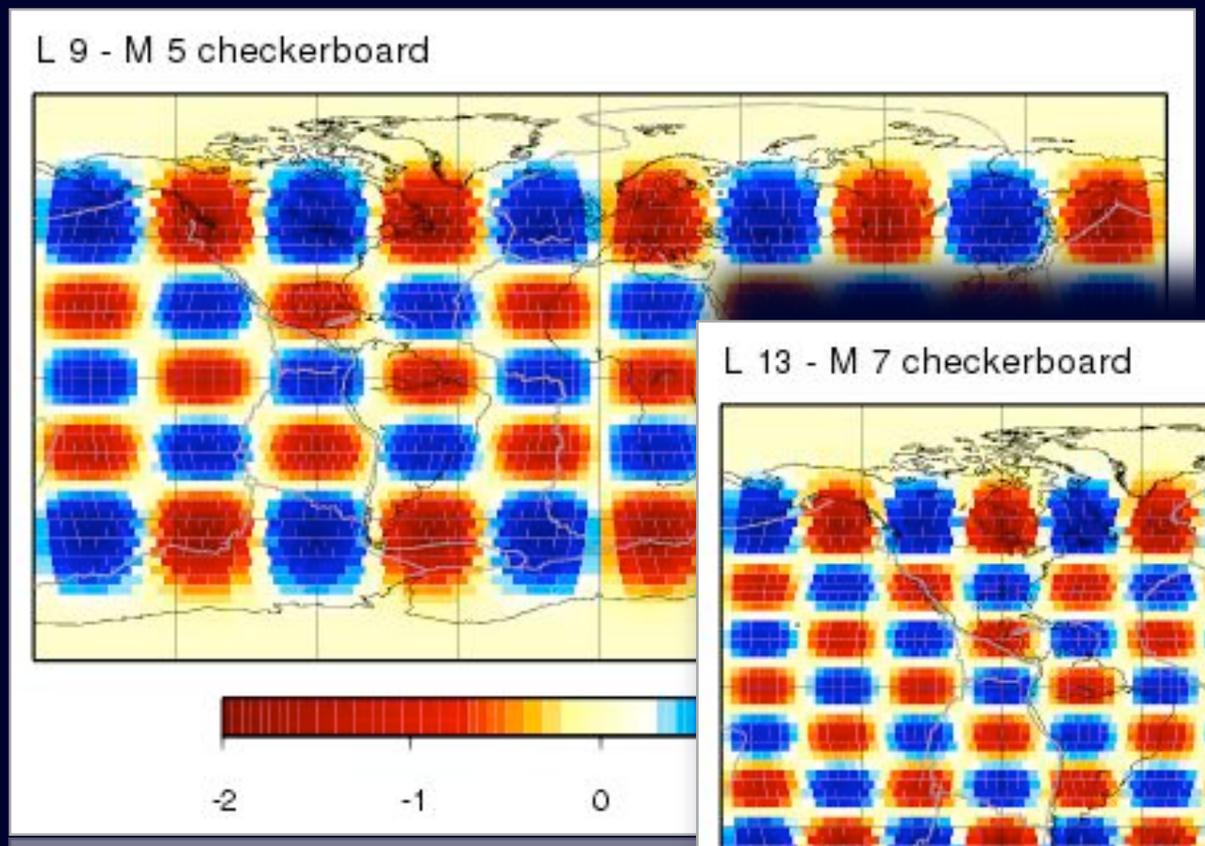

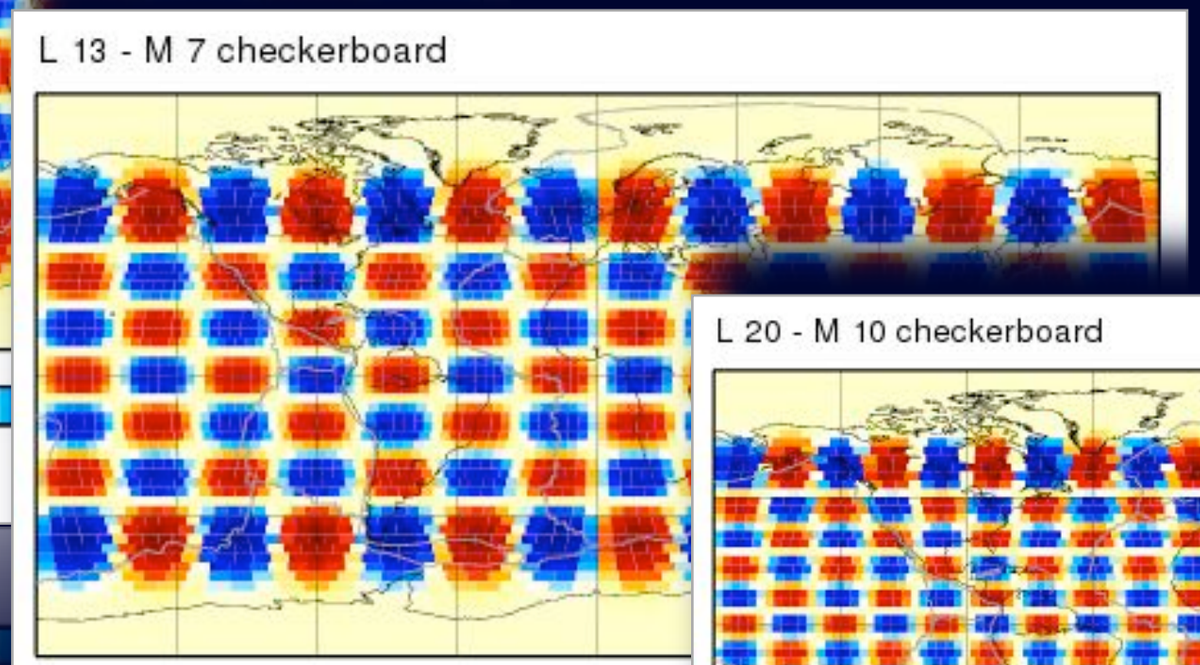

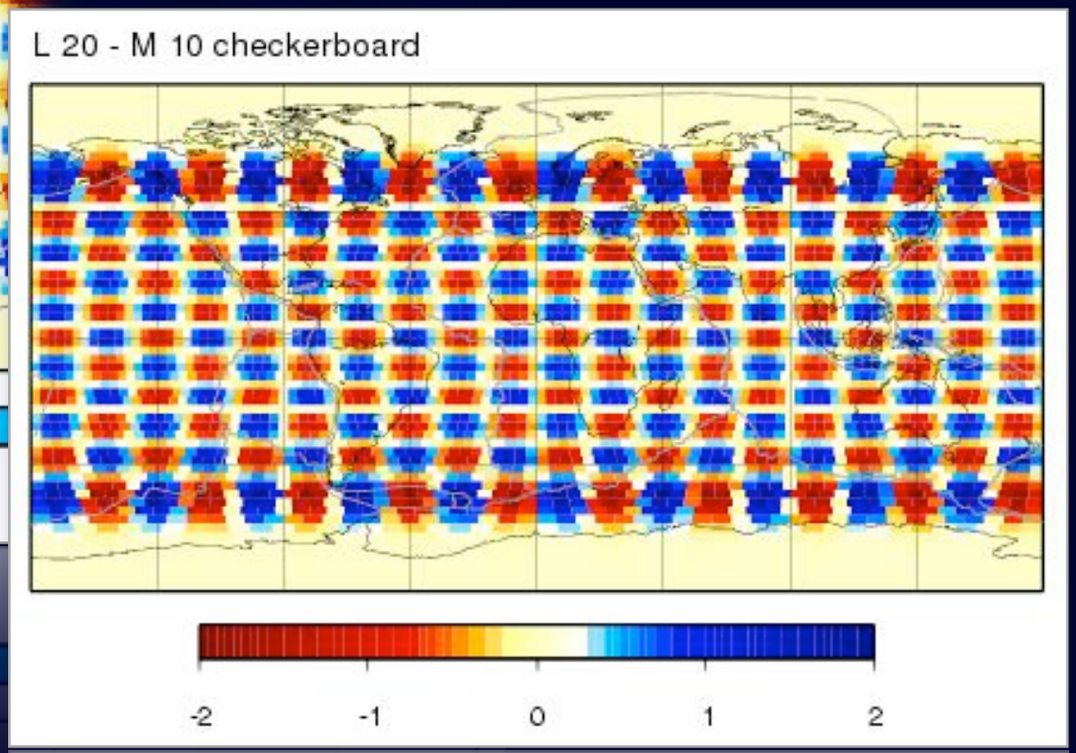

Synthetic benchmark

Rays

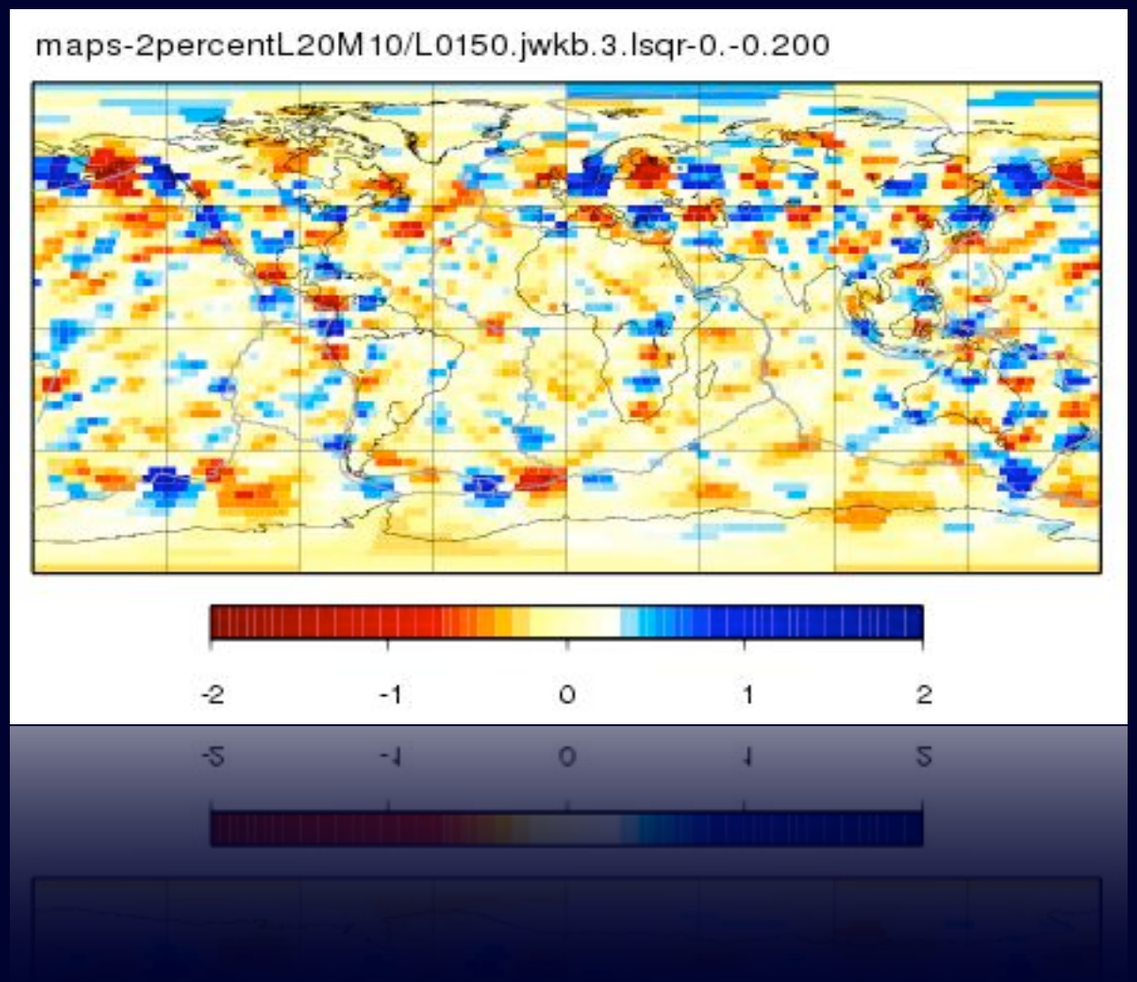

Finite-frequency

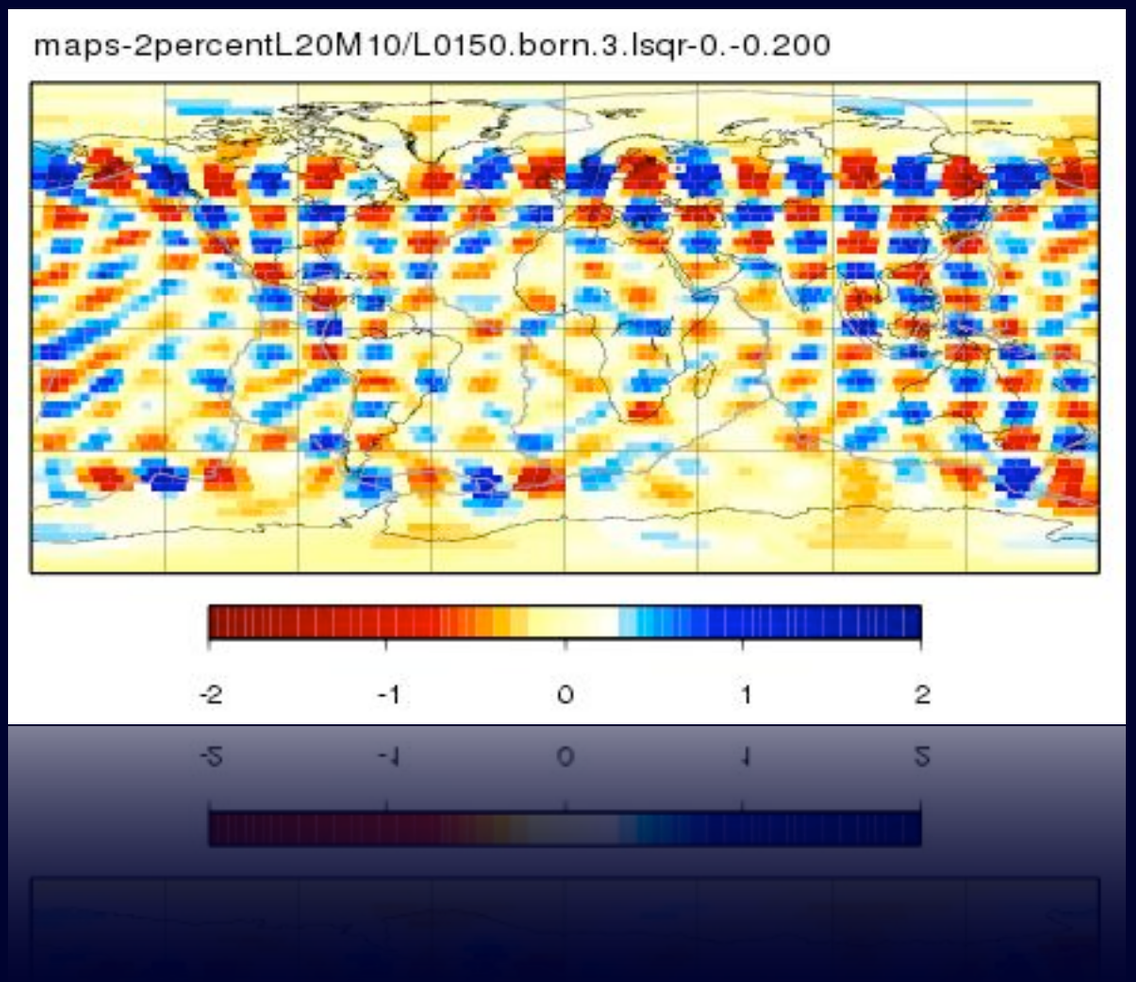

Synthetic benchmark

Rays

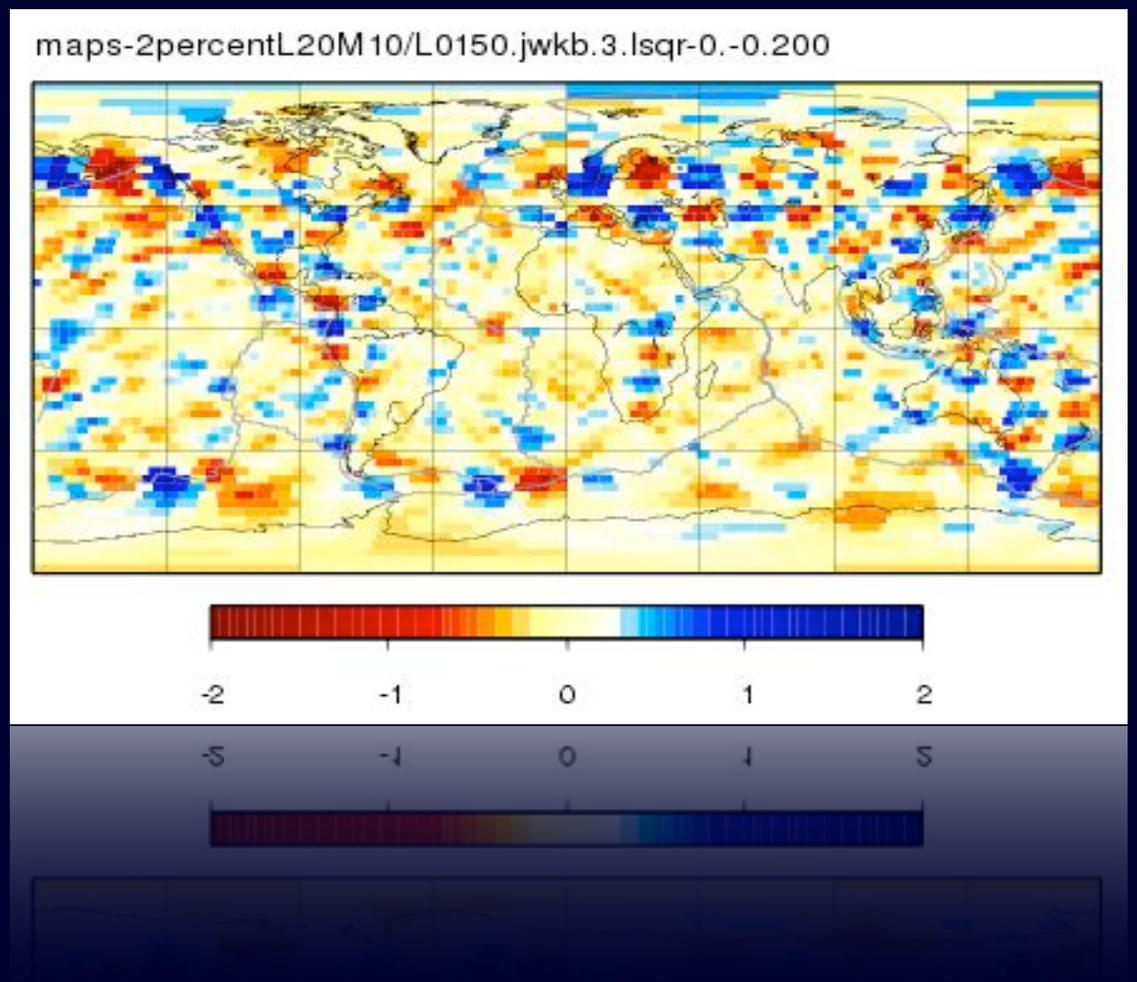

Finite-frequency

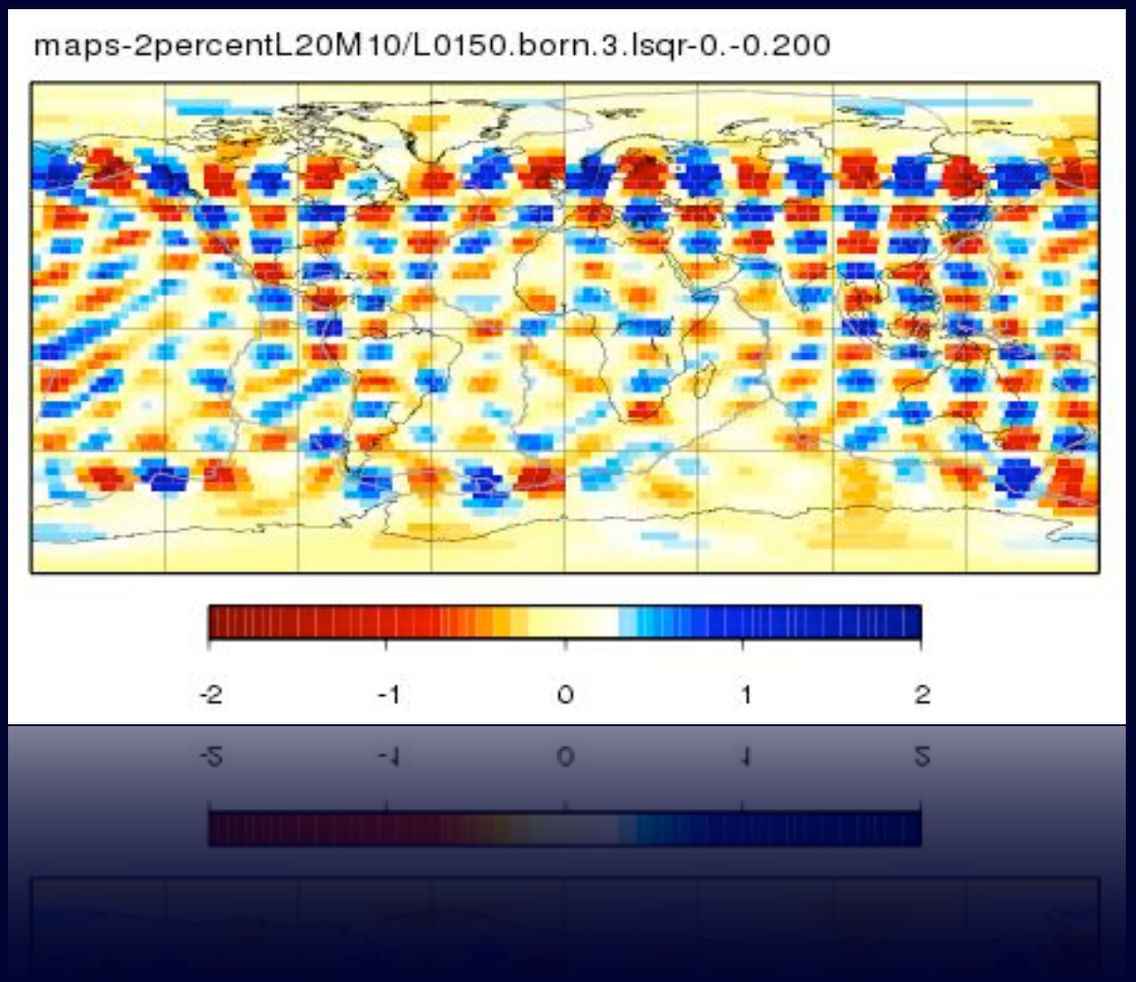

Synthetic benchmark

Rays

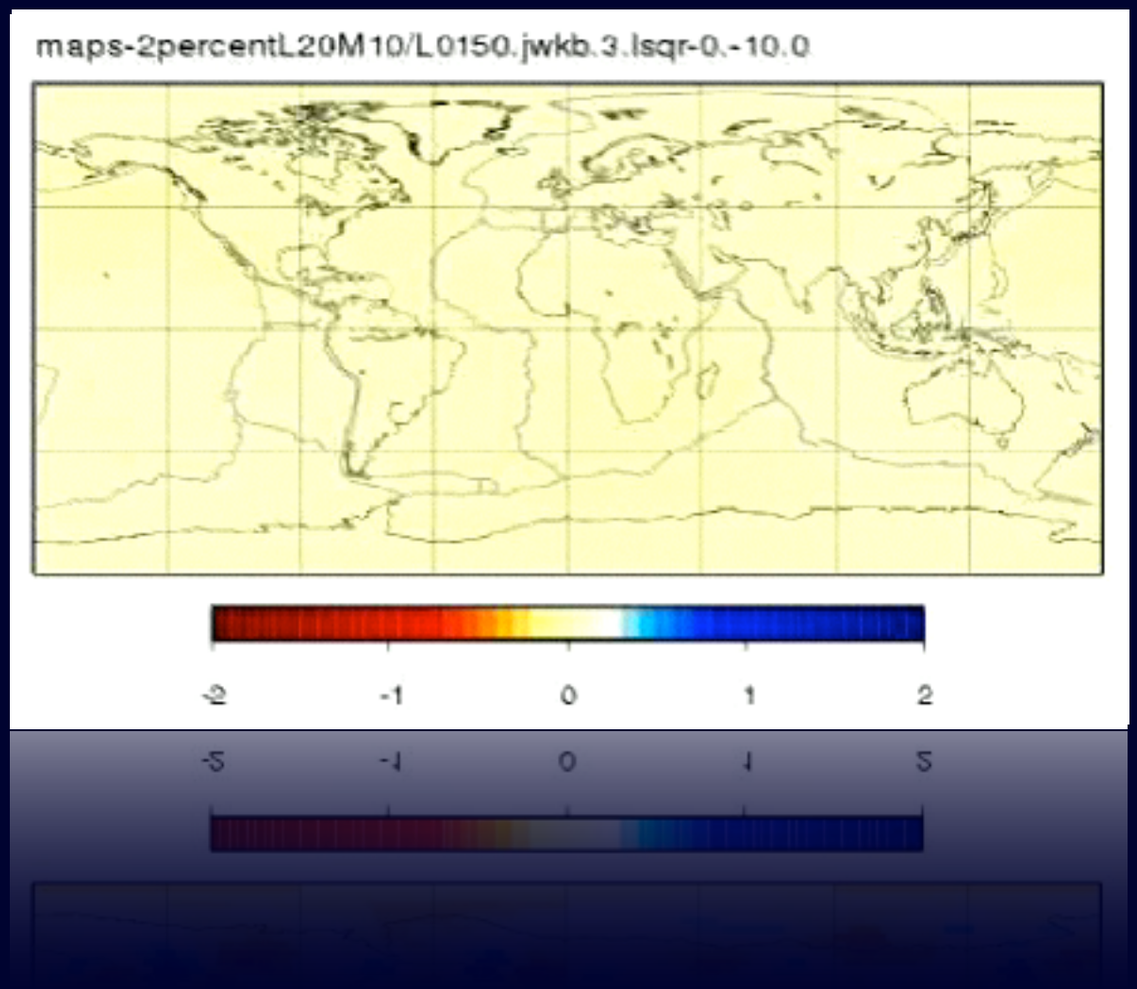

Finite-frequency

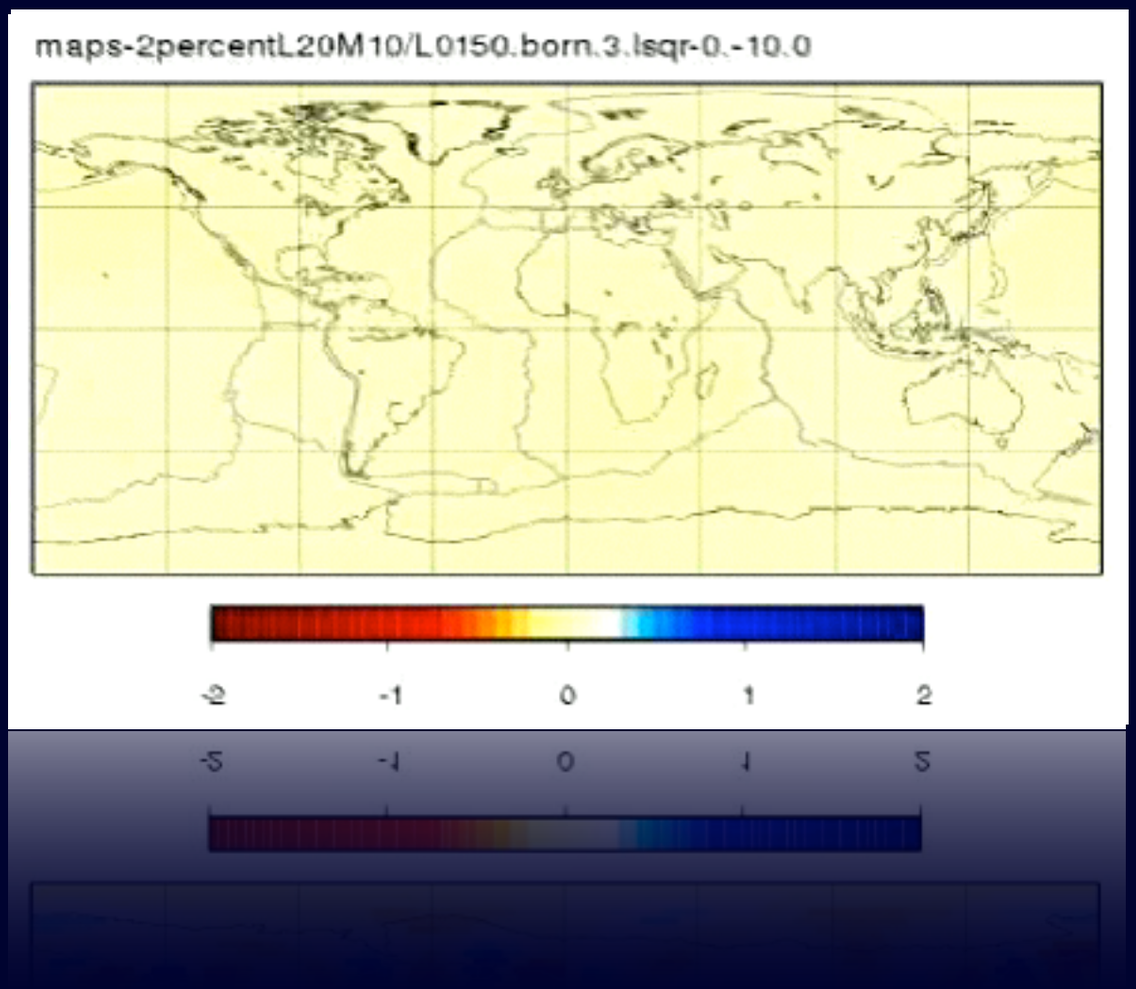

Synthetic benchmark

Rays

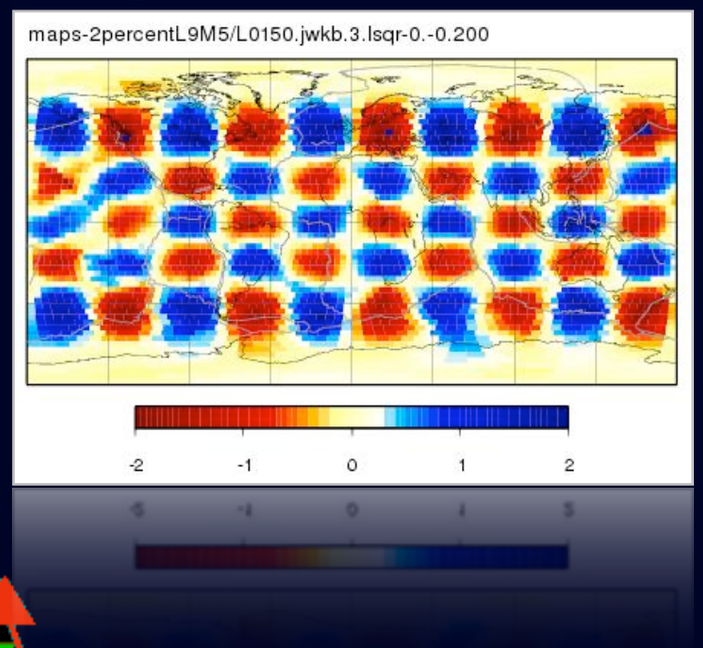

Finite-frequency

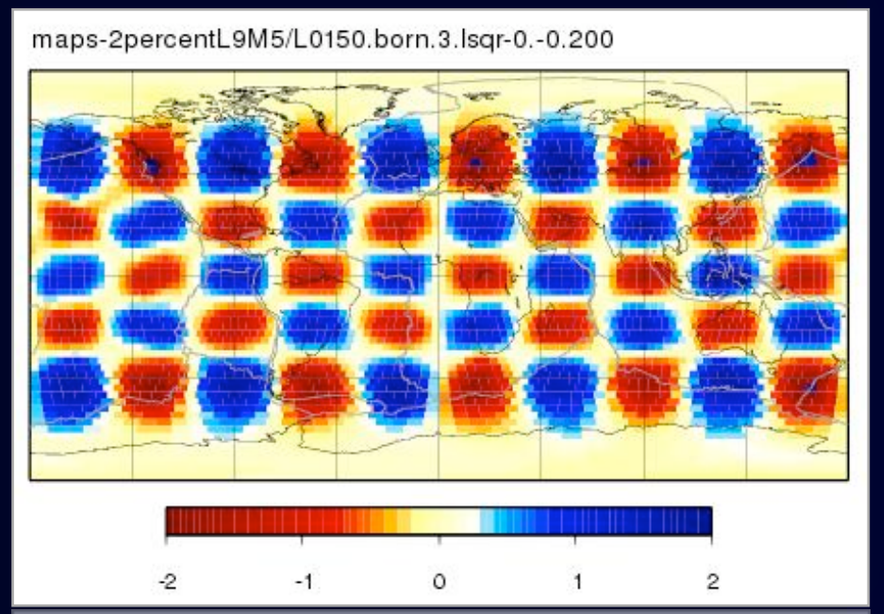

misfit

0.3
0.2
0.1
0

0.1
0.2
0.3

normalized model roughness

Daniel Peter | ETH Zurich

L 9 - M 5 checkerboard

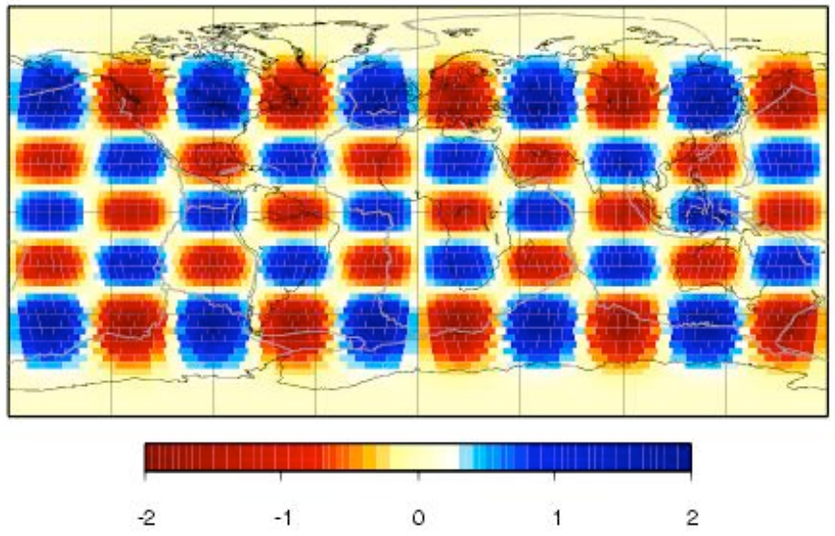

maps-2percentL9M5/L0150.jwkb.3.lsqr-0.-0.200

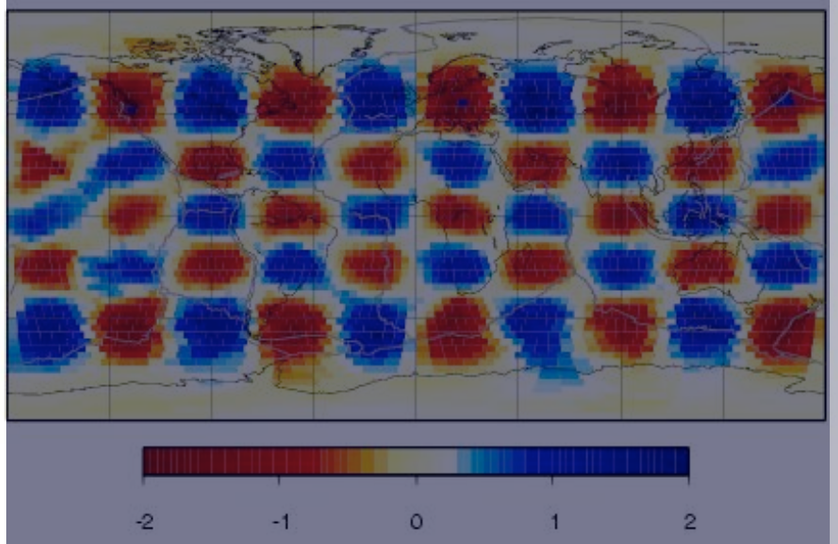

maps-2percentL9M5/L0150.born.3.lsqr-0.-0.200

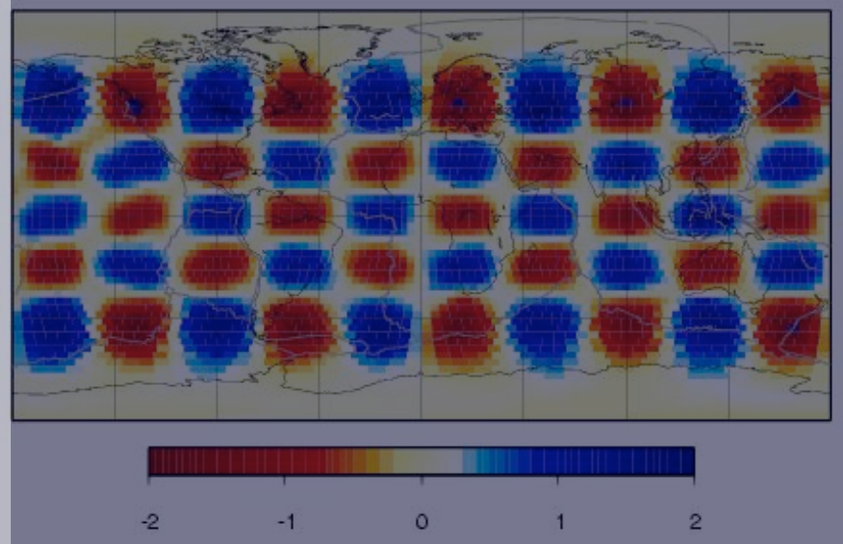

L 13 - M 7 checkerboard

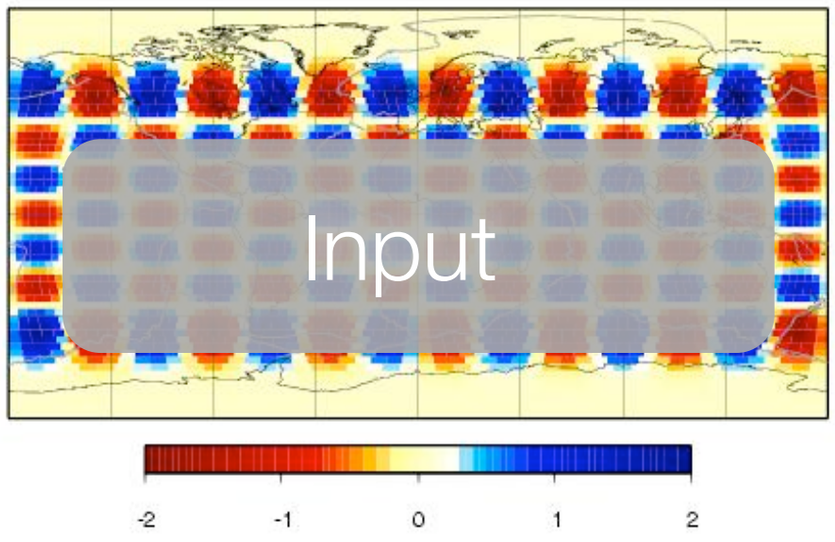

maps-2percentL13M7/L0150.jwkb.3.lsqr-0.-0.200

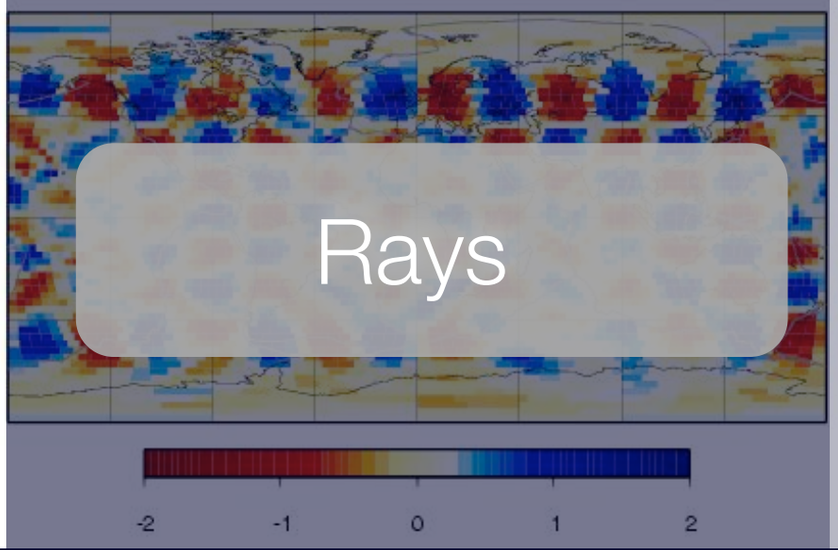

maps-2percentL13M7/L0150.born.3.lsqr-0.-0.200

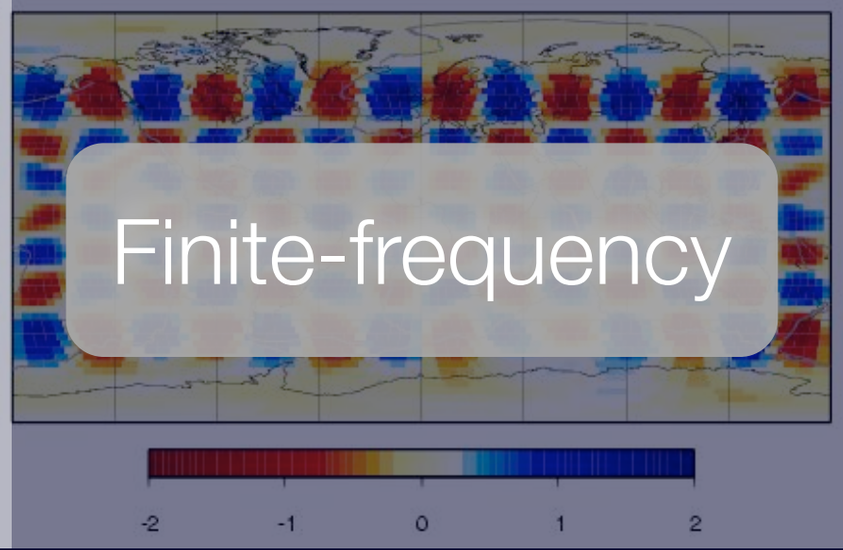

L 20 - M 10 checkerboard

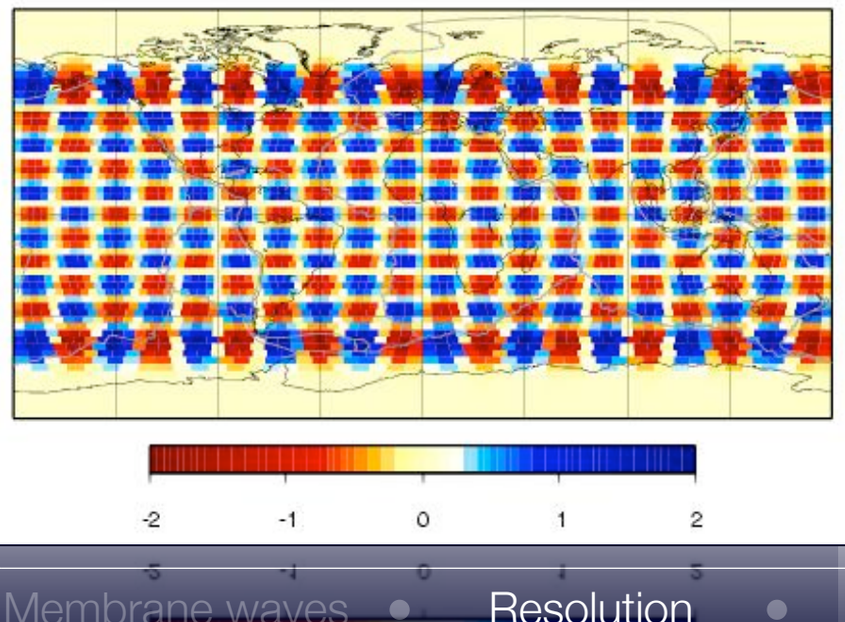

maps-2percentL20M10/L0150.jwkb.3.lsqr-0.-0.200

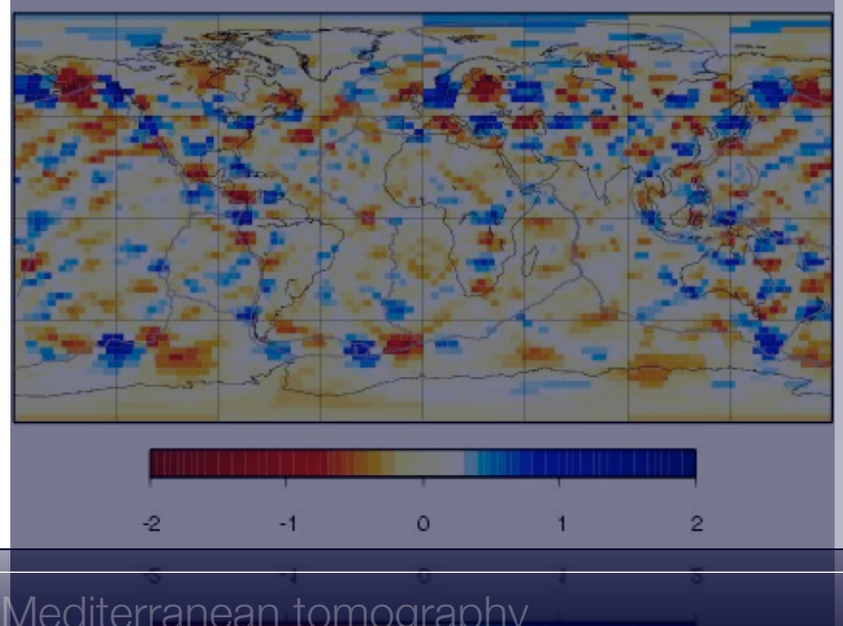

maps-2percentL20M10/L0150.born.3.lsqr-0.-0.200

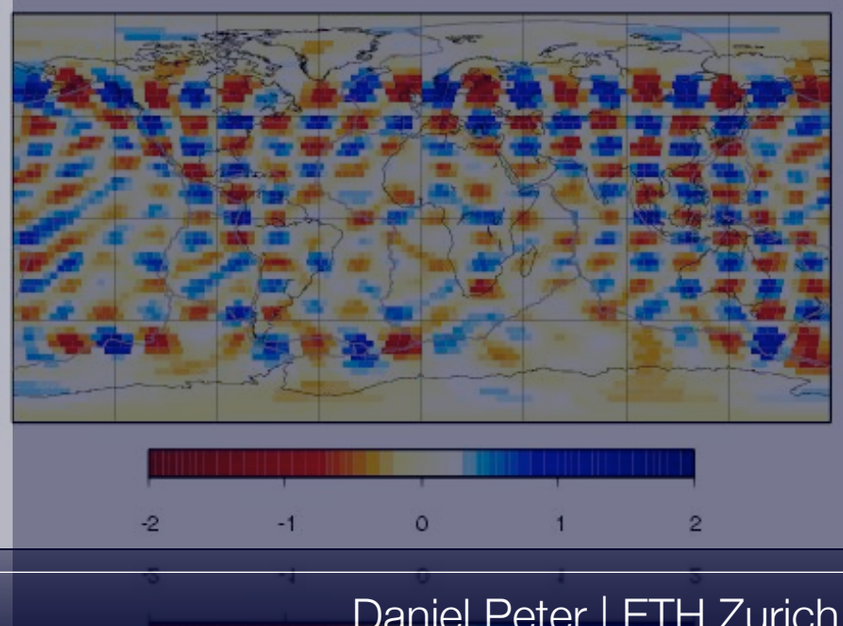

Input

Rays

Finite-frequency

L 9 - M 5 checkerboard

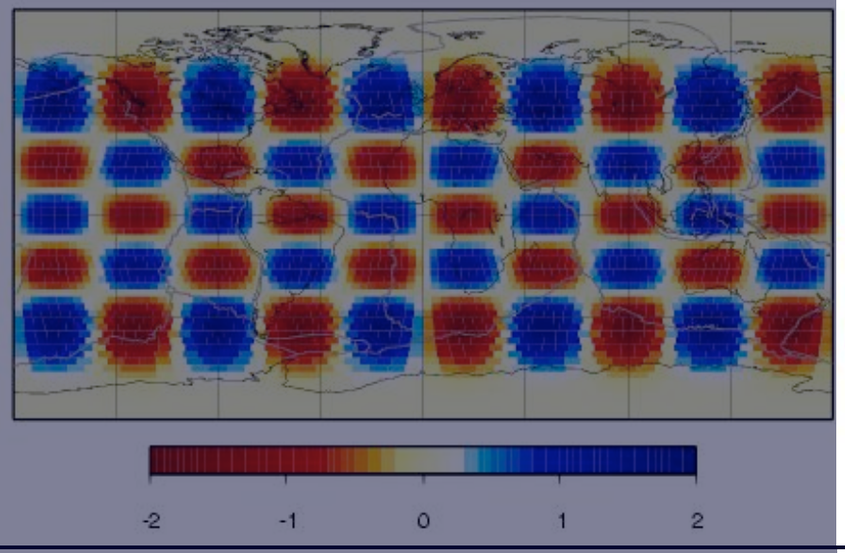

maps-2percentL9M5/L0150.jwkb.3.lsqr-0.-0.200

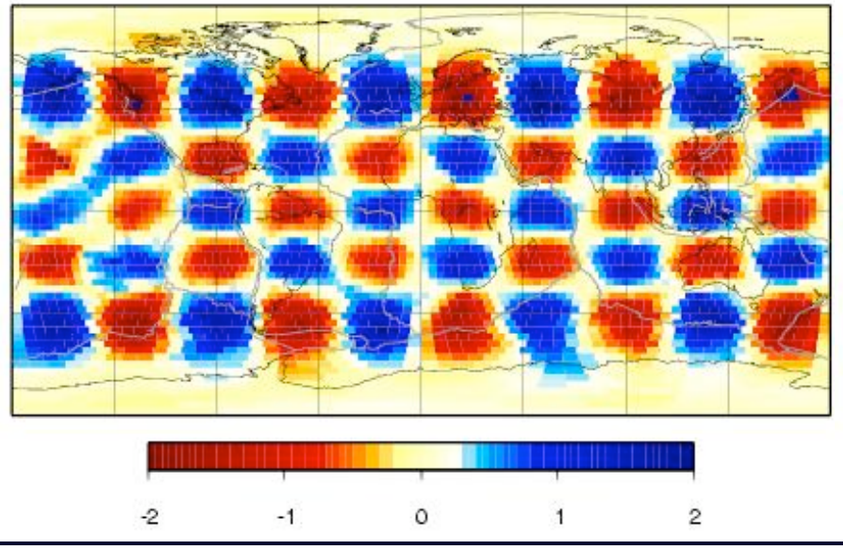

maps-2percentL9M5/L0150.born.3.lsqr-0.-0.200

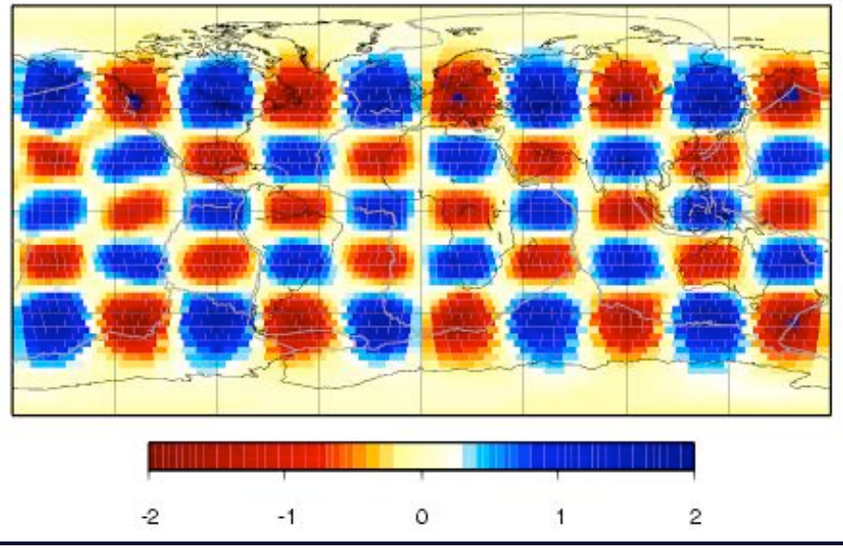

L 13 - M 7 checkerboard

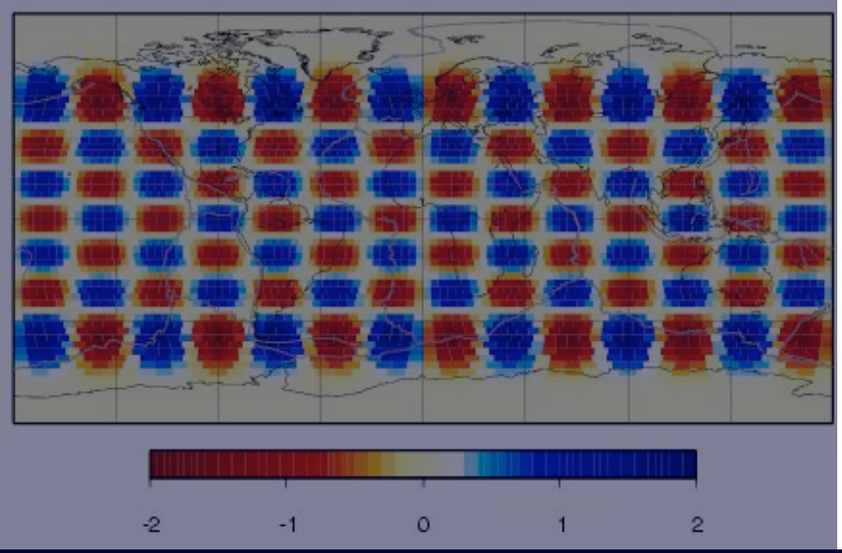

maps-2percentL13M7/L0150.jwkb.3.lsqr-0.-0.200

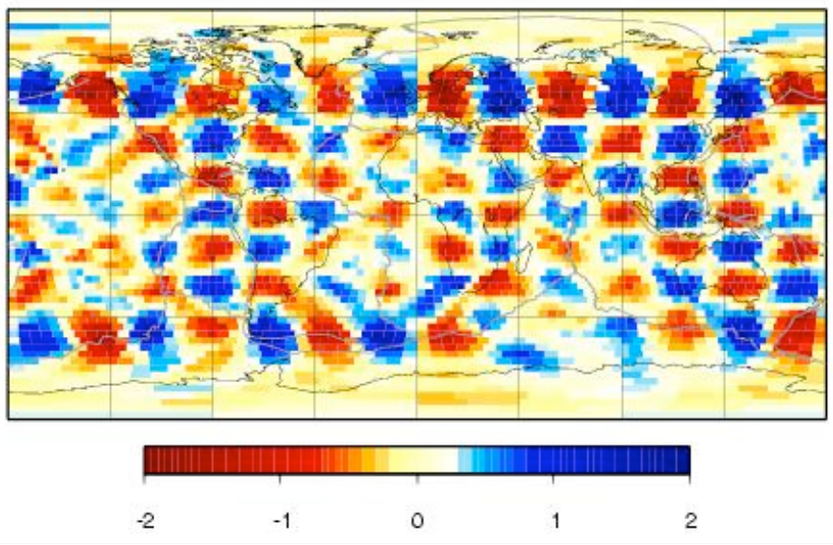

maps-2percentL13M7/L0150.born.3.lsqr-0.-0.200

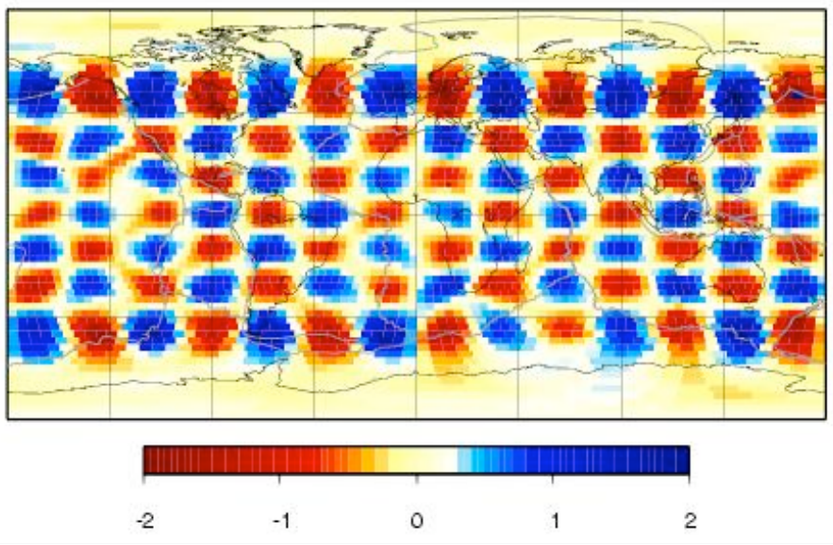

L 20 - M 10 checkerboard

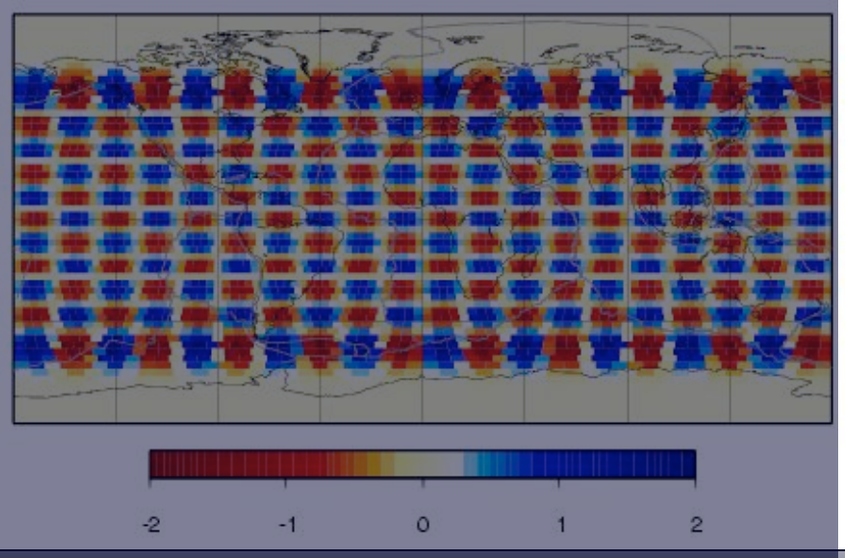

maps-2percentL20M10/L0150.jwkb.3.lsqr-0.-0.200

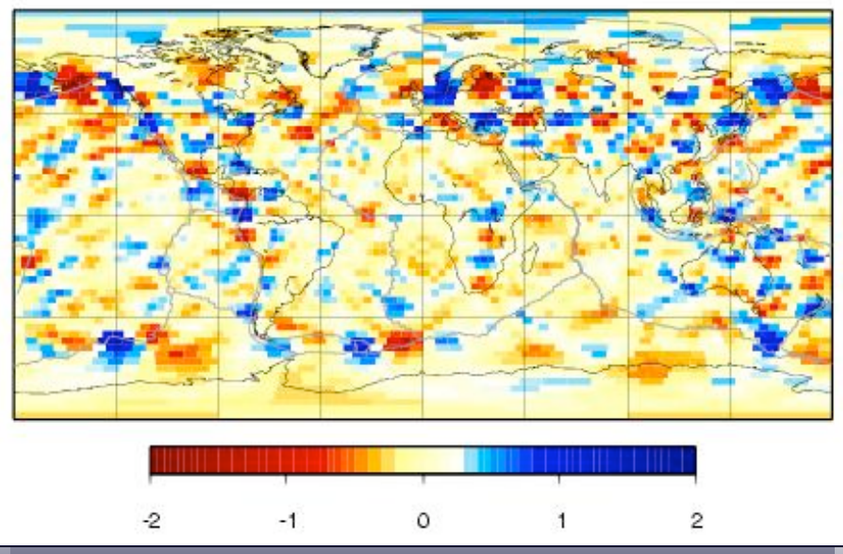

maps-2percentL20M10/L0150.born.3.lsqr-0.-0.200

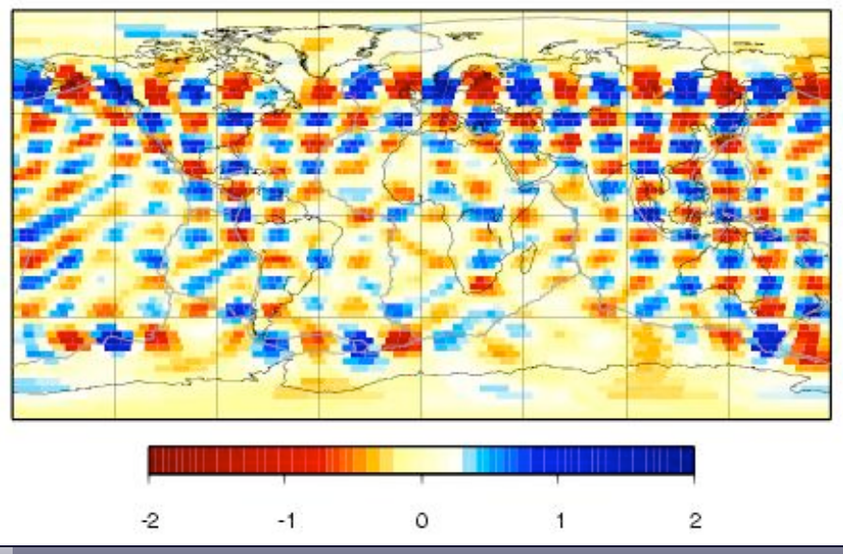

Outline

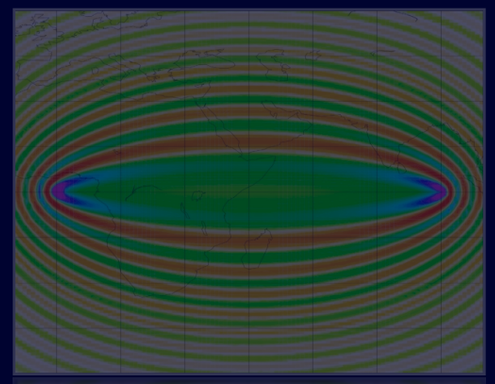

- Forward modeling:
  Membrane waves and sensitivity kernels

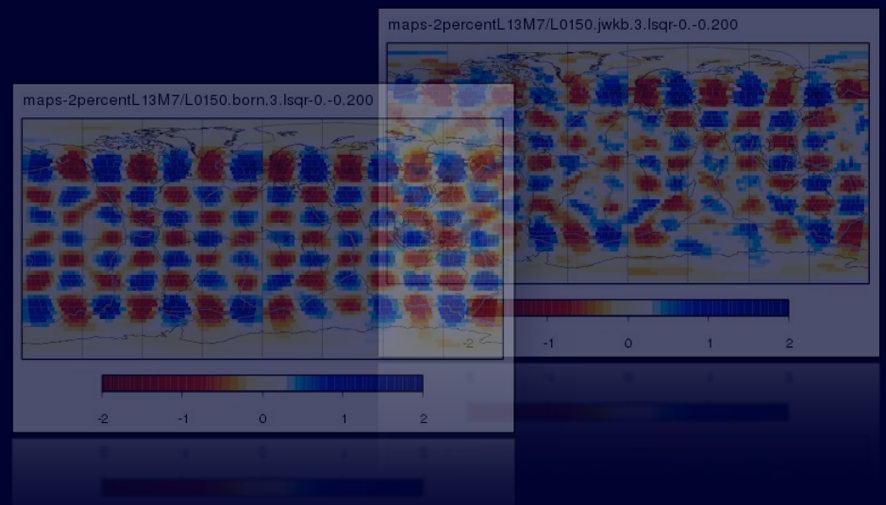

- Implications on tomography:
  Resolution benchmark

- Application to 3-D seismology:
  Mediterranean tomography

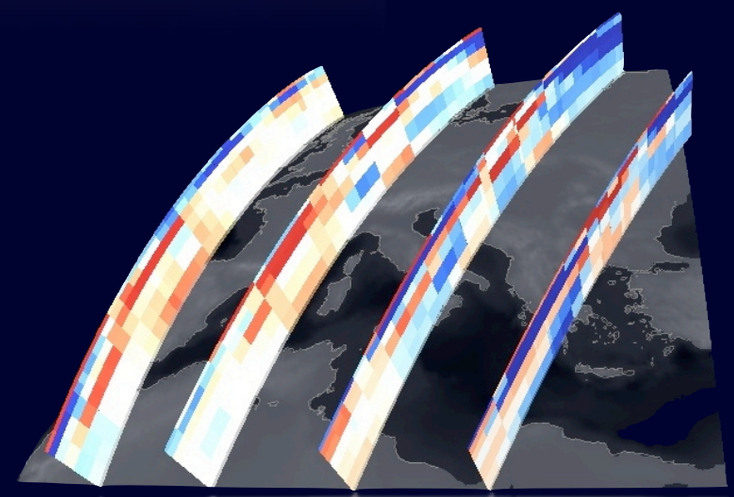

Surface wave dispersion

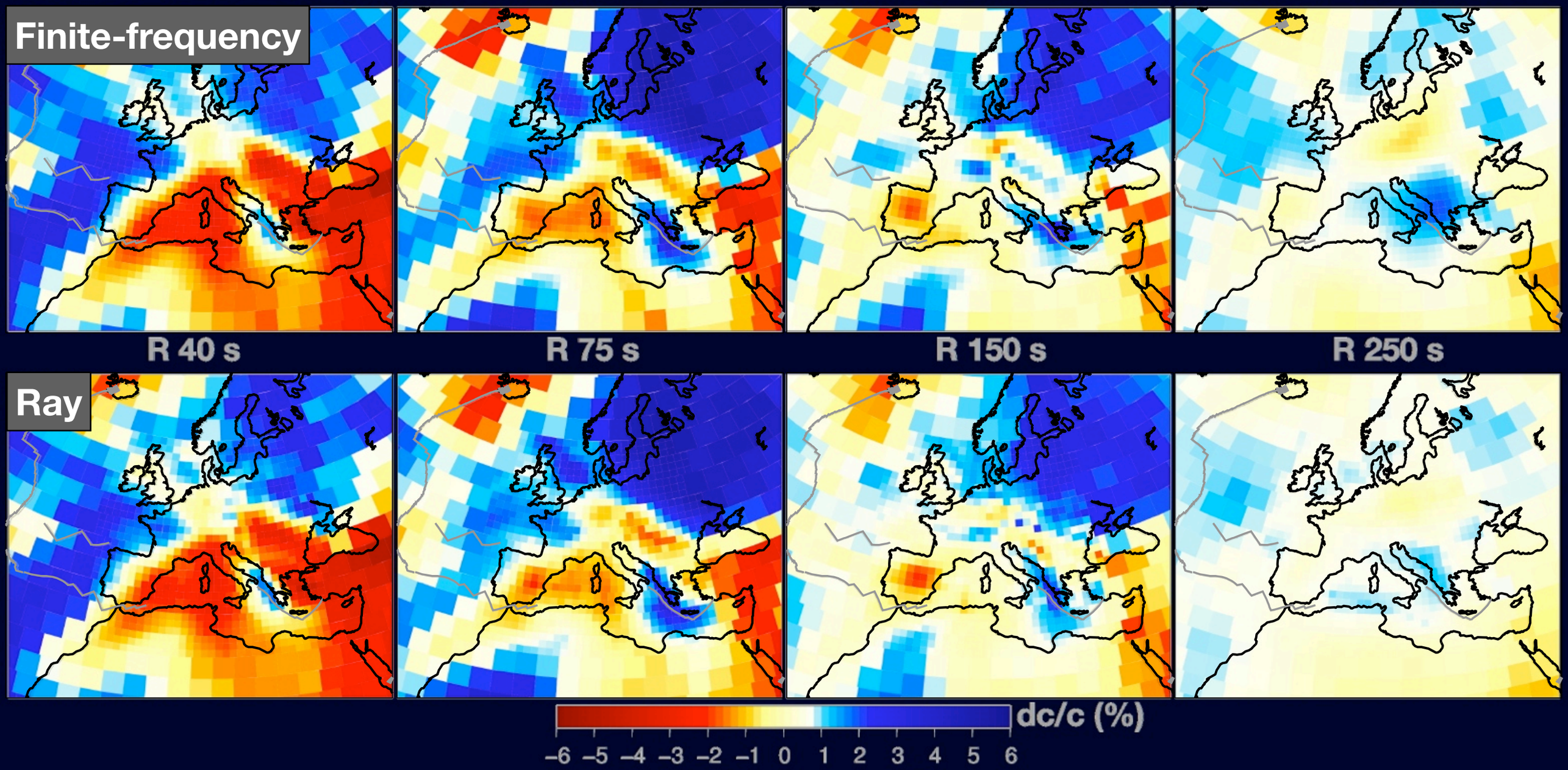

Daniel Peter | ETH Zurich

Vs profiles (Southern Italy)

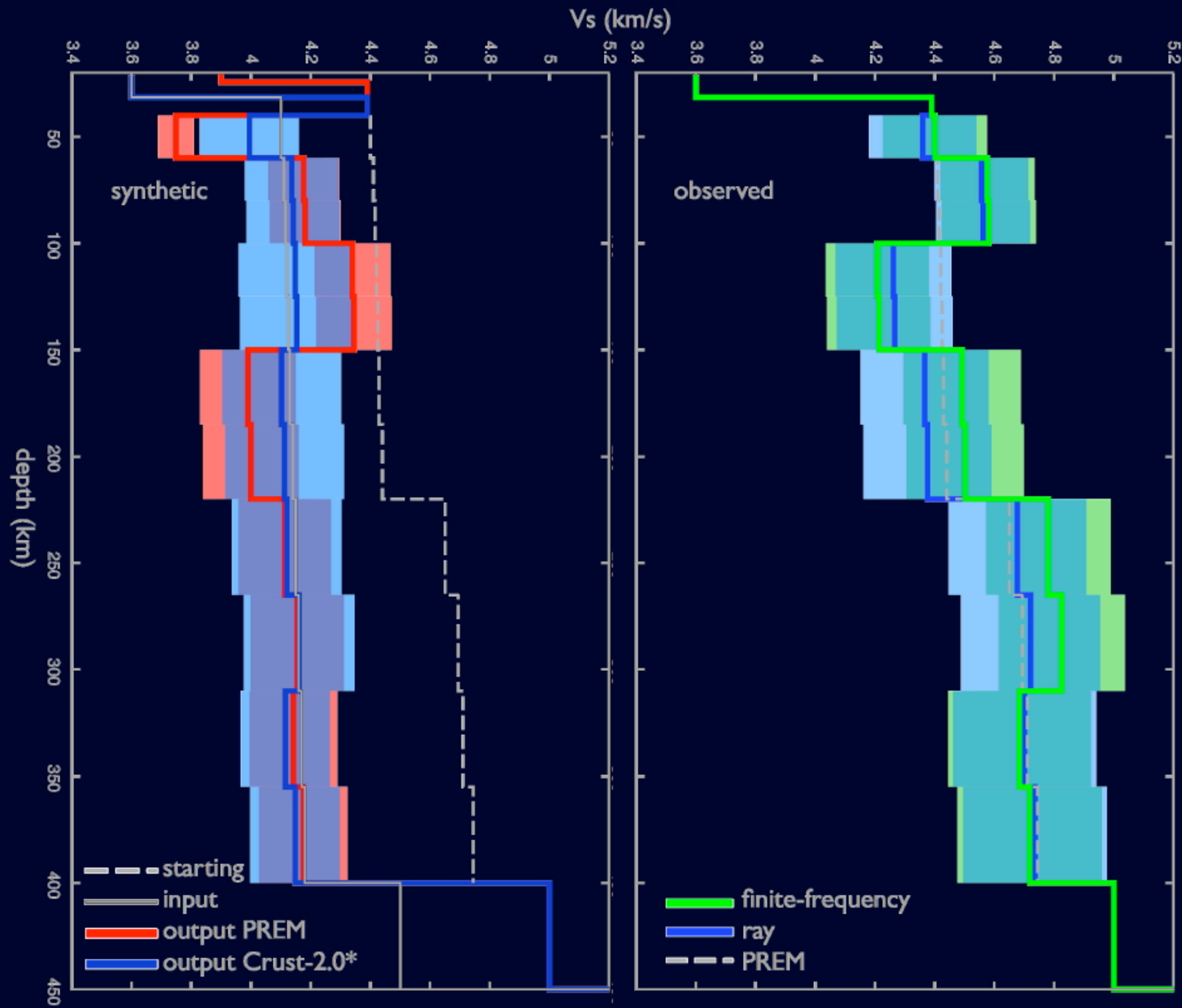

Horizontal cross-sections

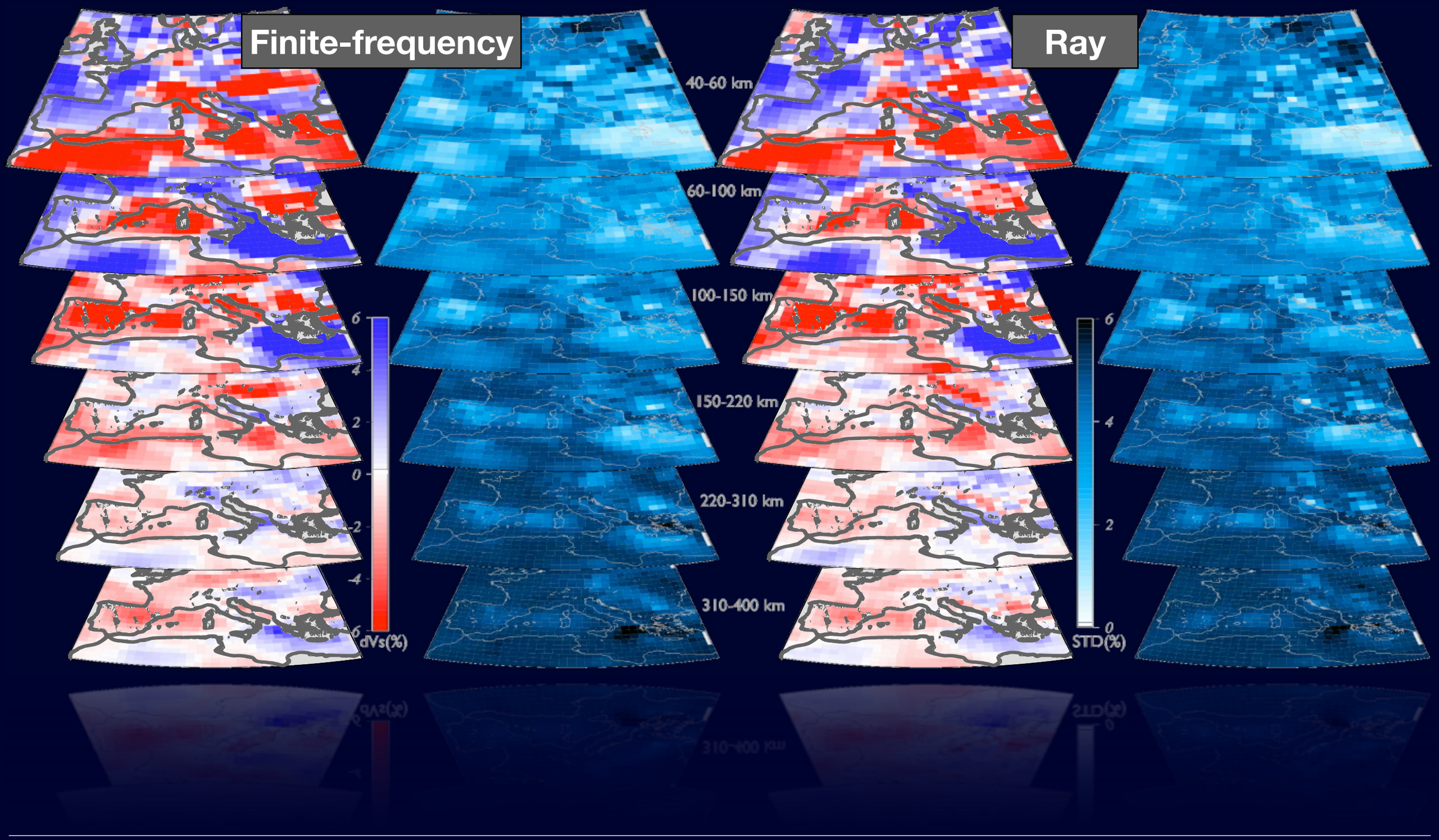

Horizontal cross-sections

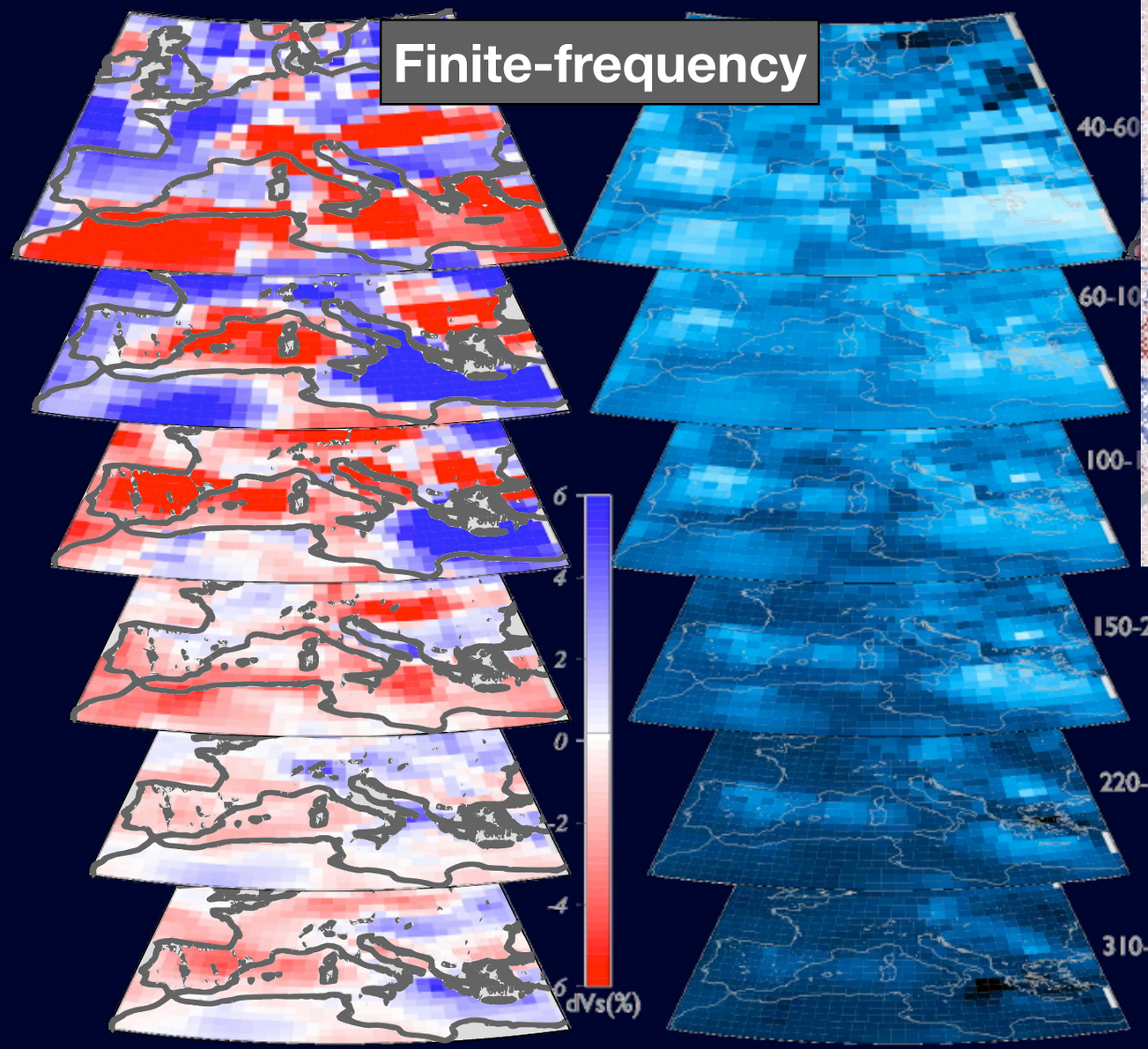

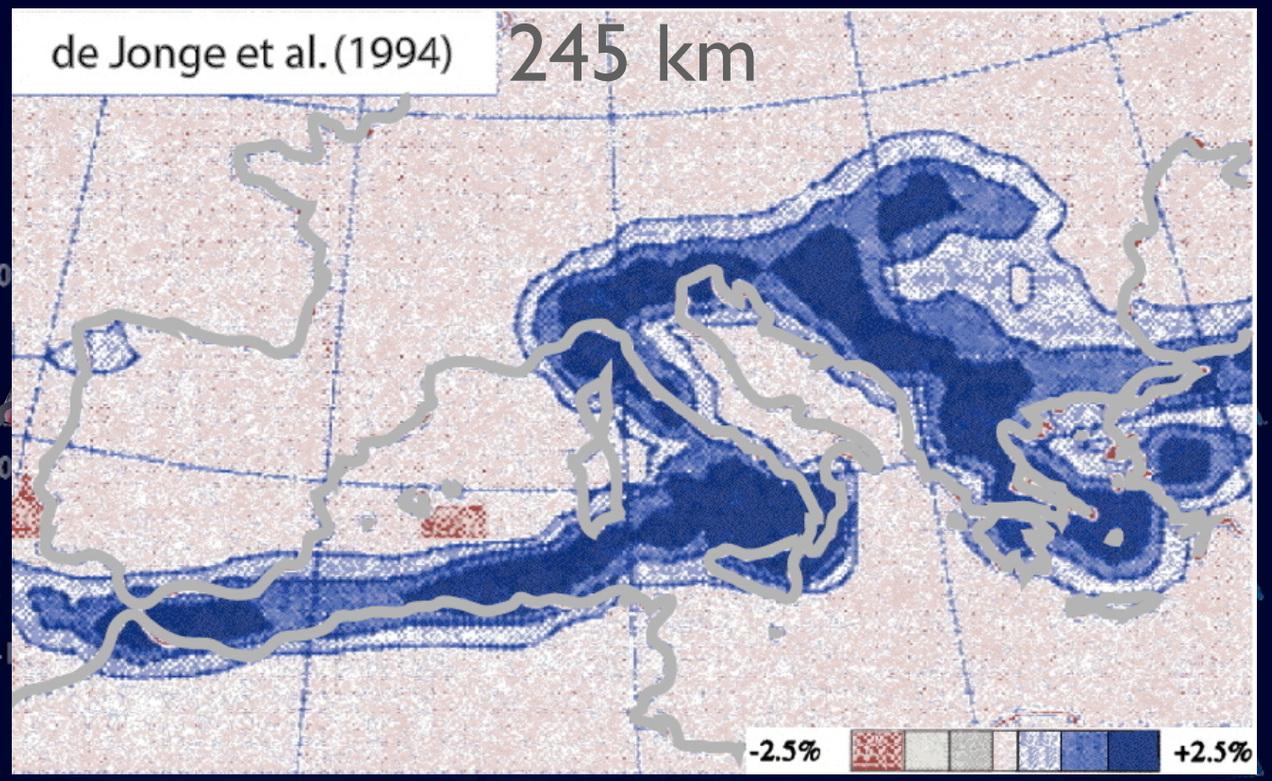

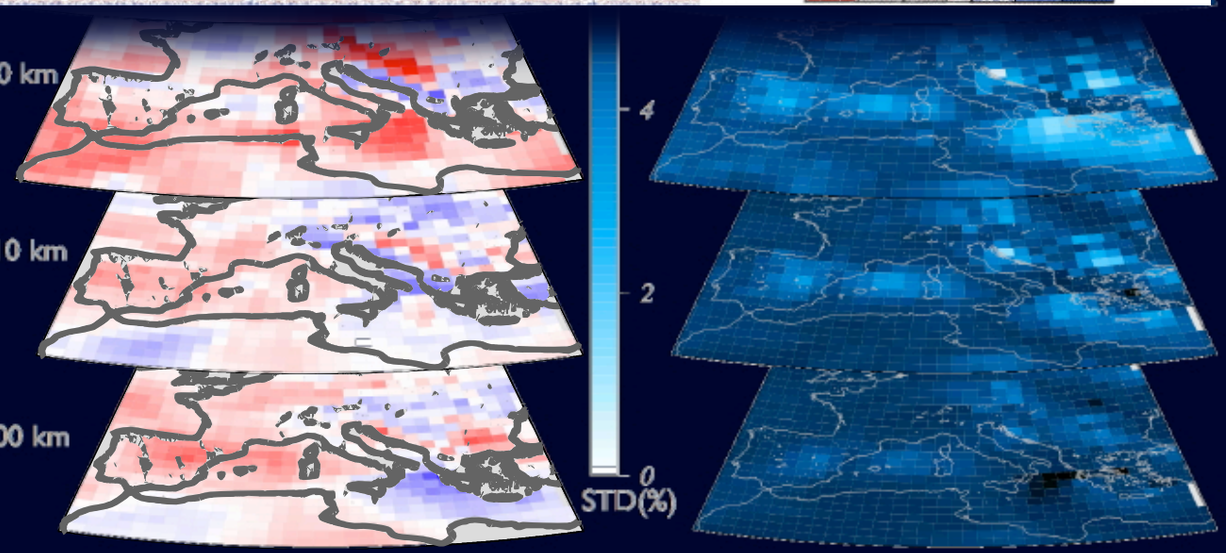

Horizontal cross-sections

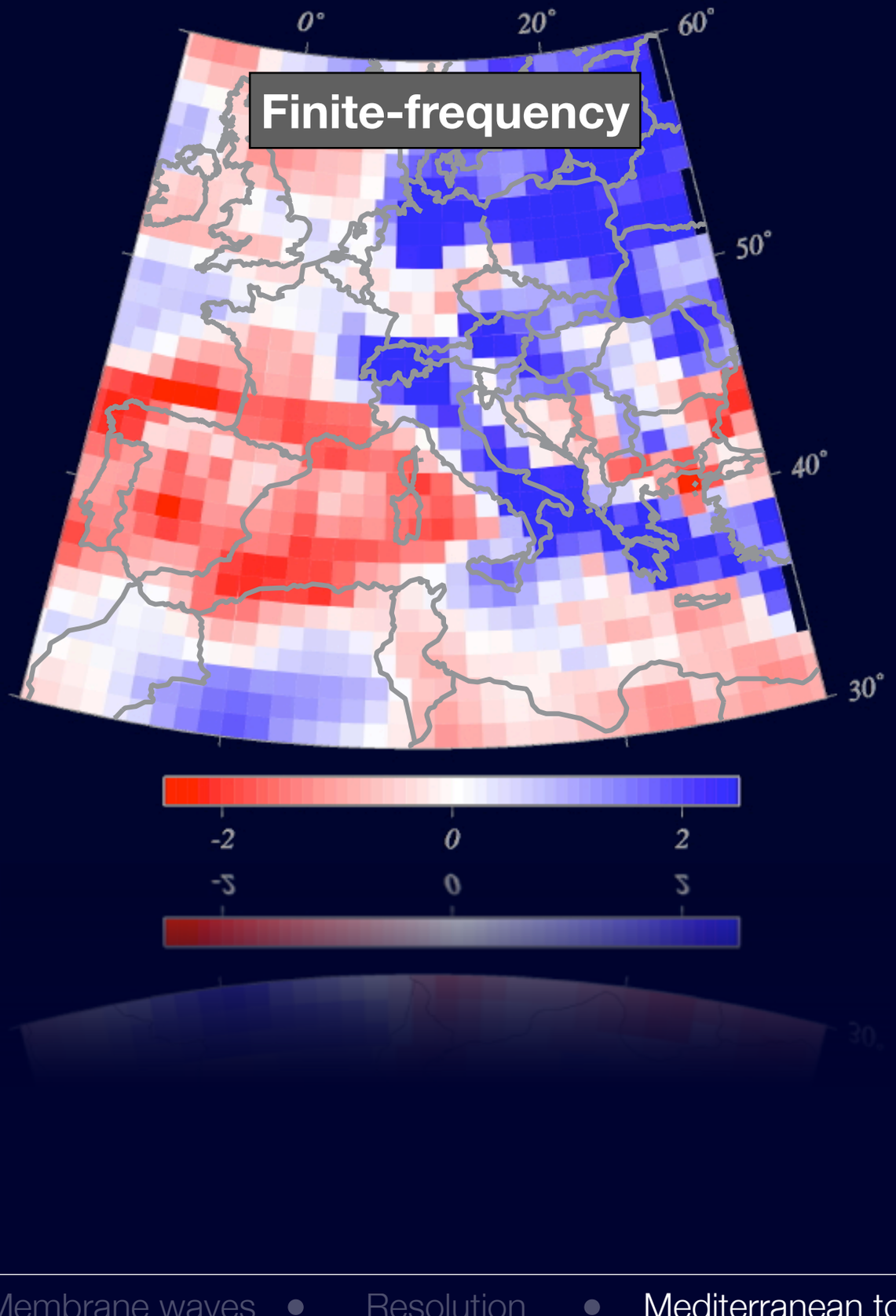

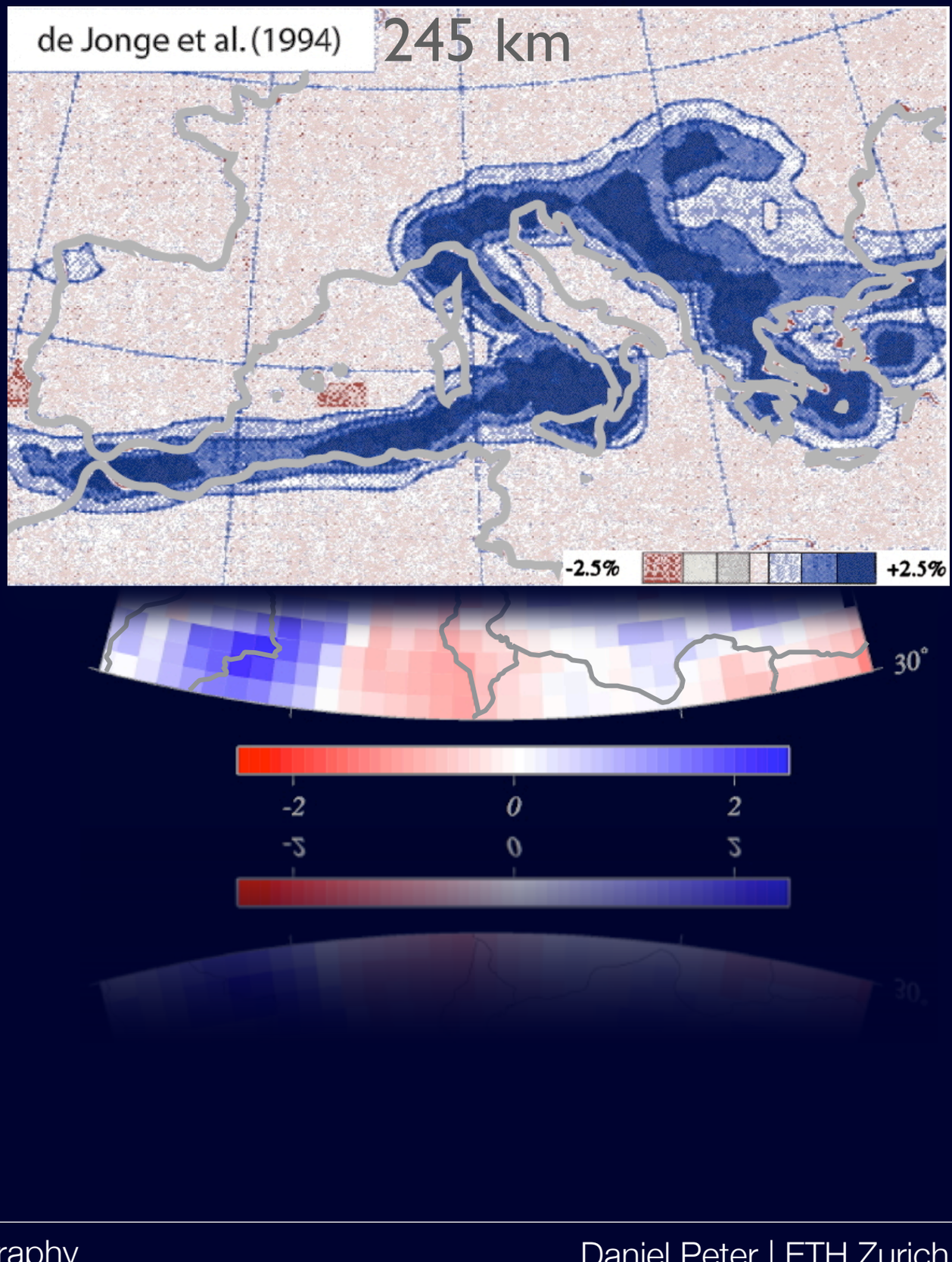

Horizontal cross-sections

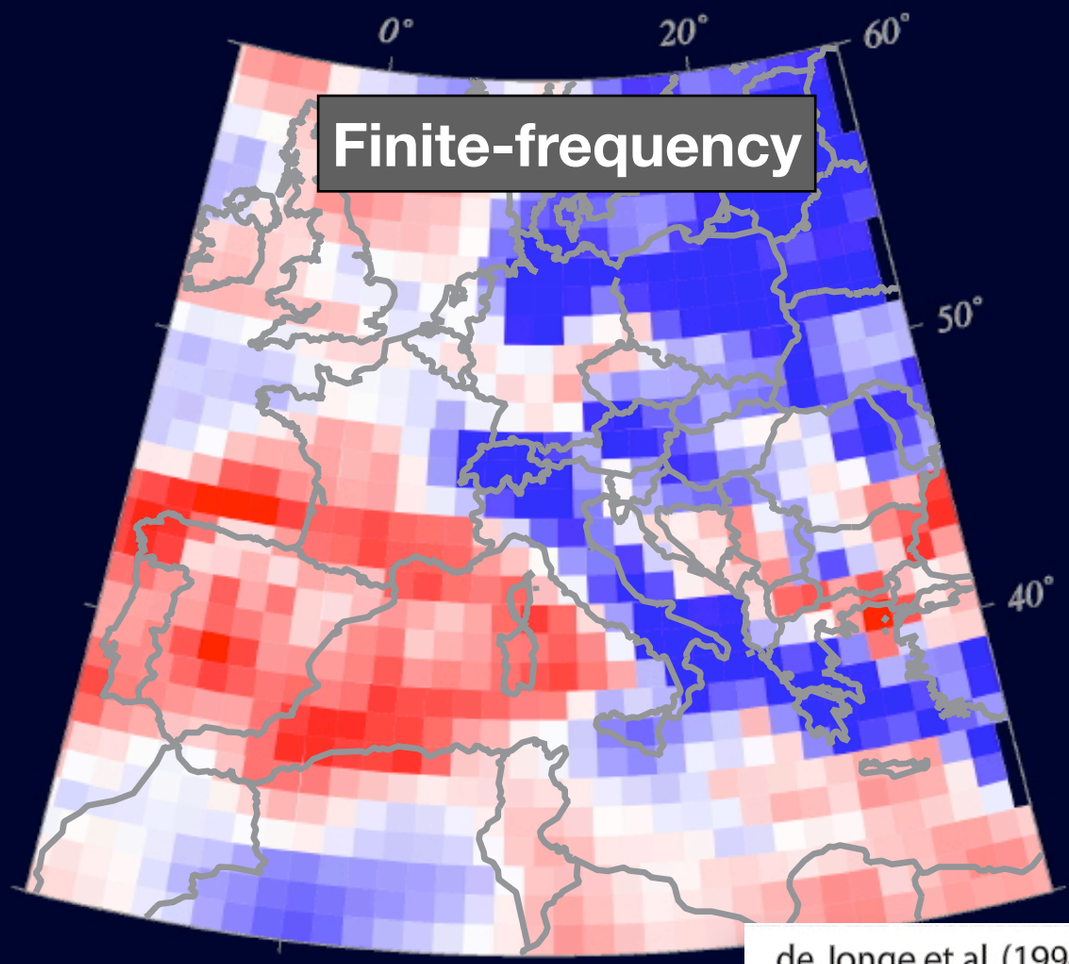

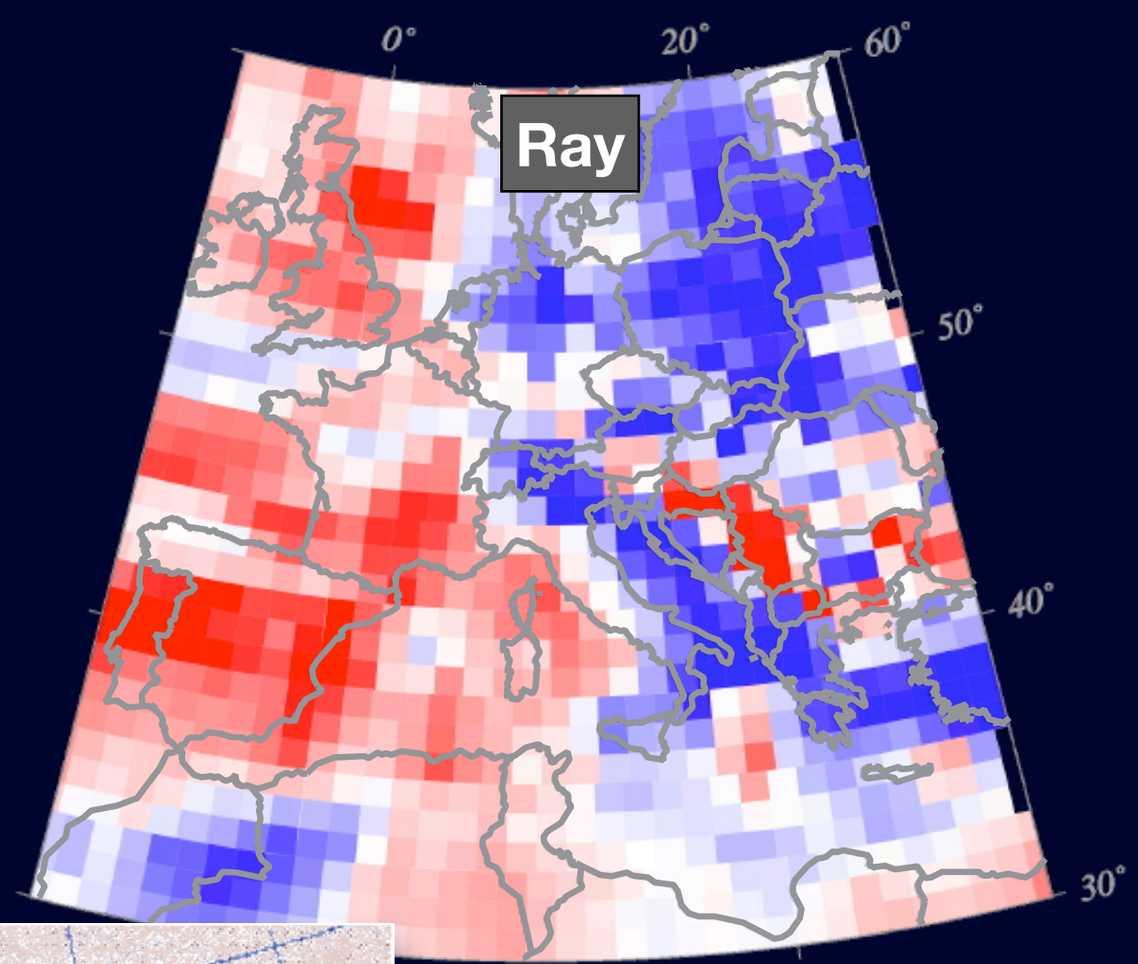

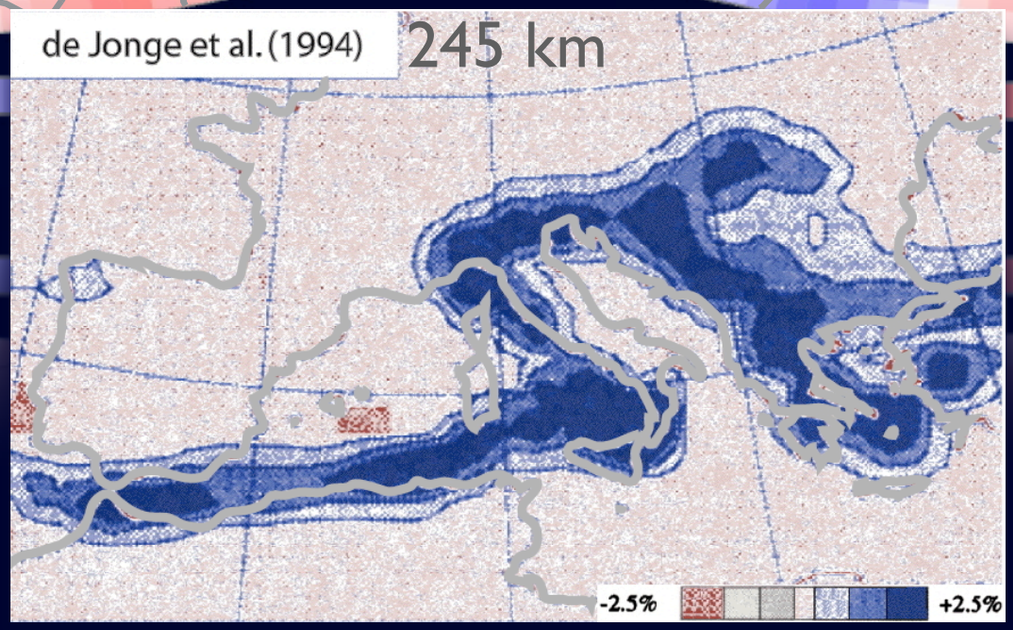

Ray tomography

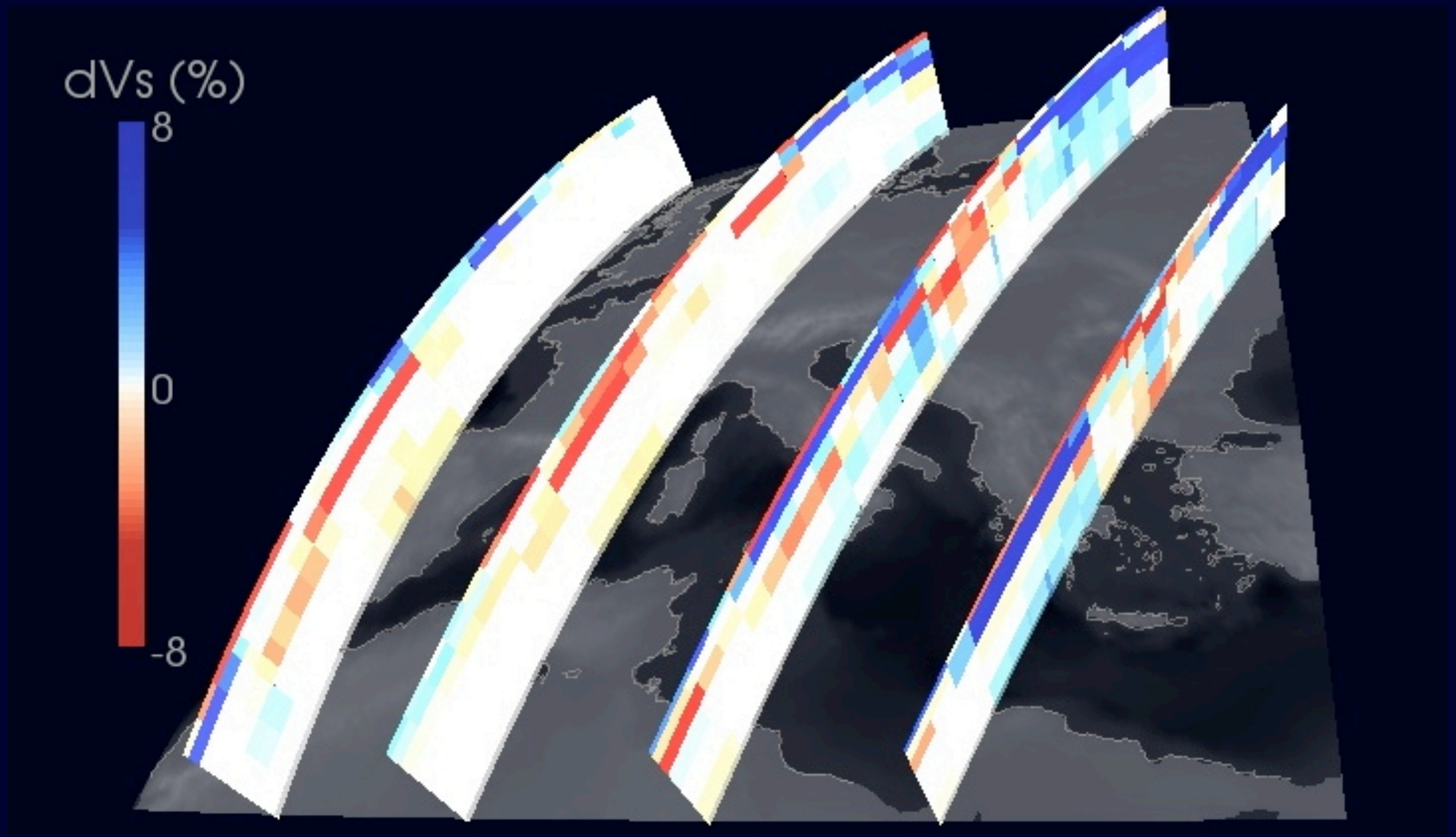

Finite-frequency tomography

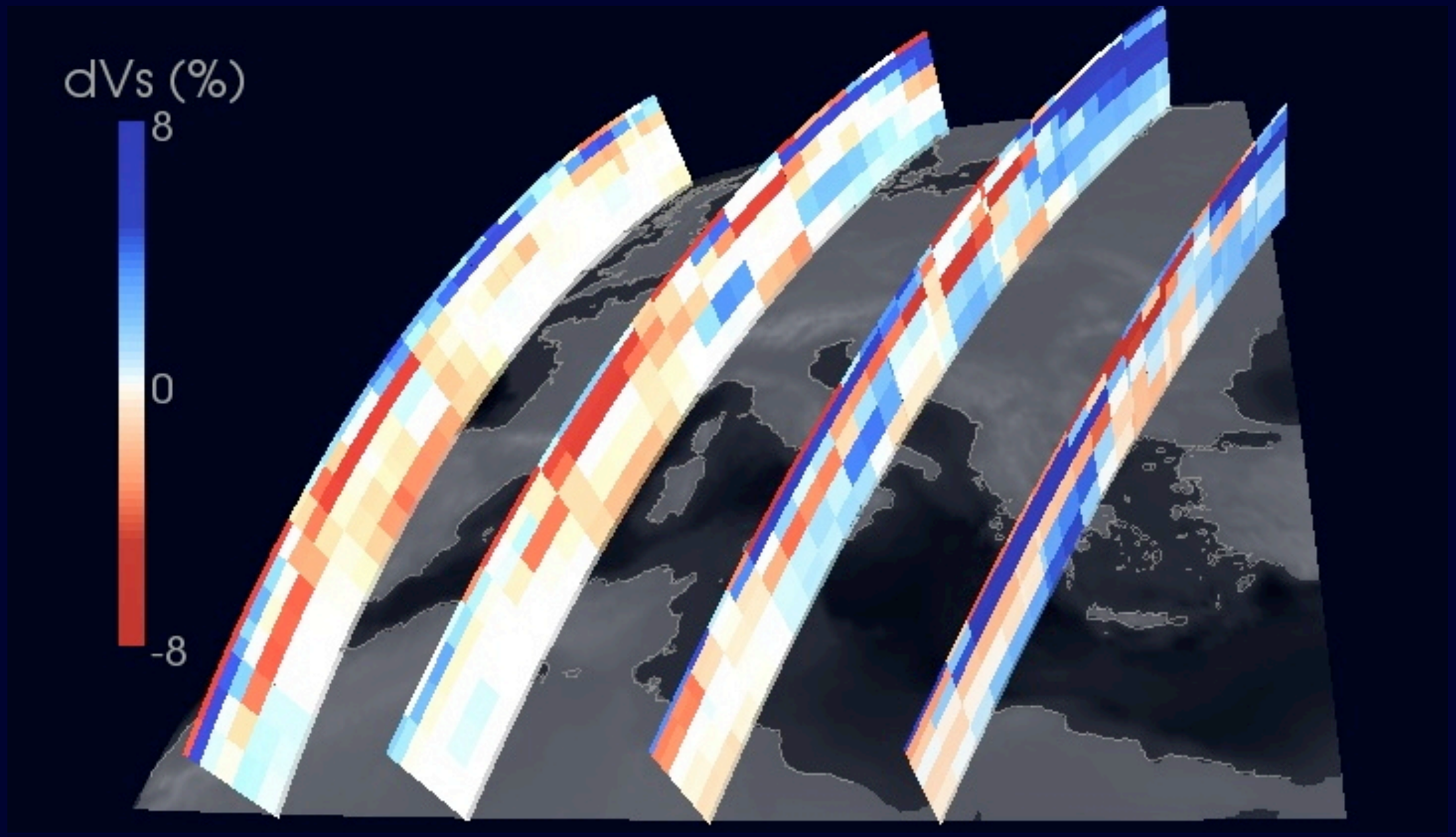

Finite-frequency tomography

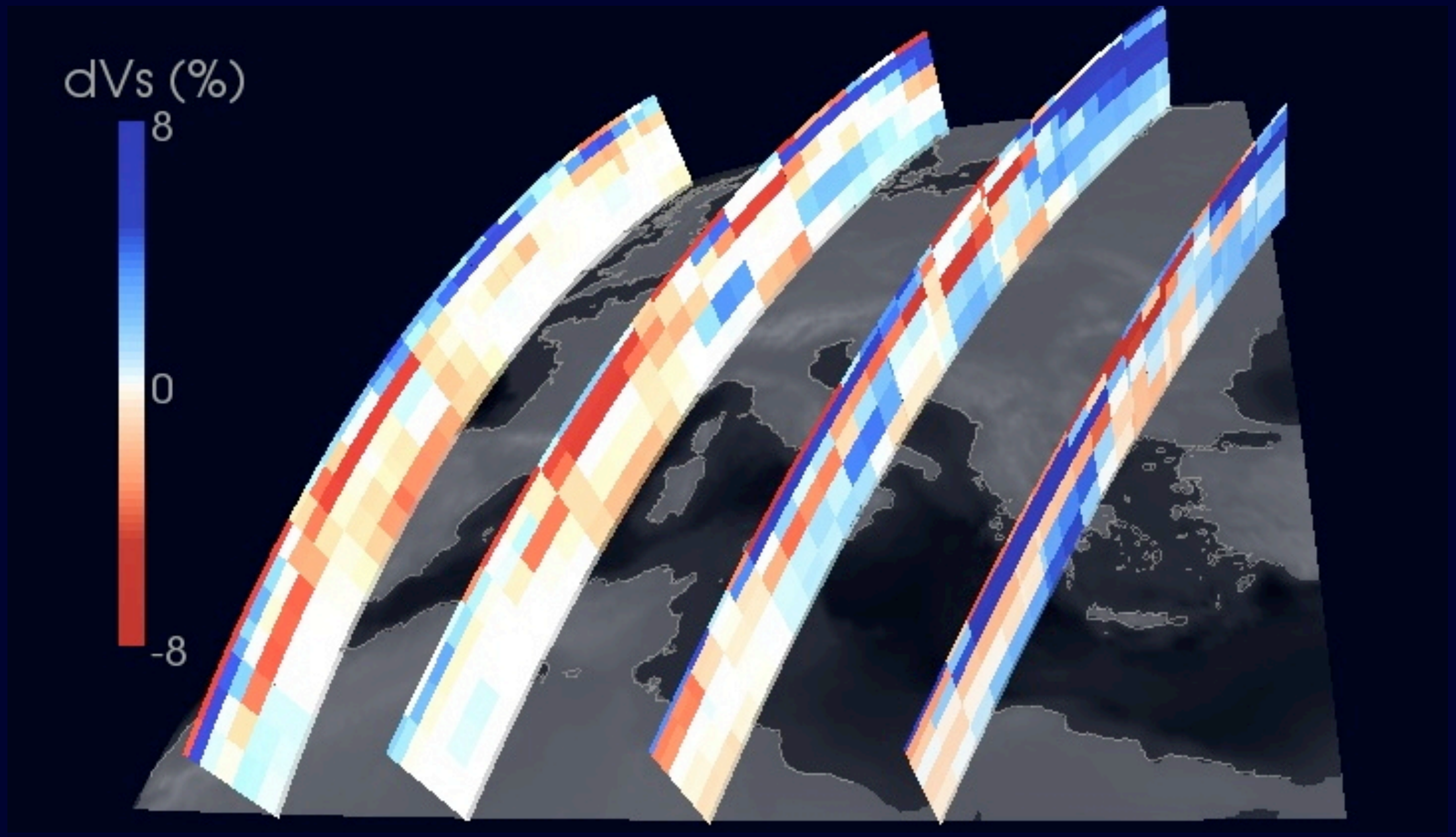

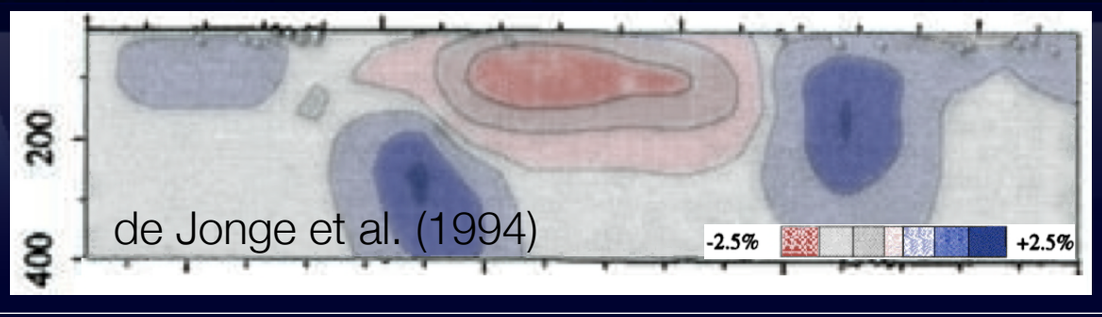

Finite-frequency tomography

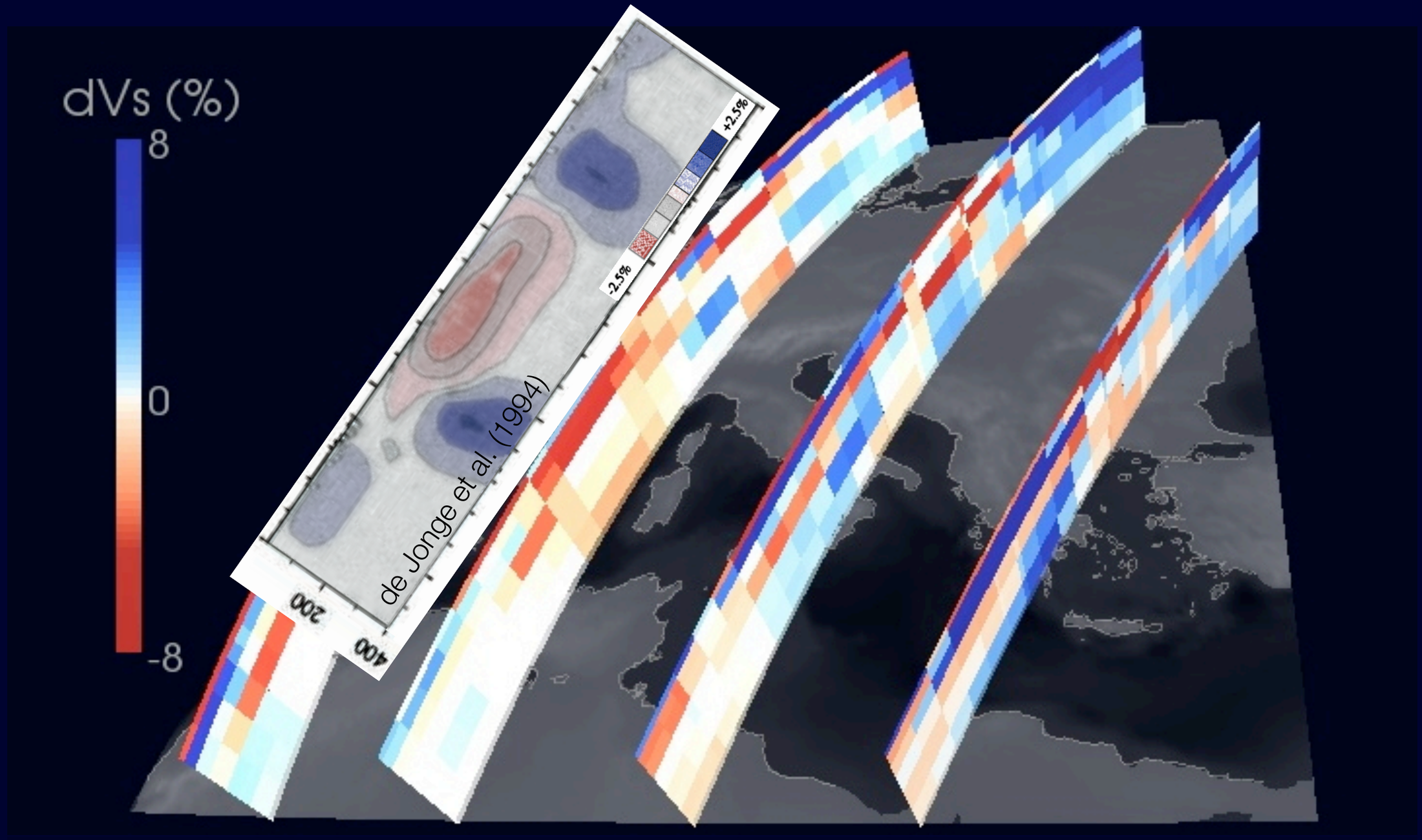

Conclusions

- Membrane waves simplify numerical simulations of surface waves

- Adjoint methods accelerate the computation of numerical sensitivity kernels

- Finite-frequency theory leads to higher image resolution

Outlook

- Membrane modeling
  - Mesh optimization

- Sensitivity kernels
  - Wavelet compression

- Adjoint methods
  - 3-D sensitivity kernels

Mesh optimization

2-D wave equation

$$\left[\frac{1}{c^2(\mathbf{x})}\partial_t^2 - \nabla_1^2\right] s(\mathbf{x},\mathbf{t}) = \mathbf{f}(\mathbf{x_s},\mathbf{t})$$

solved by a finite-differences approximation (Heikes & Randall 1994)

$$\nabla_1^2 s\Big|_{T_0} \approx \frac{1}{A_0}\sum_{i=1}^{N}\frac{l_i}{L_i}\left(s_i - s_0\right)$$

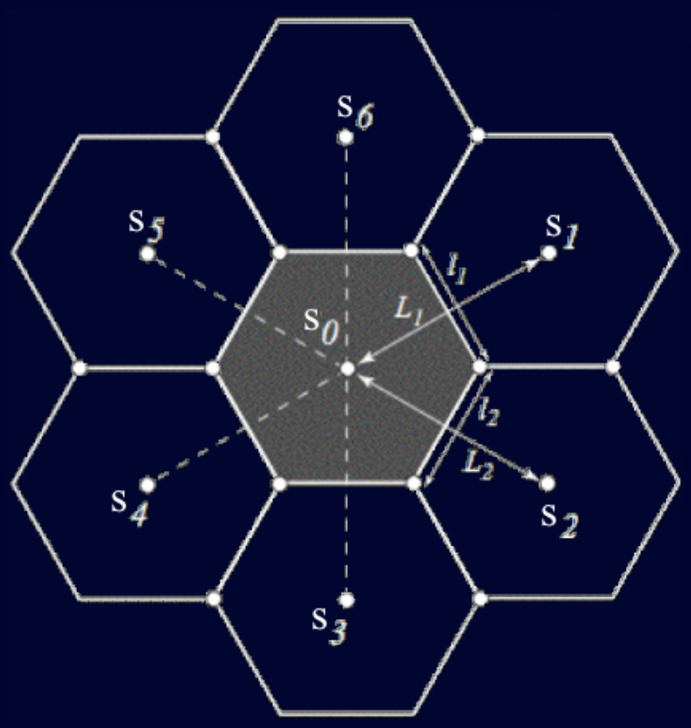

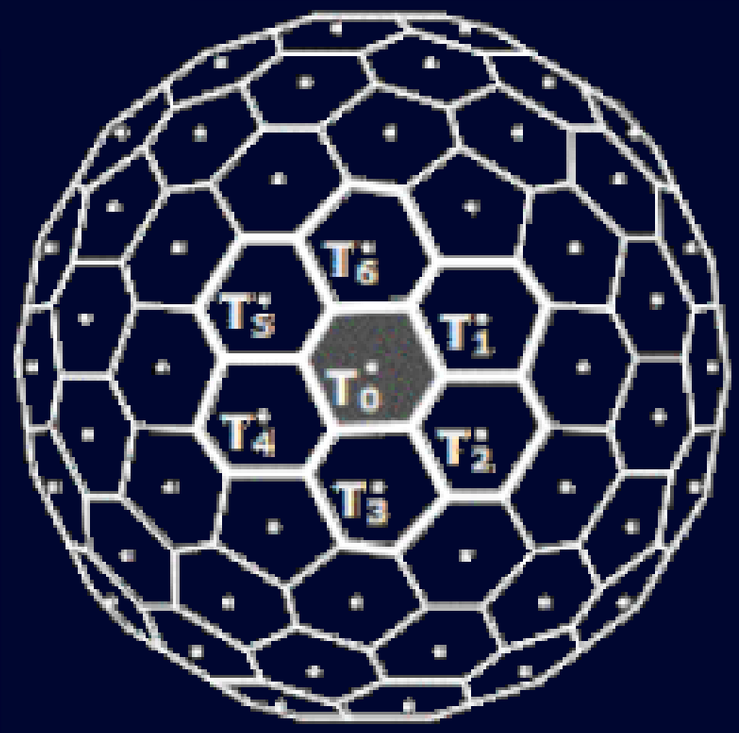

Tape (2003)

Mesh optimization

cell distortion by
mesh refinement

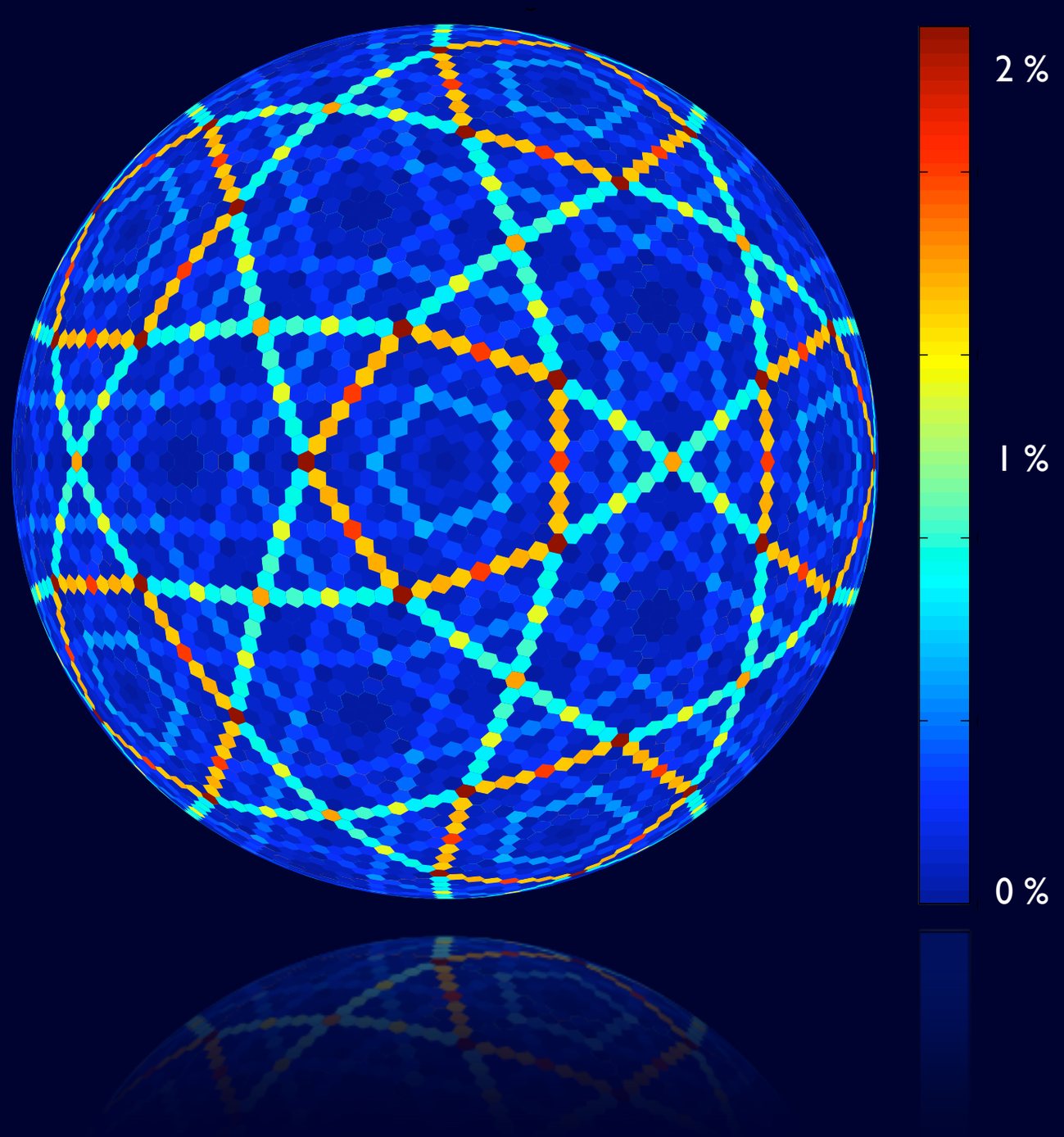

relax

Mesh optimization

mesh relaxation

by electrostatic forces

$$F_i = \frac{1}{4\pi\epsilon} \sum_{j \neq i}^{N} \frac{q_i q_j}{\|\mathbf{r_i} - \mathbf{r_j}\|^2}$$

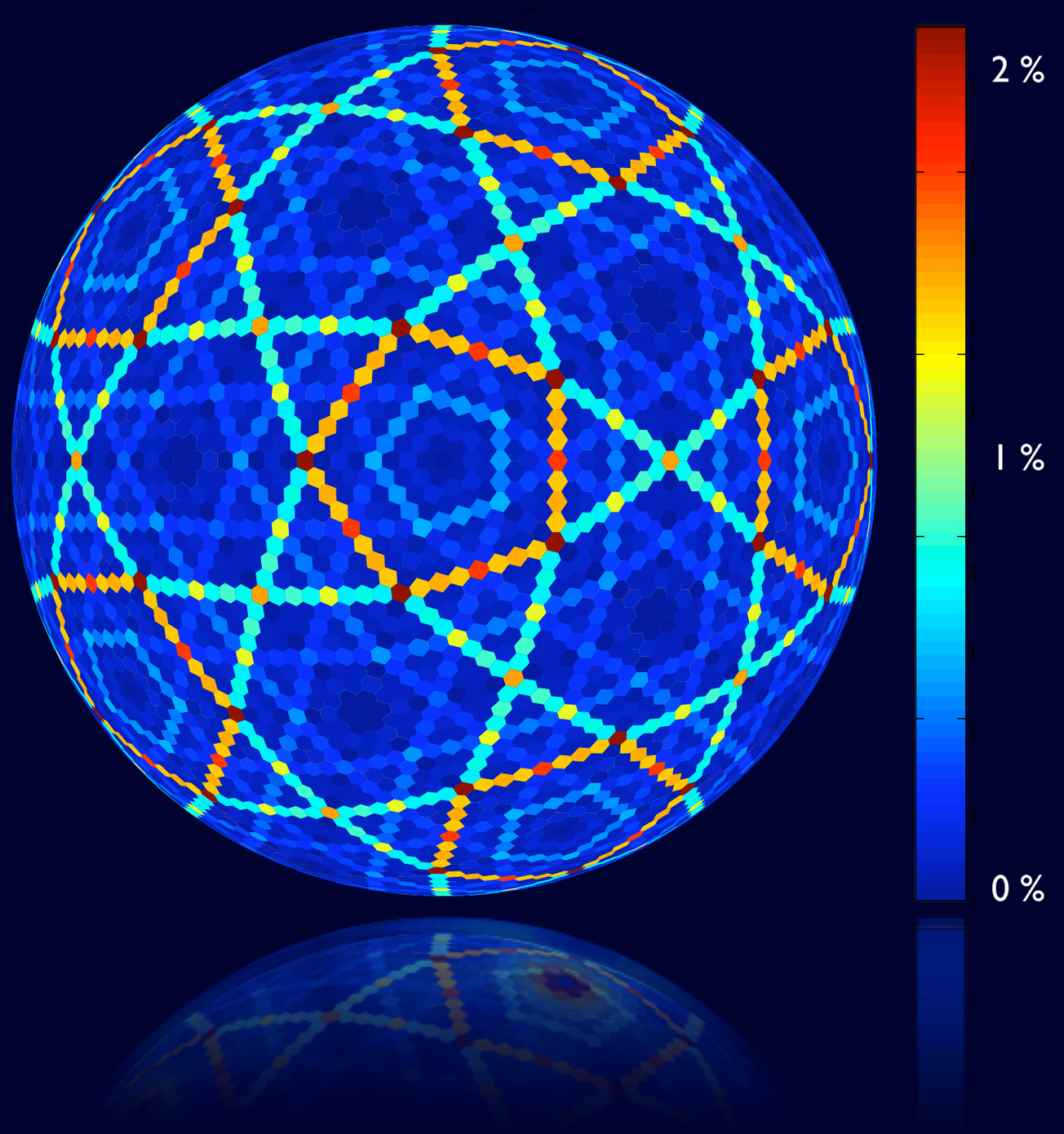

Mesh optimization

mesh relaxation

by electrostatic forces

$$F_i = \frac{1}{4\pi\epsilon} \sum_{j \neq i}^{N} \frac{q_i q_j}{\|\mathbf{r_i} - \mathbf{r_j}\|^2}$$

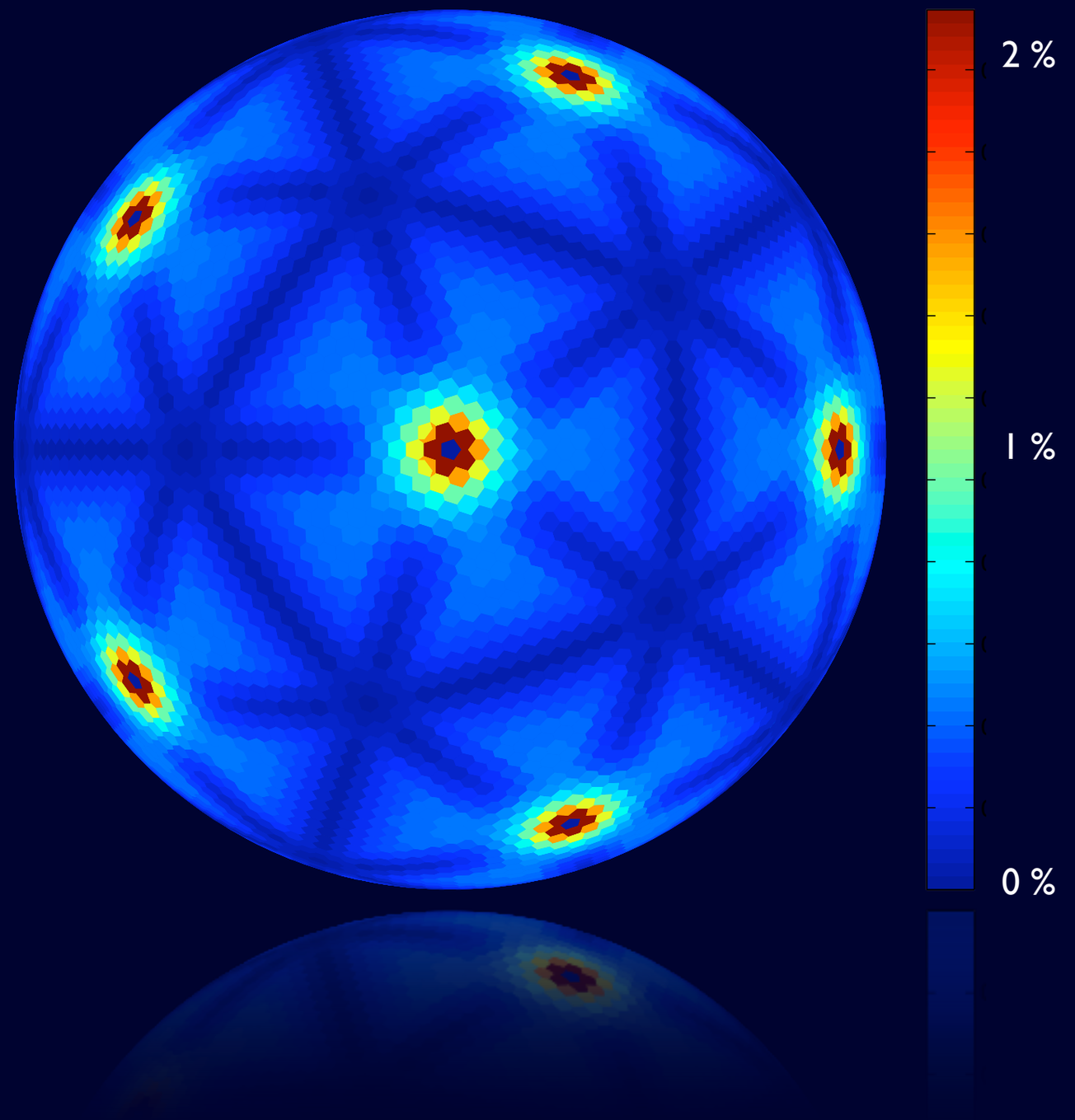

Outlook

- Membrane modeling
  - Mesh optimization

- Sensitivity kernels
  - Wavelet compression

- Adjoint methods
  - 3-D sensitivity kernels

Wavelet compression

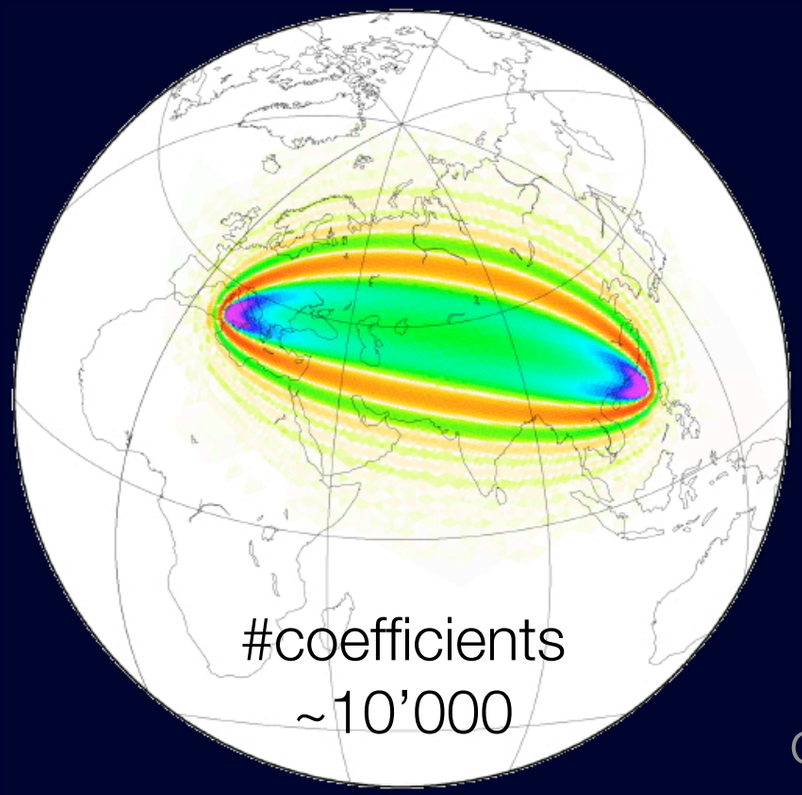

#coefficients
~10’000

wavelet
coefficients:

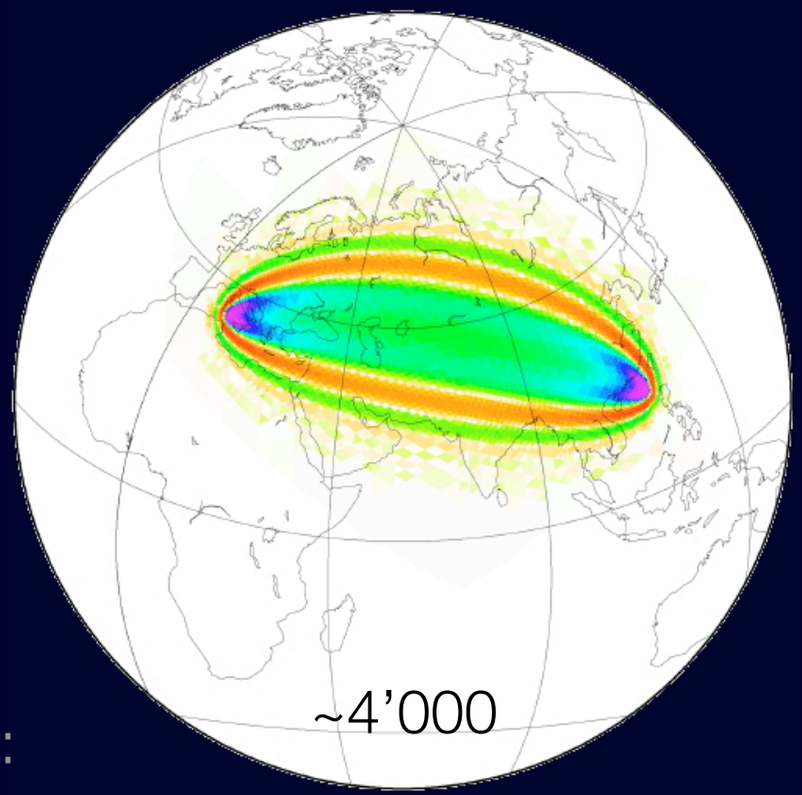

~4’000

wavelet basis

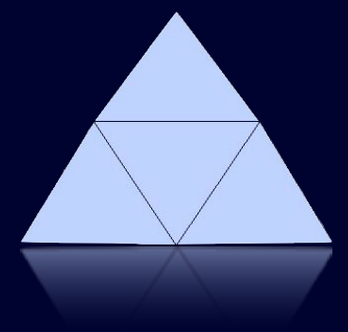

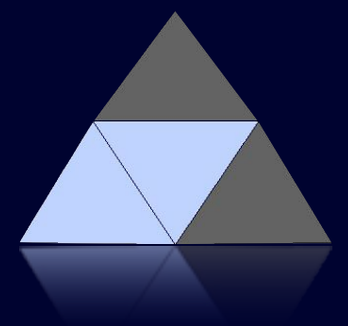

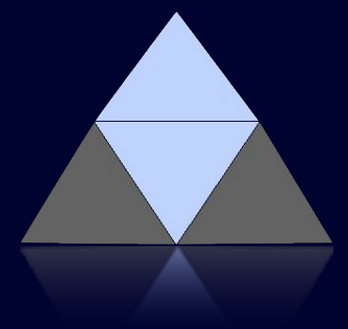

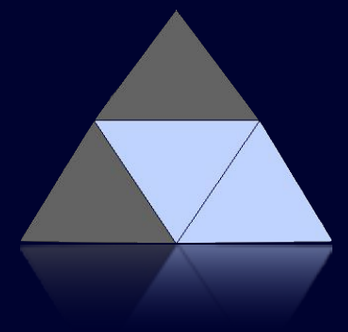

~250’000 total

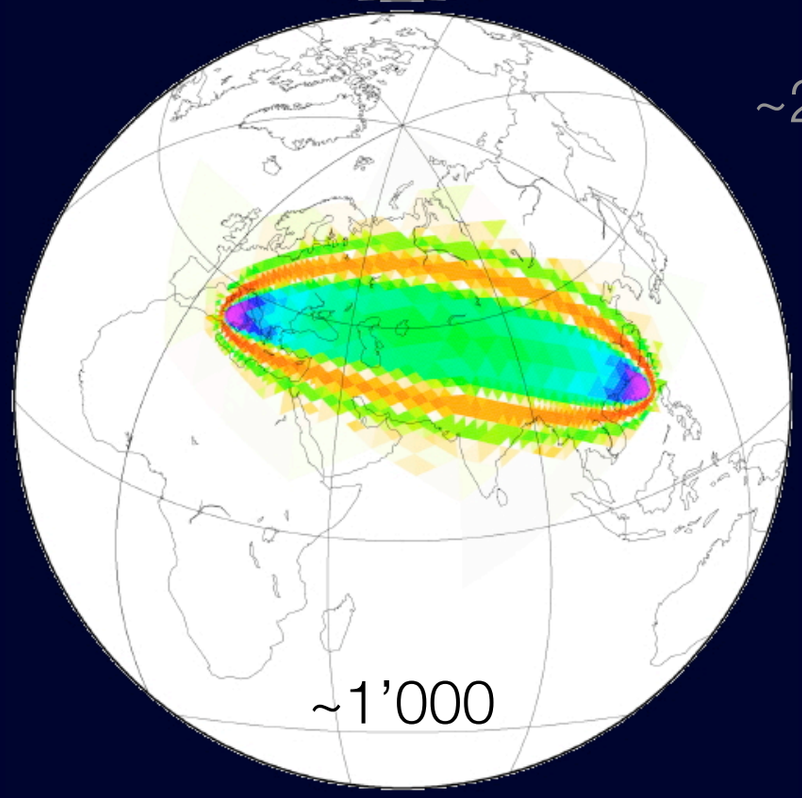

~1’000

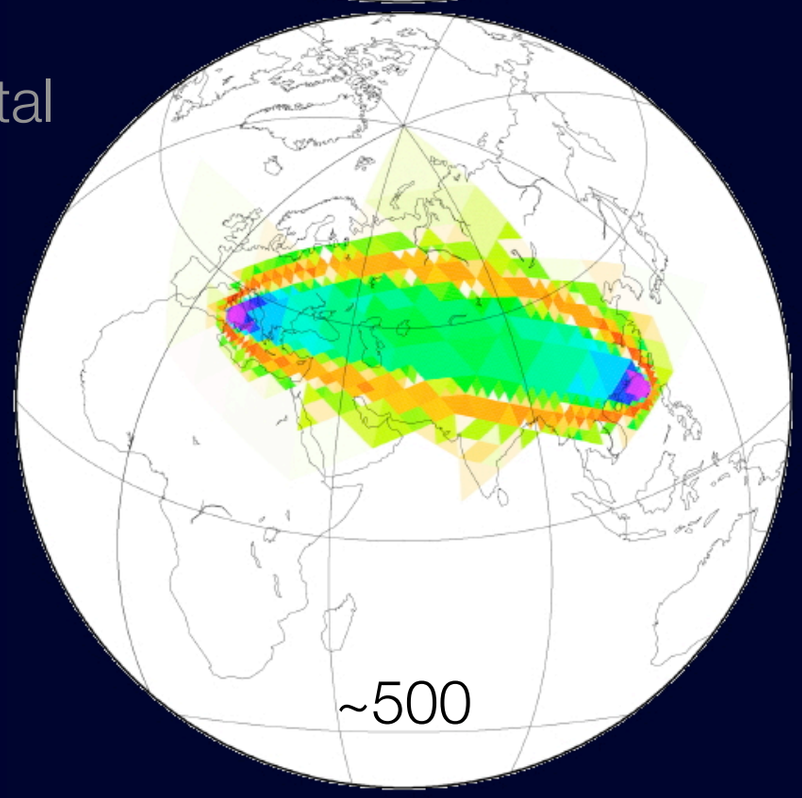

~500

Outlook

- Membrane modeling
  - Mesh optimization
- Sensitivity kernels
  - Wavelet compression
- Adjoint methods
  - 3-D sensitivity kernels

3-D Surface wave kernel

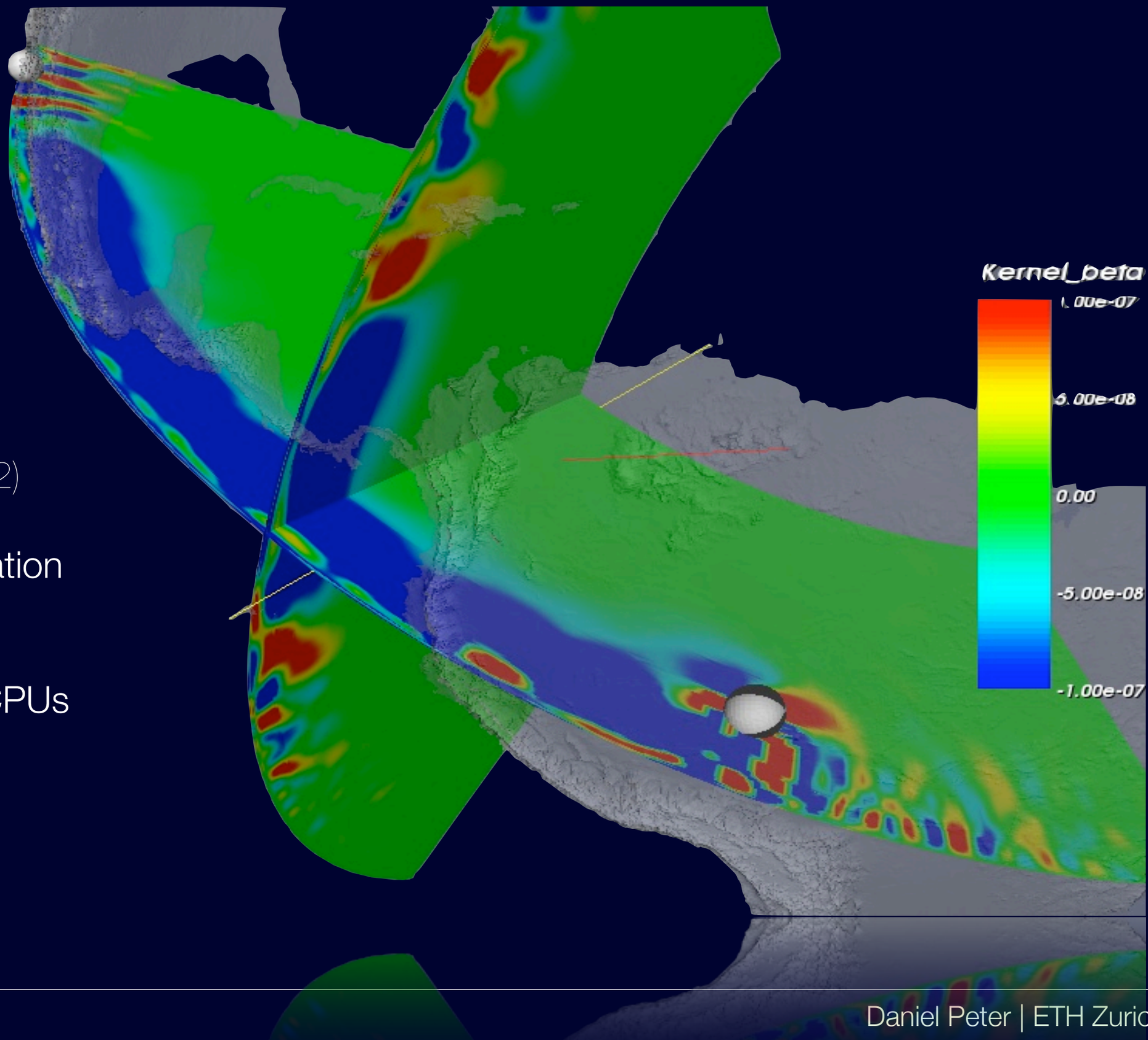

SPECFEM3D
(Komatitsch et al. 2002)

single kernel calculation
10^6 GFlop

~7 hours on 24 CPUs
(40 GFlop/s)

3-D Surface wave kernel

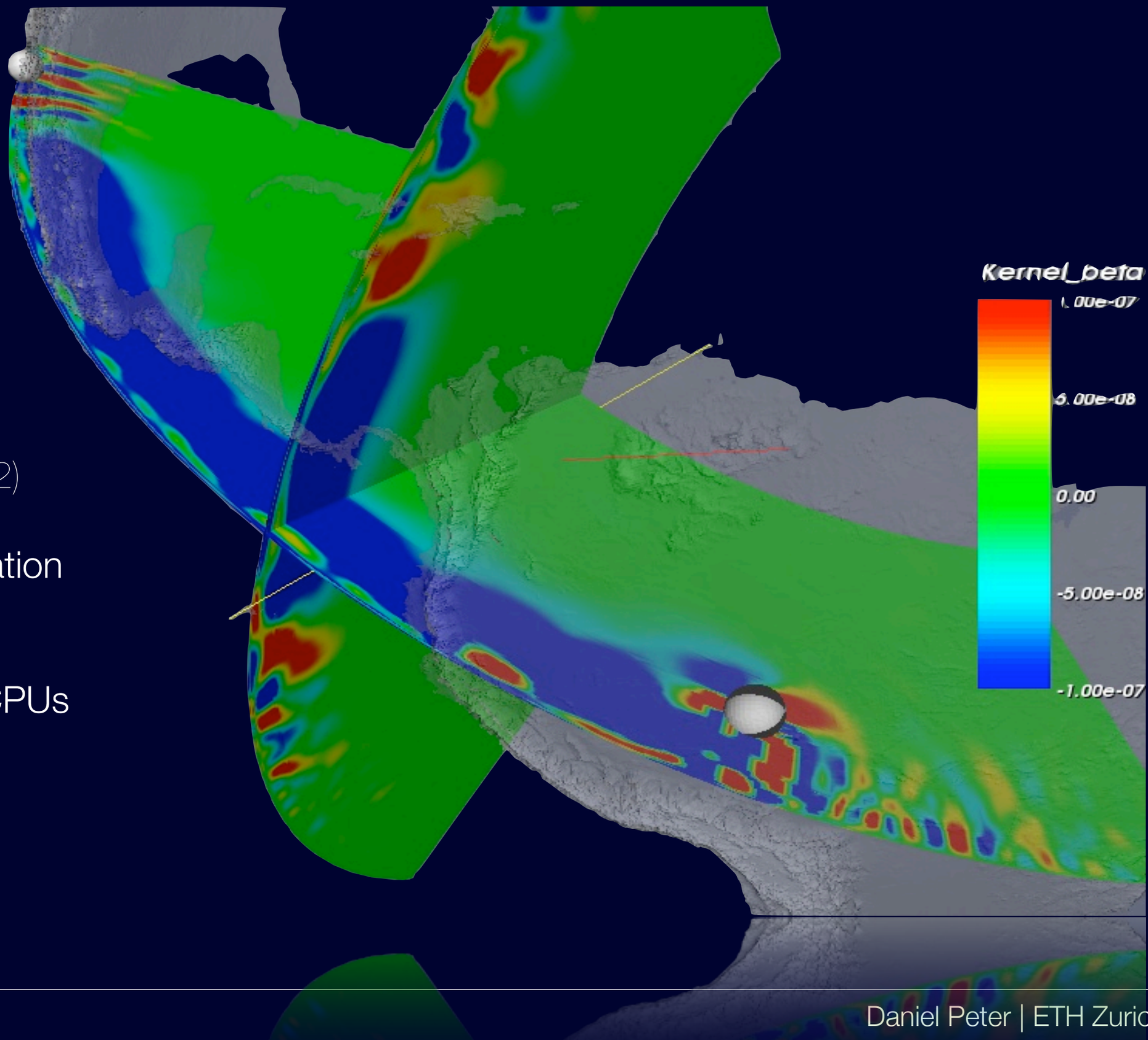

SPECFEM3D
(Komatitsch et al. 2002)

single kernel calculation
10^6 GFlop

~7 hours on 24 CPUs
(40 GFlop/s)

Acknowledgements

Data
Bill Fry, Lapo Boschi, Göran Ekström

Tomographic models
Jeannot Trampert, John Woodhouse

Tomographic imaging
Lapo Boschi, Frédéric Deschamps

Membrane wave modeling
Carl Tape, John Woodhouse

Ray modeling
John Woodhouse, Lapo Boschi

Adjoint method

Adjoint source for cross-correlation measurements (Tromp et al. 2005)

$$\bar{f}^{\dagger}(\mathbf{x},t) = \frac{1}{N}\partial_t s(\mathbf{x_r}, T-t)\delta(\mathbf{x}-\mathbf{x_r})$$

Adjoint method

Adjoint source for cross-correlation measurements (Tromp et al. 2005)

$$\bar{f}^\dagger(\mathbf{x},t) = \frac{1}{N}\partial_t s(\mathbf{x_r}, T-t)\delta(\mathbf{x}-\mathbf{x_r})$$

Time-reversal, adjoint simulation

$$\bar{s}^\dagger(\mathbf{x}', \mathbf{x_r}, T-t) = \frac{1}{N}\int_0^{T-t} G(\mathbf{x}', \mathbf{x_r}, T-t-t')\partial_t s(\mathbf{x_r}, T-t')dt'$$

Adjoint method

Adjoint source for cross-correlation measurements (Tromp et al. 2005)

$$\bar{f}^\dagger(\mathbf{x},t) = \frac{1}{N}\partial_t s(\mathbf{x_r}, T-t)\delta(\mathbf{x}-\mathbf{x_r})$$

Time-reversal, adjoint simulation

$$\bar{s}^\dagger(\mathbf{x}', \mathbf{x_r}, T-t) = \frac{1}{N}\int_0^{T-t} G(\mathbf{x}', \mathbf{x_r}, T-t-t')\partial_t s(\mathbf{x_r}, T-t')dt'$$

Phase-velocity sensitivity kernel

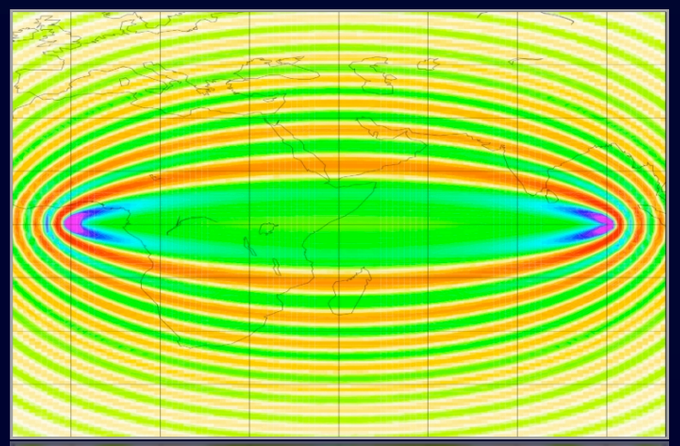

$$K(\mathbf{x}, \mathbf{x_r}) = -\frac{1}{T_0}\int_0^T \frac{2}{c_0^2(\mathbf{x})}\bar{s}^\dagger(\mathbf{x}, \mathbf{x_r}, T-t)\partial_t^2 s(\mathbf{x},t)dt$$

Forward benchmark

- Travel time predictions

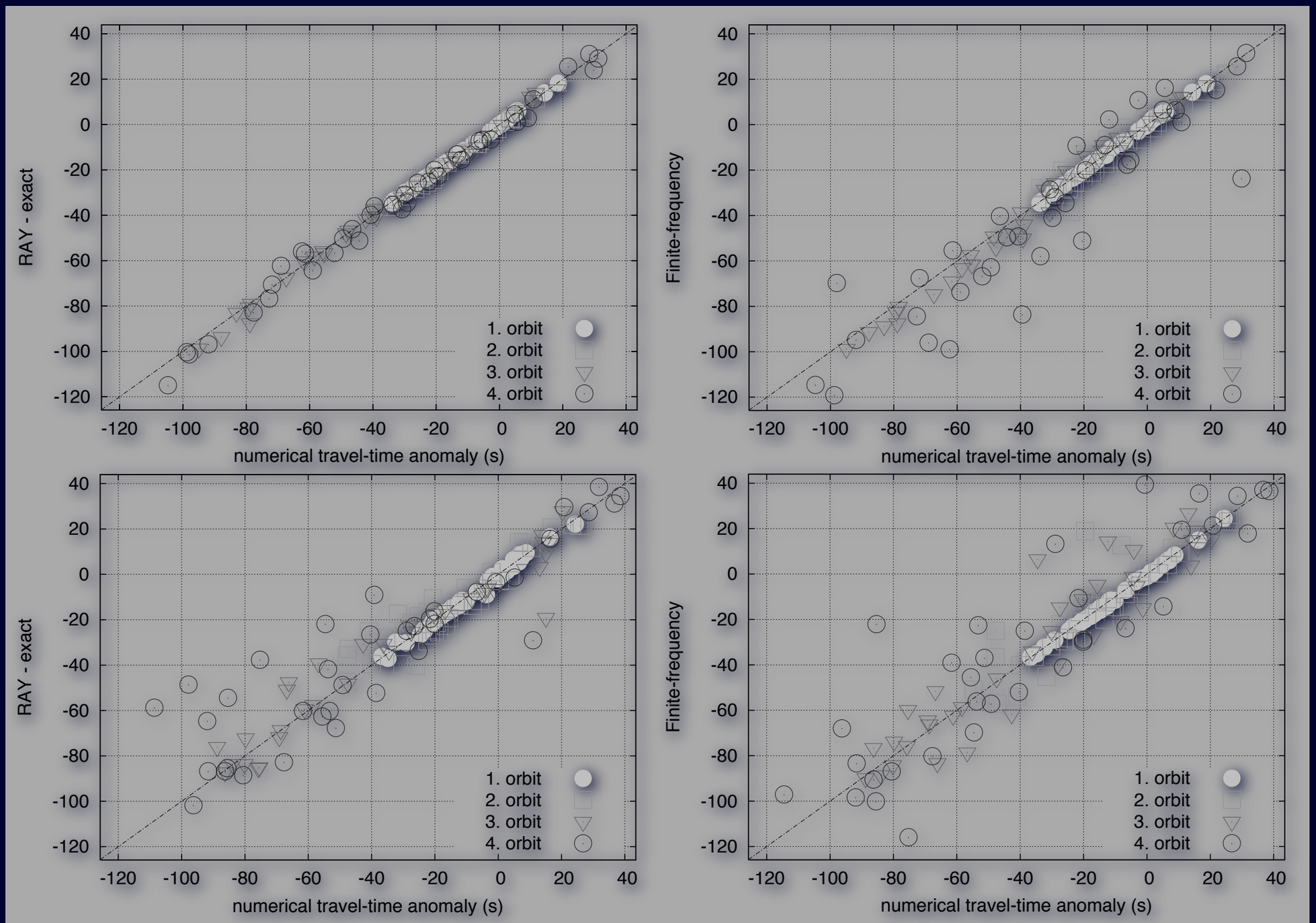

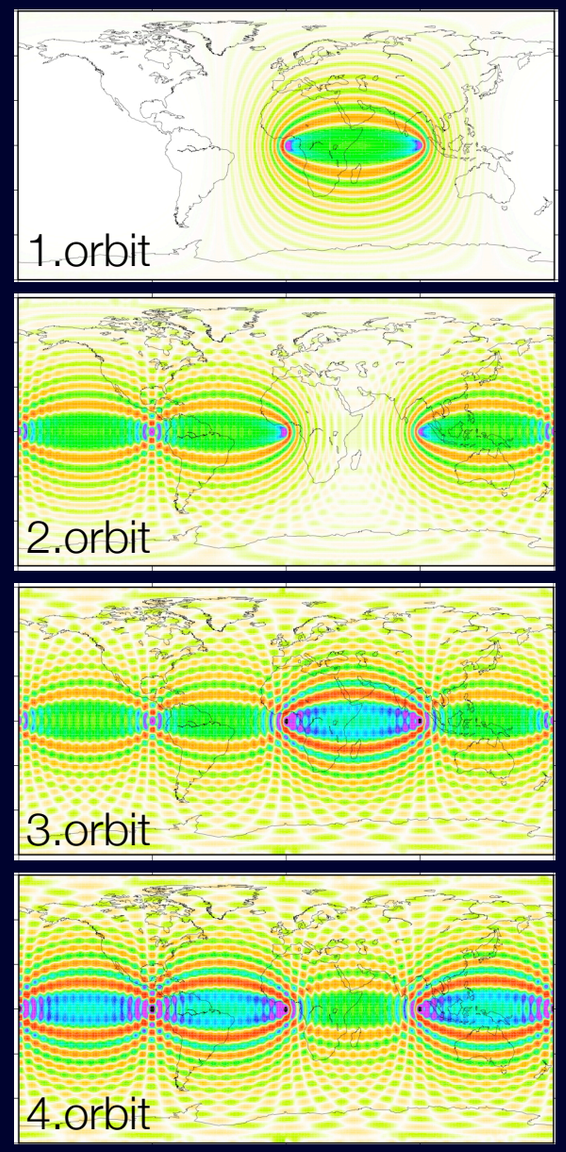

Multiple ray paths

- Travel time predictions

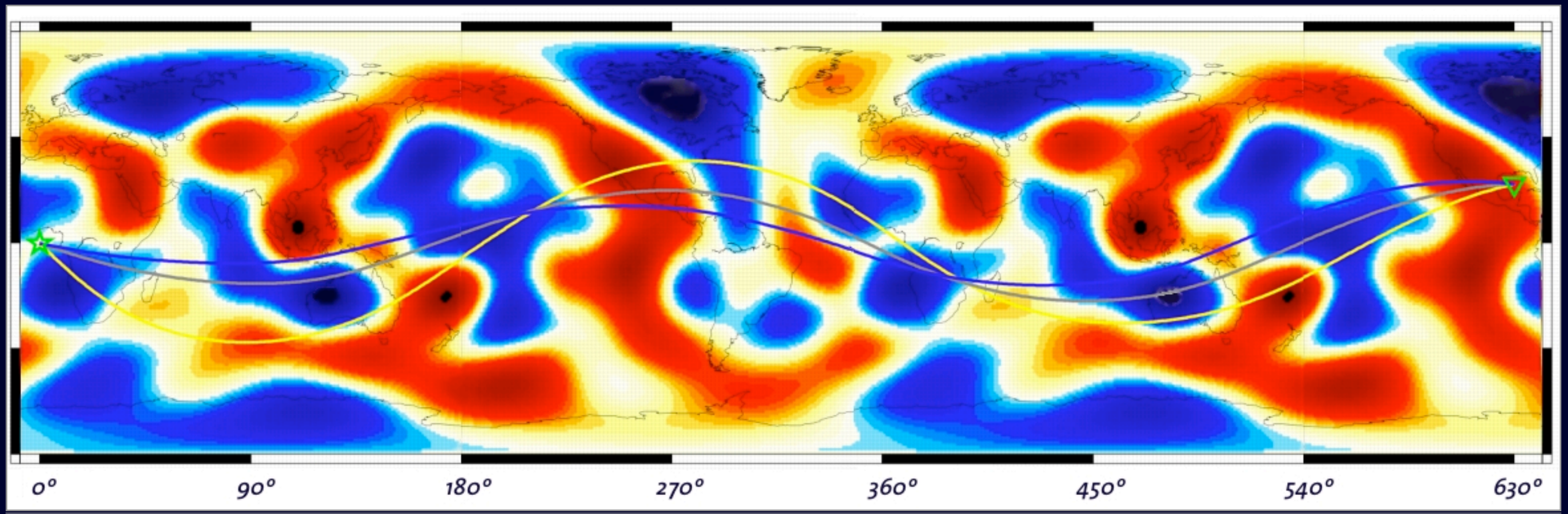

Multiple ray paths

- Travel time predictions

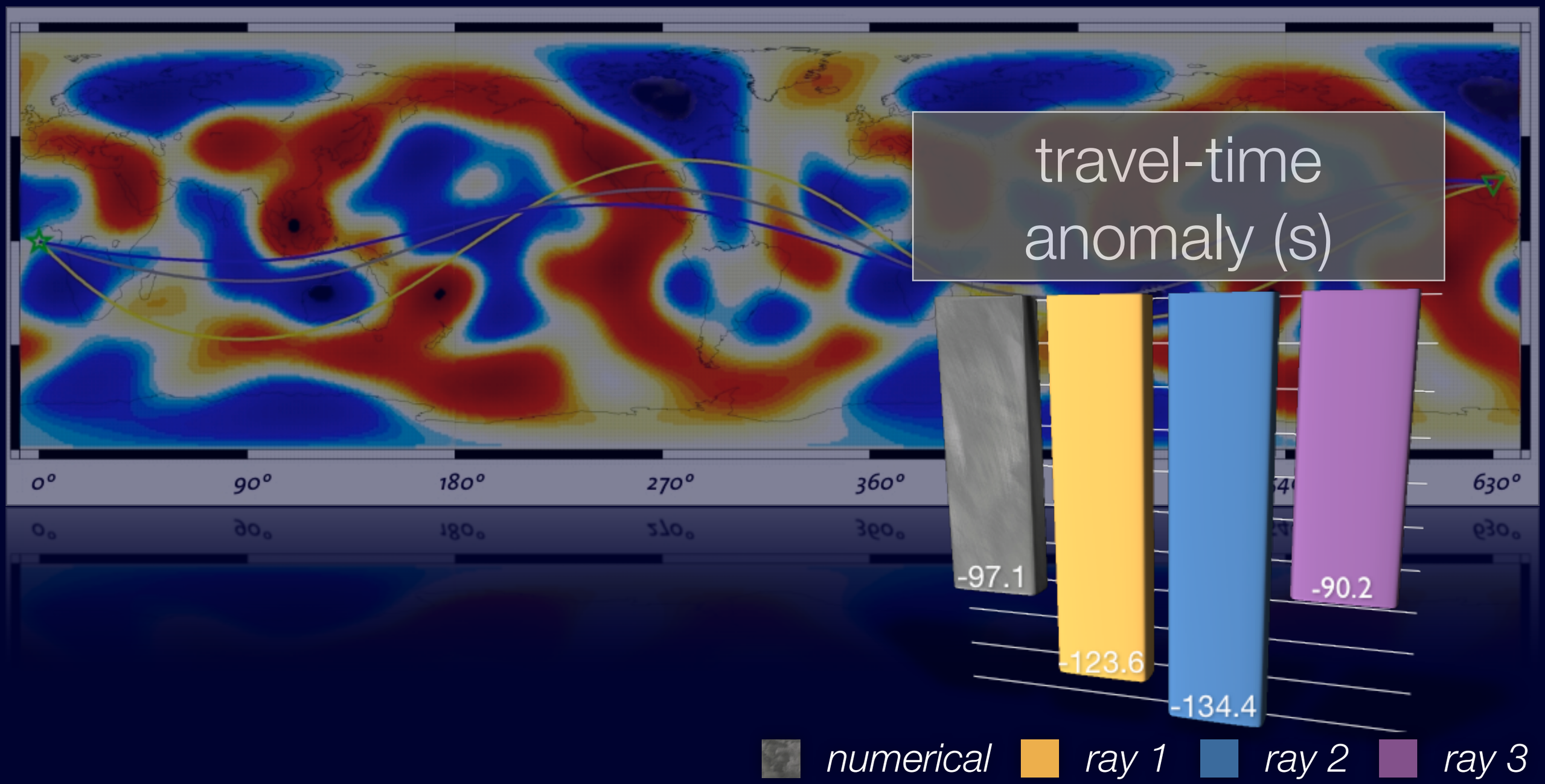

Asymptotic membrane waves

- Waveform predictions

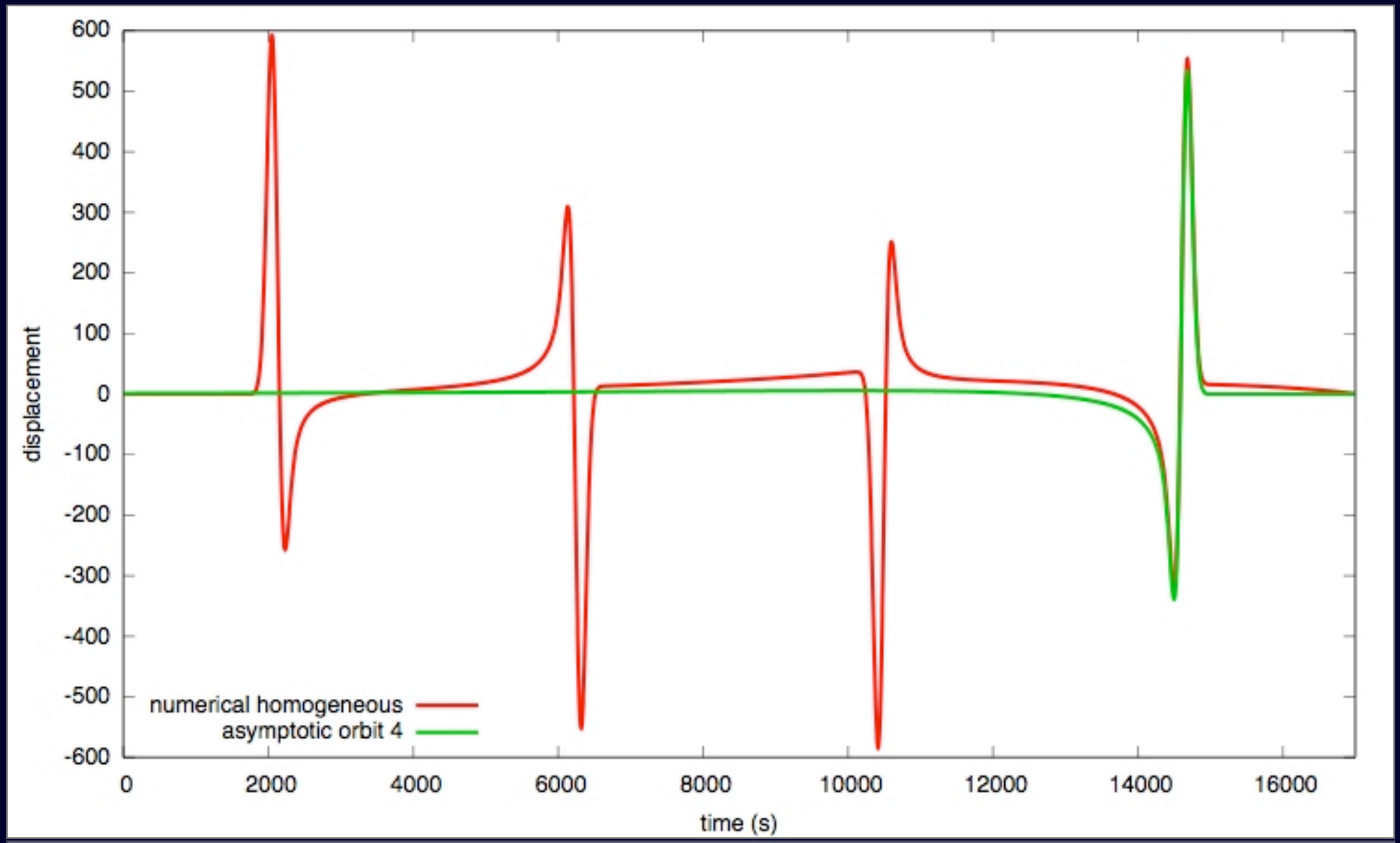

Multiple ray paths

- Waveform predictions

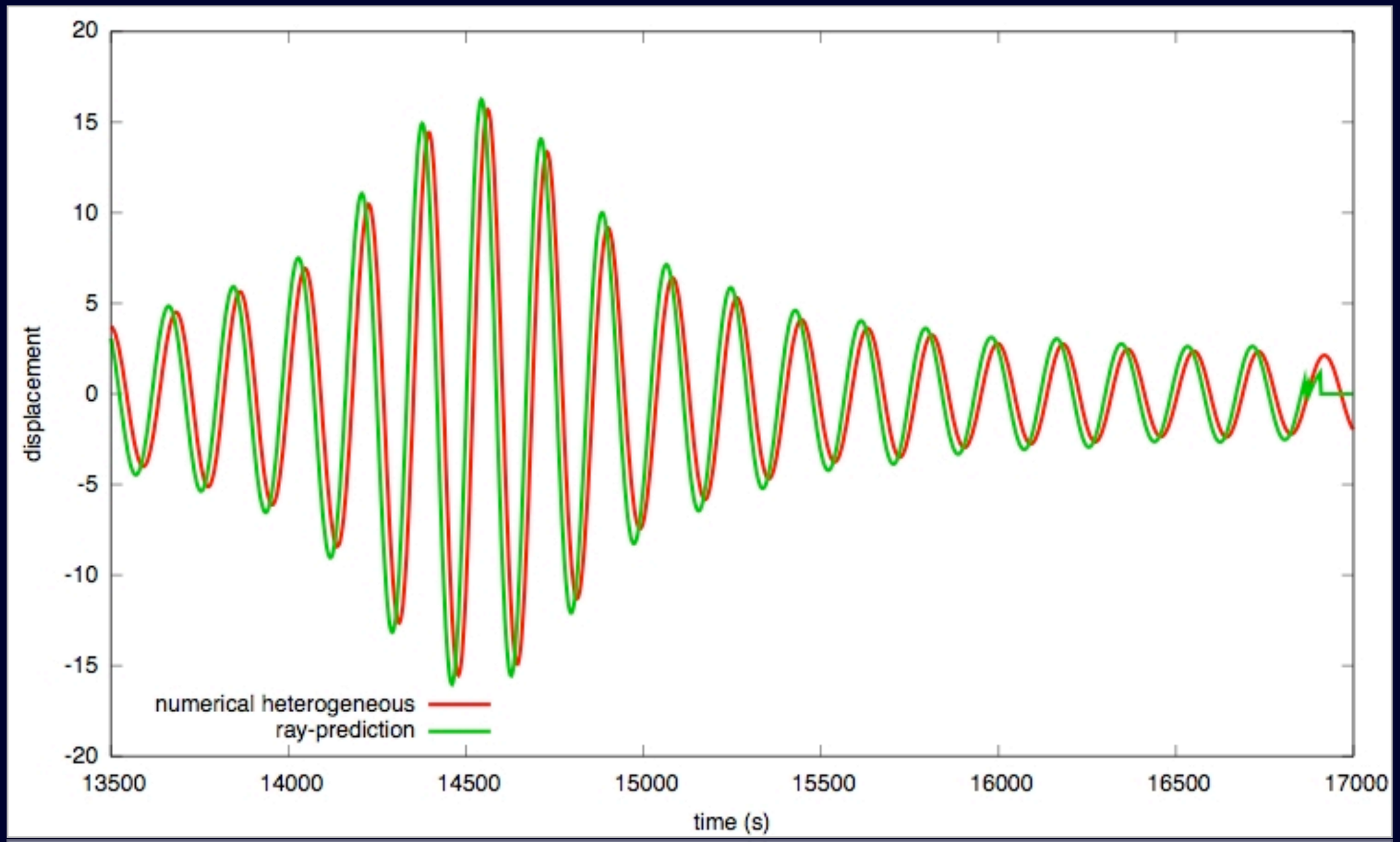

Shorter Wavelengths

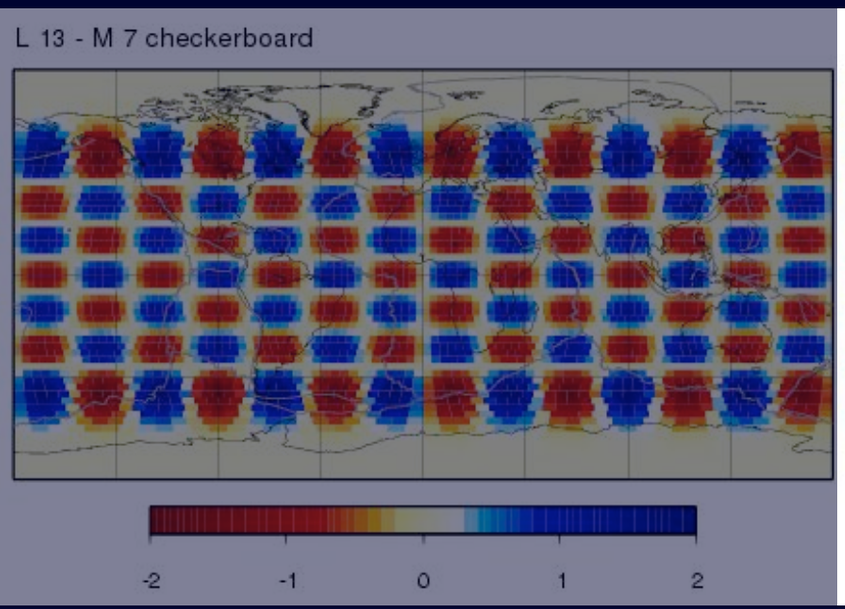

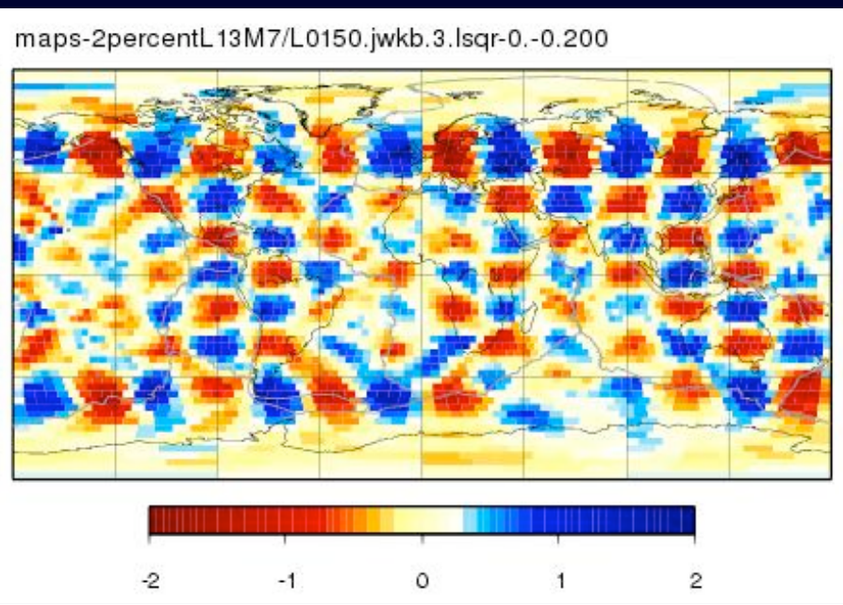

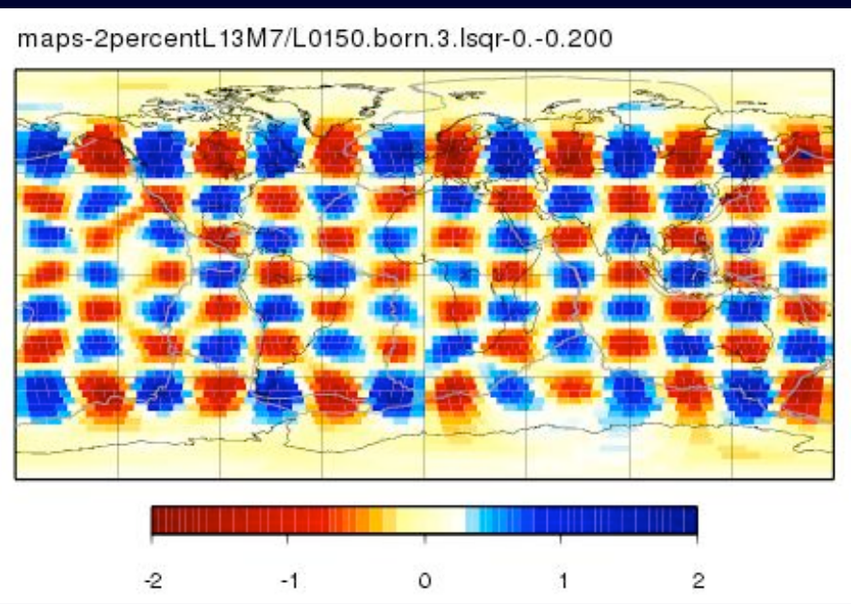

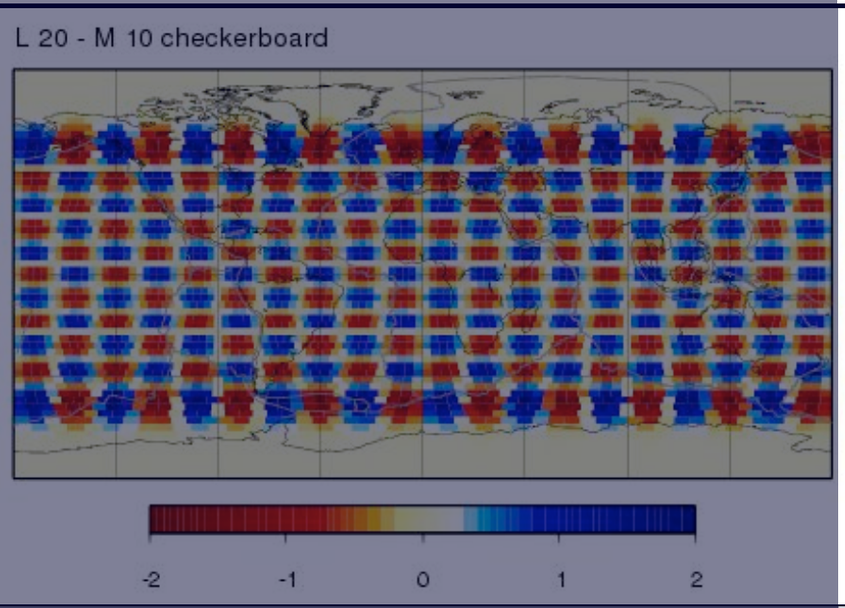

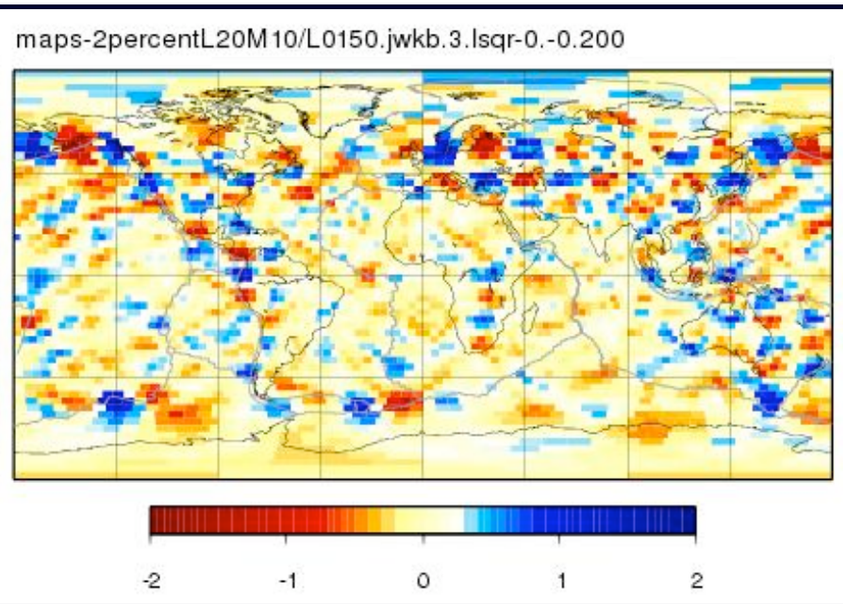

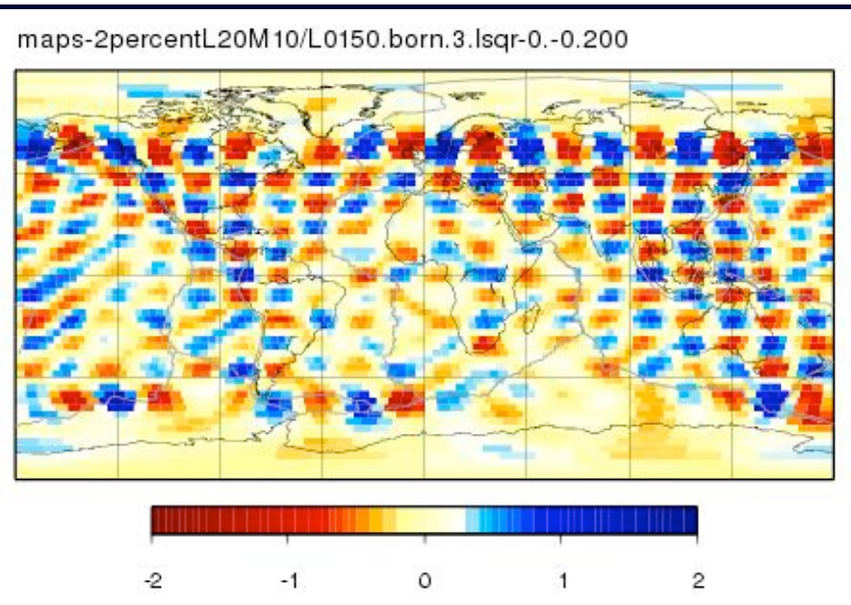

Shorter Wavelengths

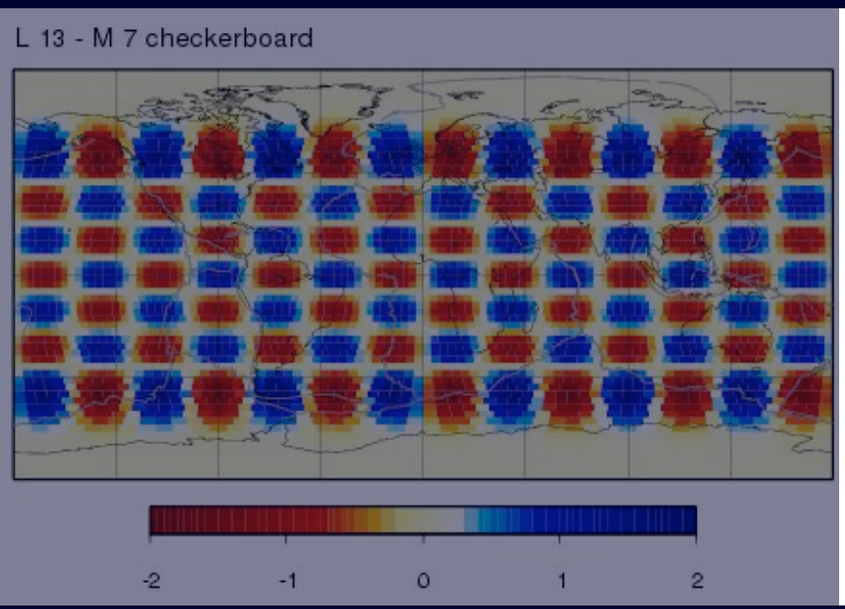

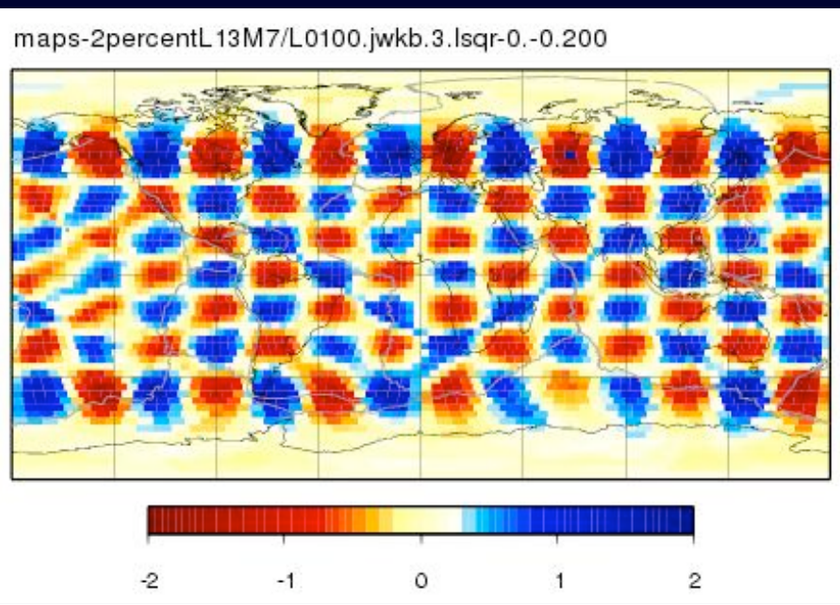

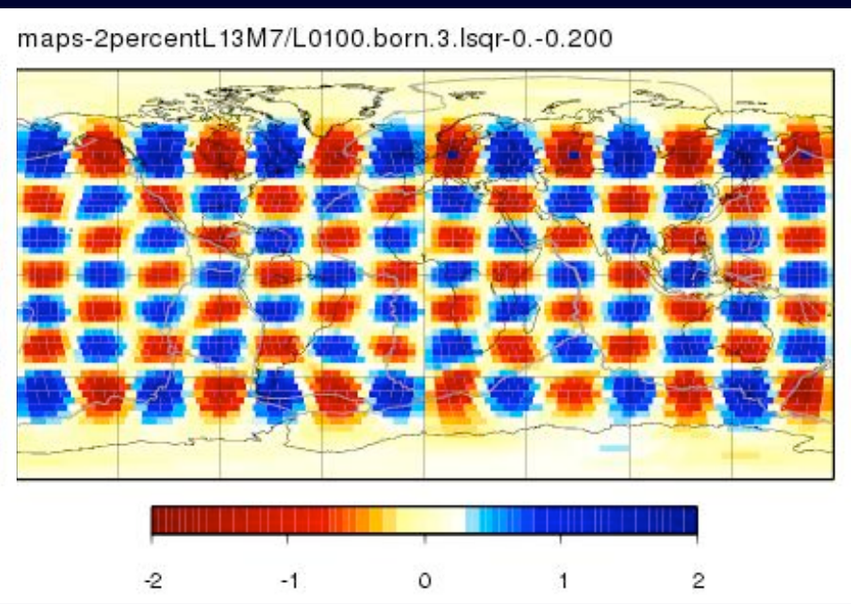

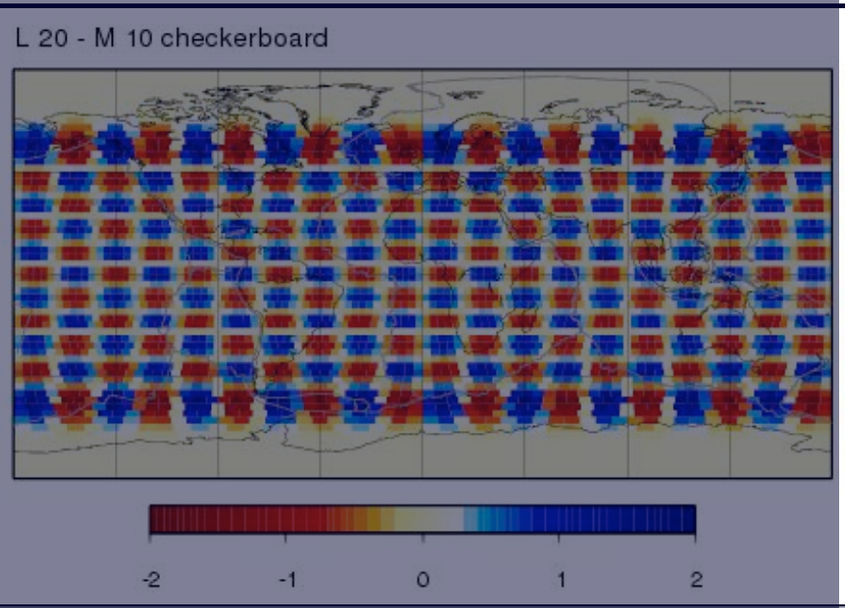

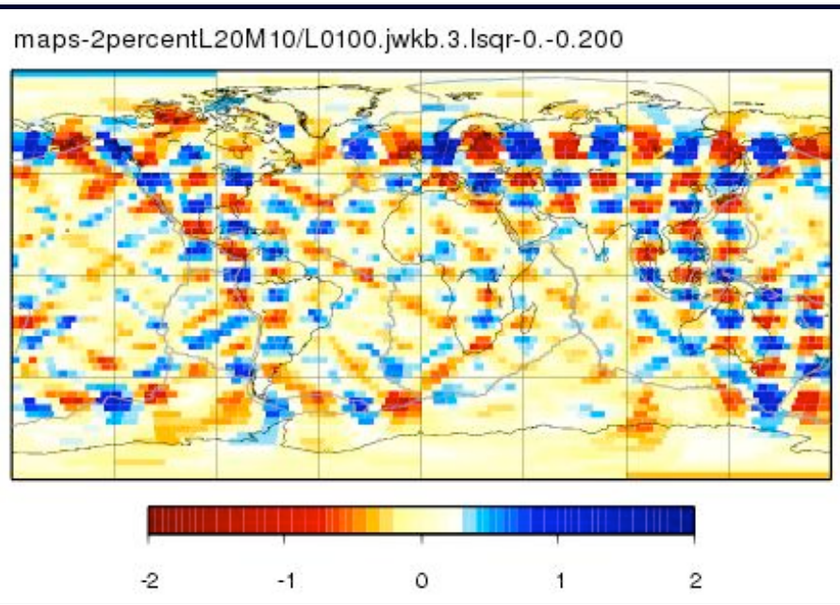

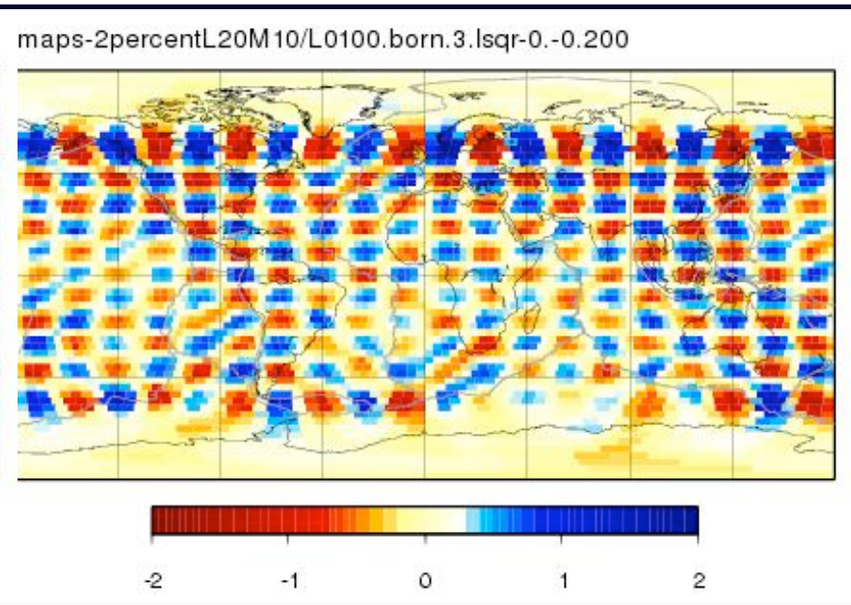

Iterative inversions

Rays

Finite-frequency

L 20 - M 10 checkerboard

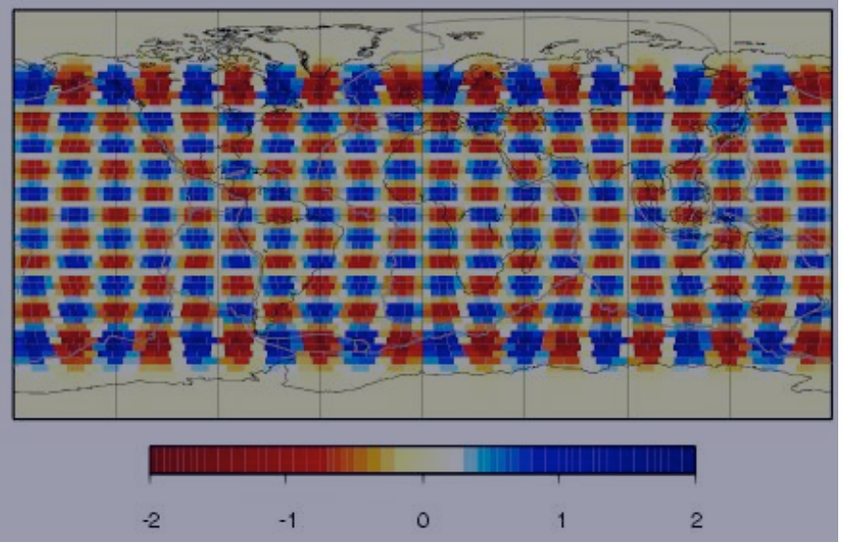

maps-2percentL20M10/L0150.jwkb.3.lsqr-0.-0.200

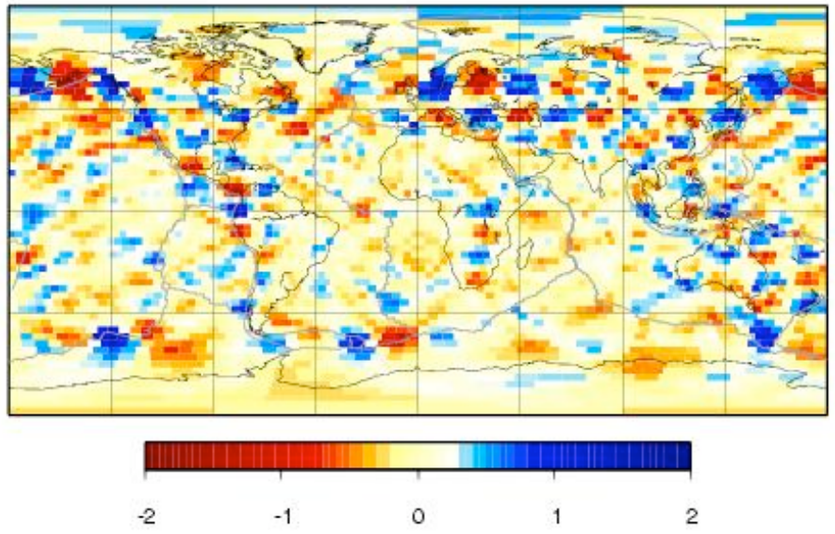

maps-2percentL20M10/L0150.born.3.lsqr-0.-0.200

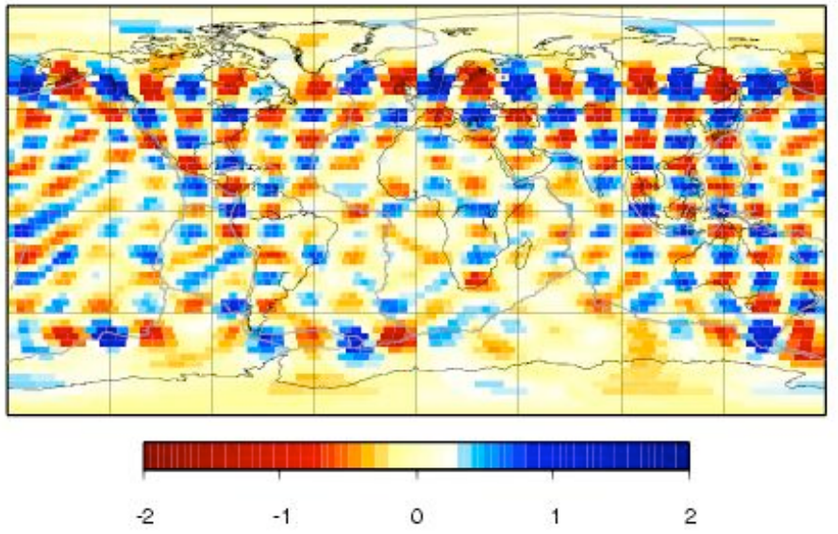

Daniel Peter | ETH Zurich

Iterative inversions

Rays

Finite-frequency

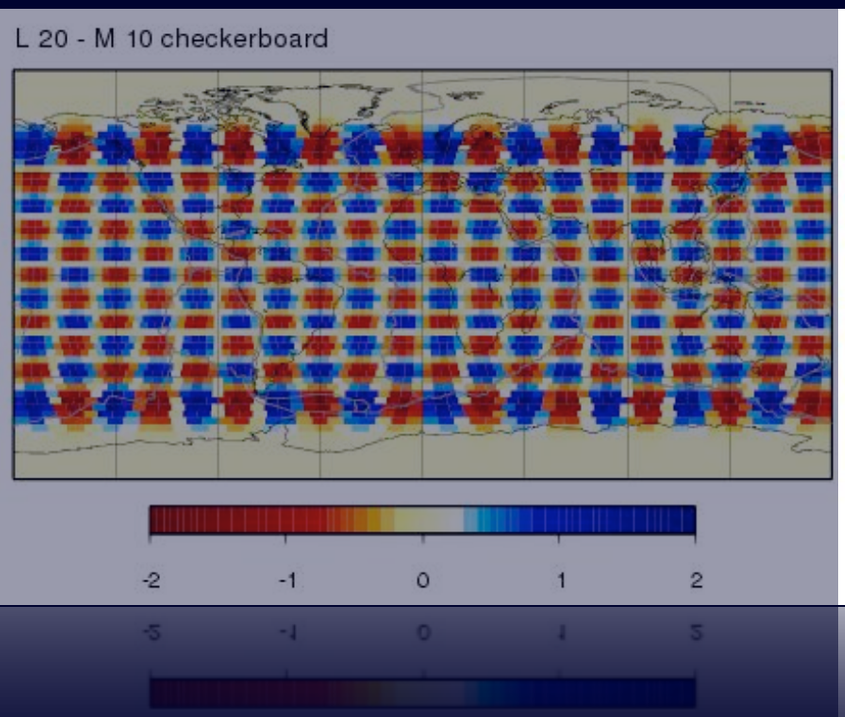

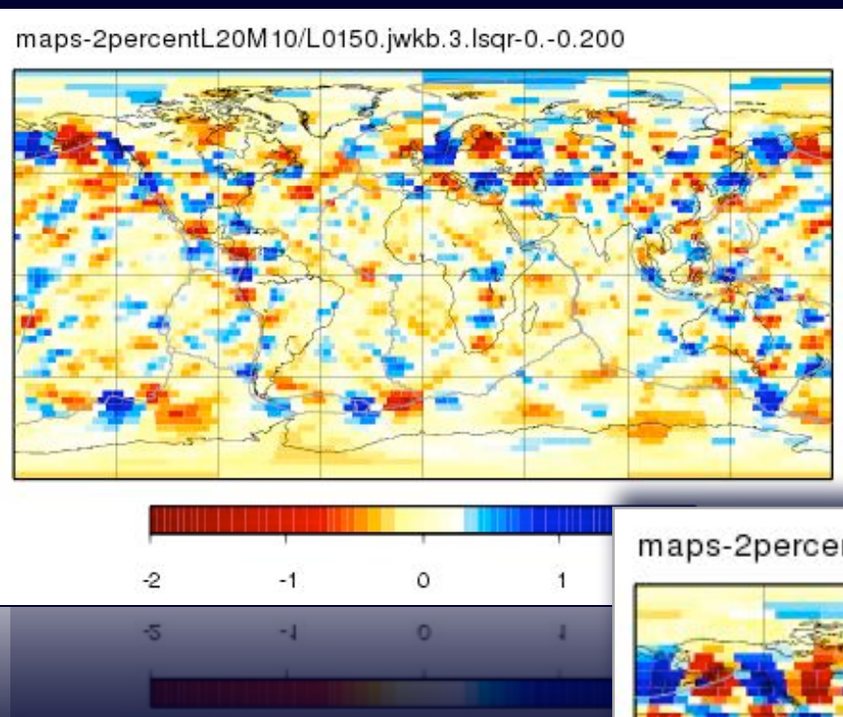

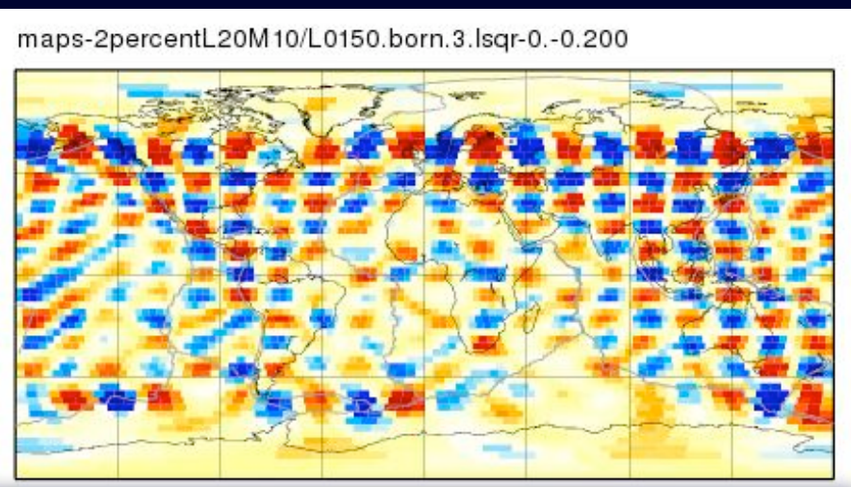

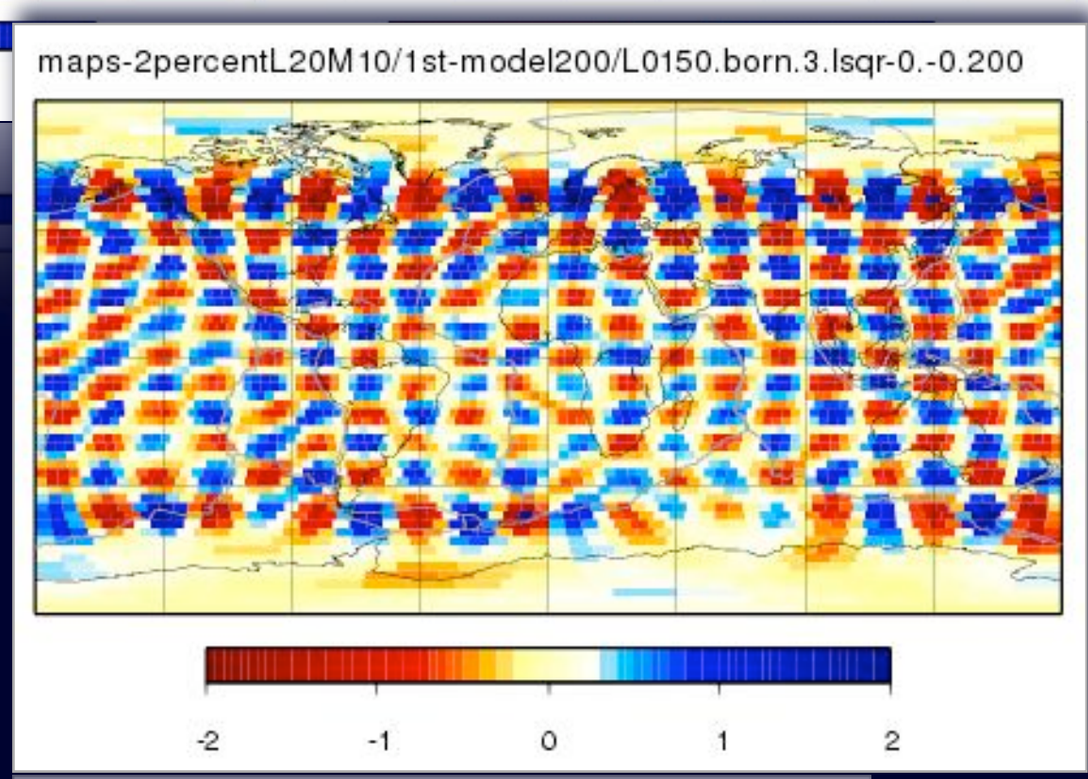

Daniel Peter | ETH Zurich

Noise

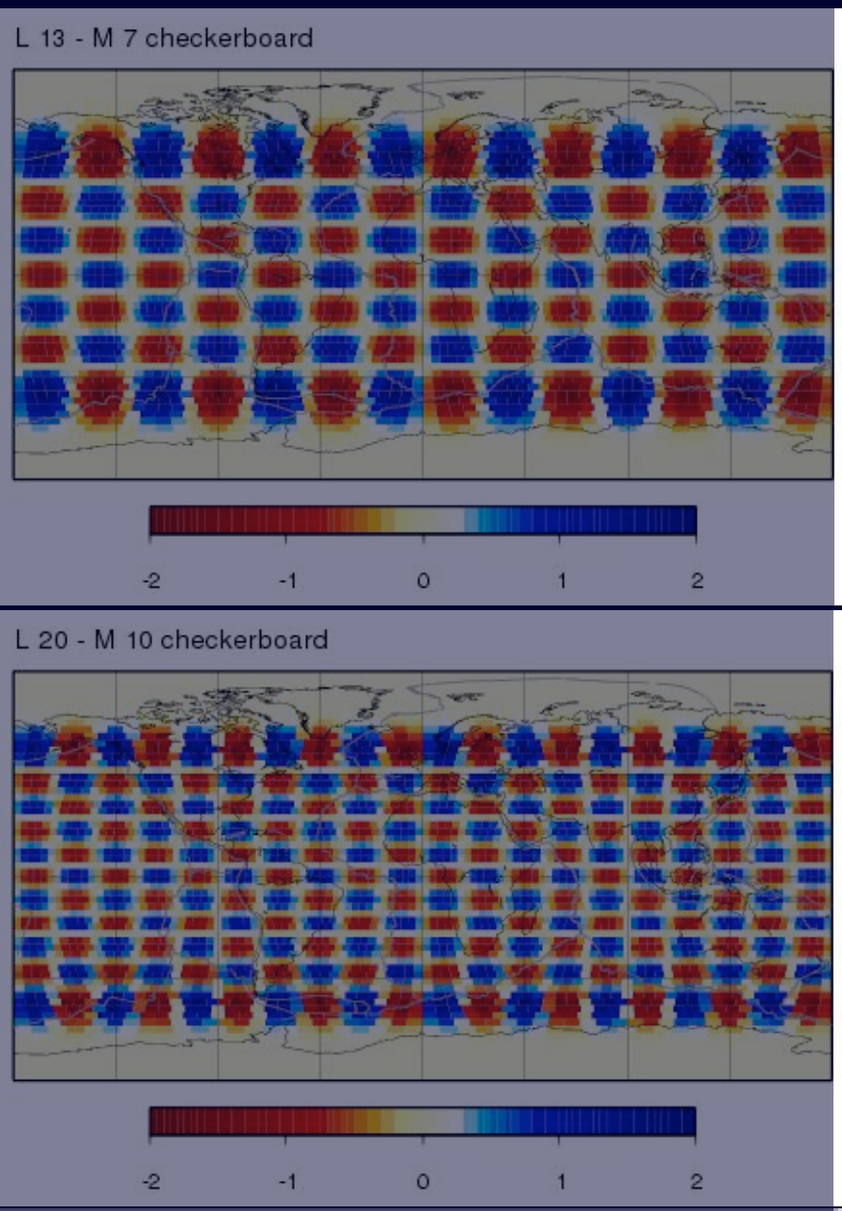
L 13 - M 7 checkerboard
-2
-1
0
1
2

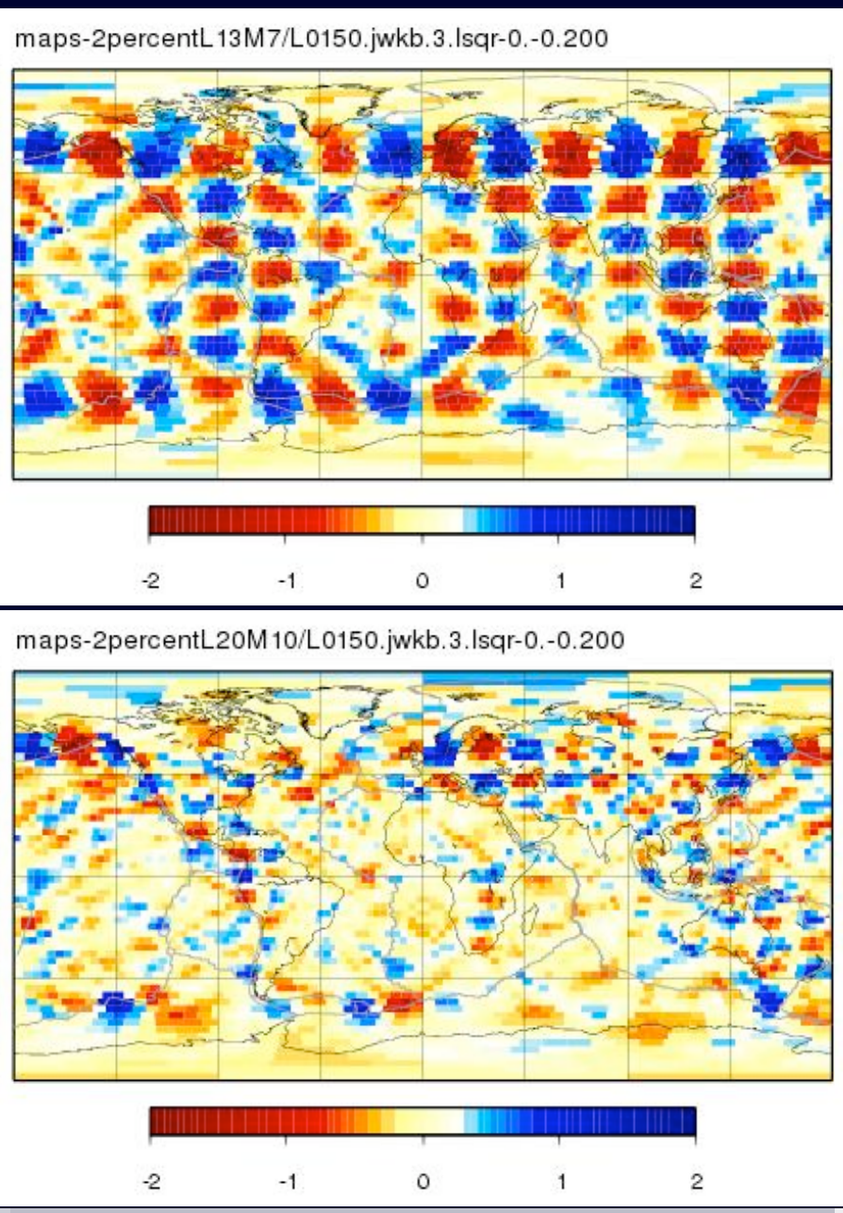
maps-2percentL13M7/L0150.jwkb.3.lsqr-0.-0.200
-2
-1
0
1
2

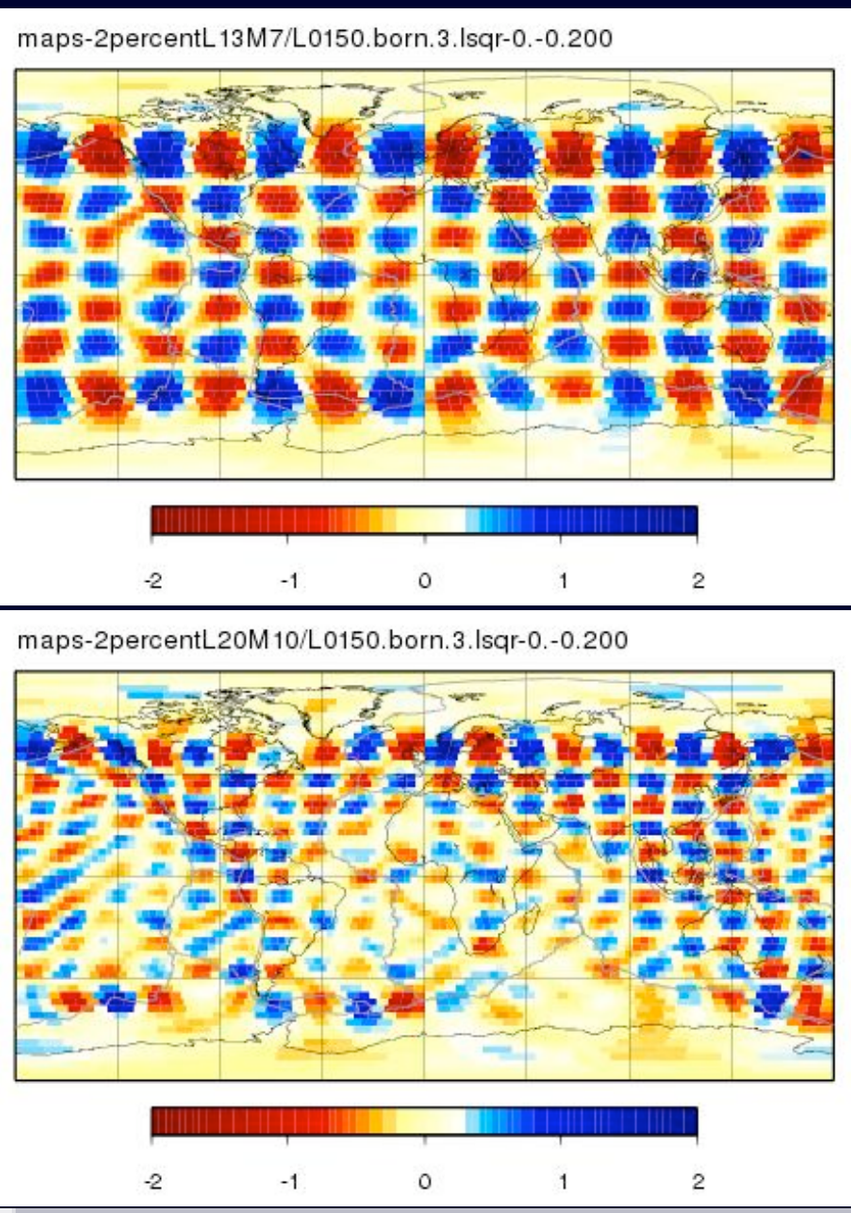
maps-2percentL13M7/L0150.born.3.lsqr-0.-0.200
-2
-1
0
1
2

L 20 - M 10 checkerboard
-2
-1
0
1
2

maps-2percentL20M10/L0150.jwkb.3.lsqr-0.-0.200
-2
-1
0
1
2

maps-2percentL20M10/L0150.born.3.lsqr-0.-0.200
-2
-1
0
1
2

Noise

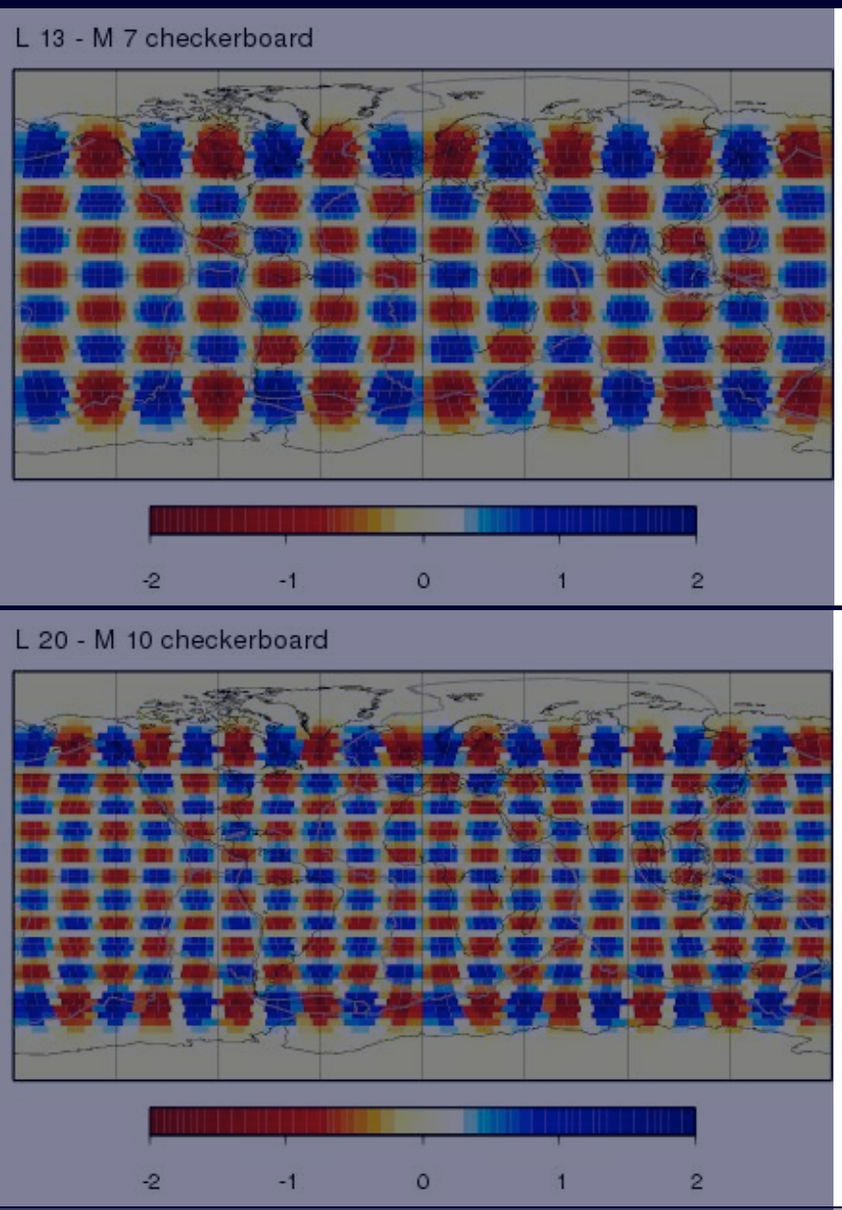
L 13 - M 7 checkerboard
-2
-1
0
1
2

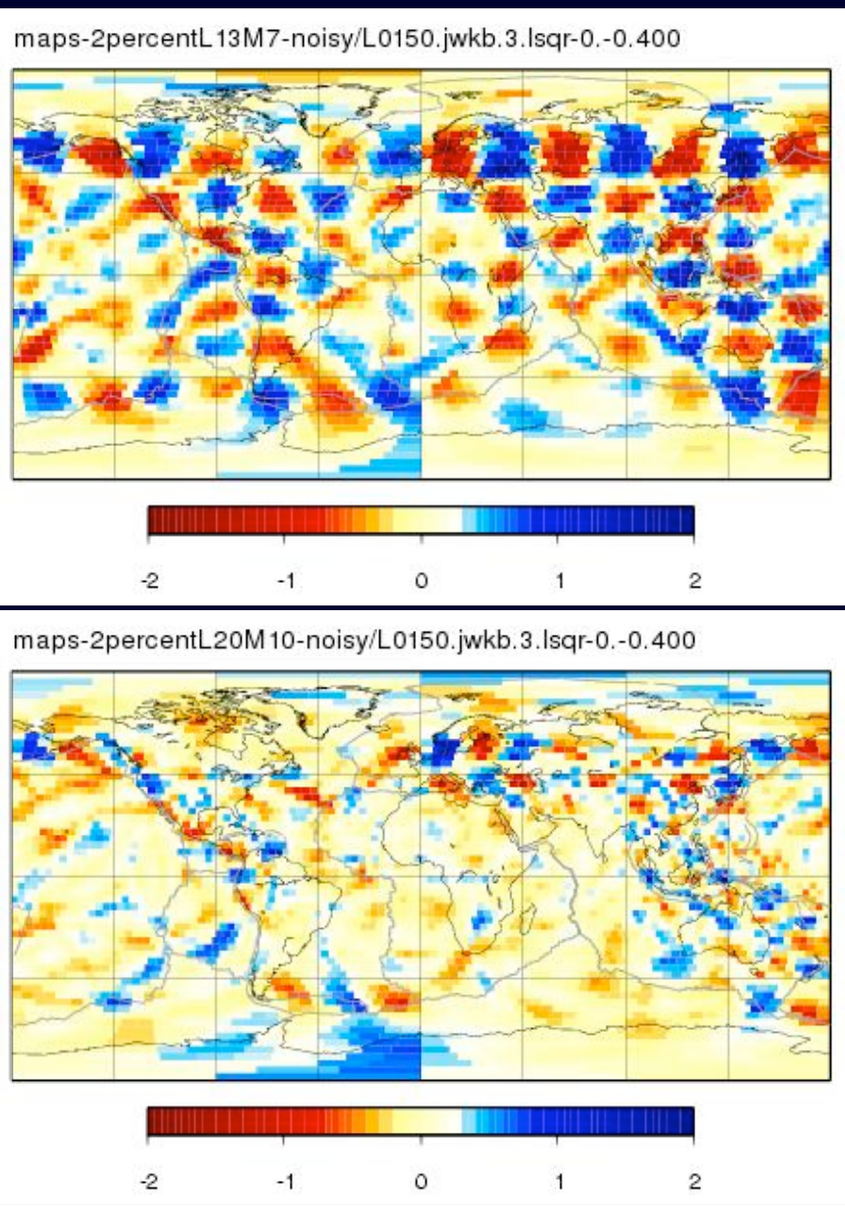
maps-2percentL13M7-noisy/L0150.jwkb.3.lsqr-0.-0.400
-2
-1
0
1
2

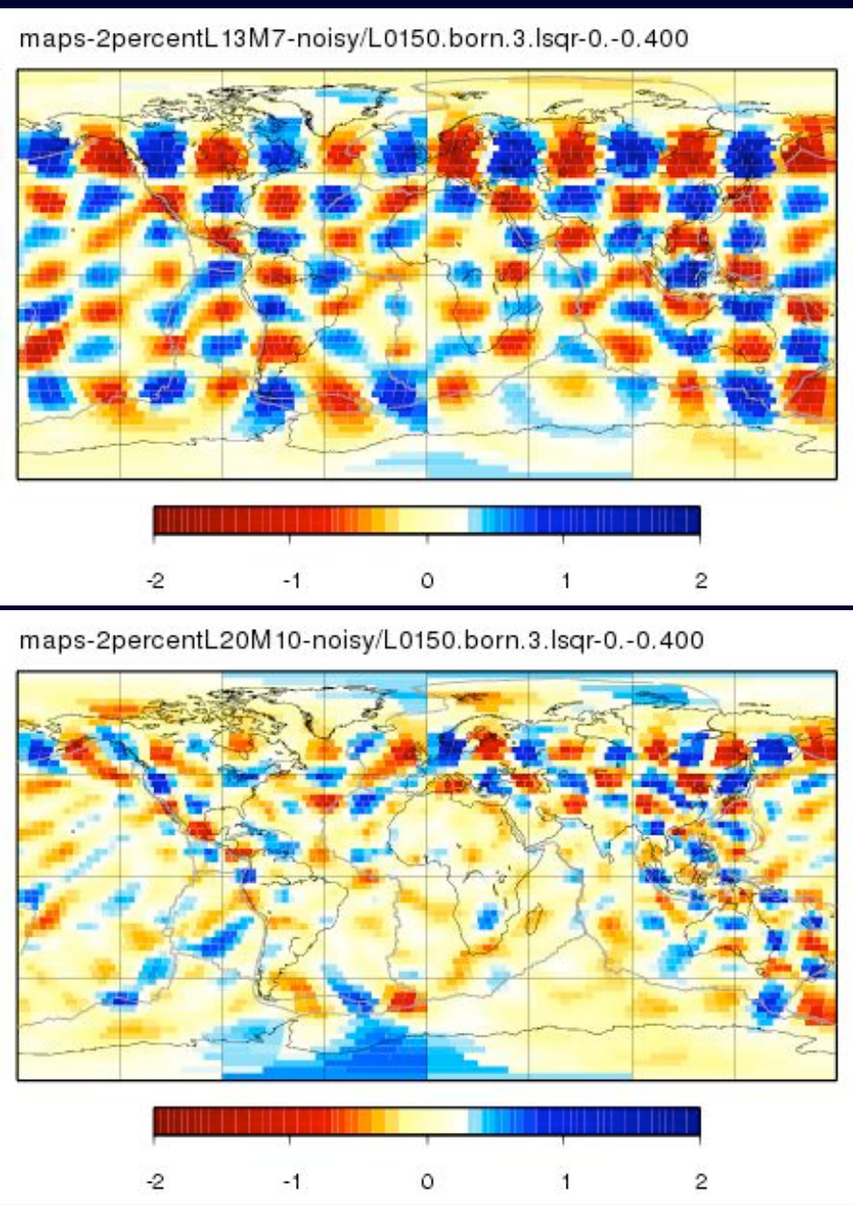
maps-2percentL13M7-noisy/L0150.born.3.lsqr-0.-0.400
-2
-1
0
1
2

L 20 - M 10 checkerboard
-2
-1
0
1
2

maps-2percentL20M10-noisy/L0150.jwkb.3.lsqr-0.-0.400
-2
-1
0
1
2

maps-2percentL20M10-noisy/L0150.born.3.lsqr-0.-0.400
-2
-1
0
1
2

Phase velocity maps

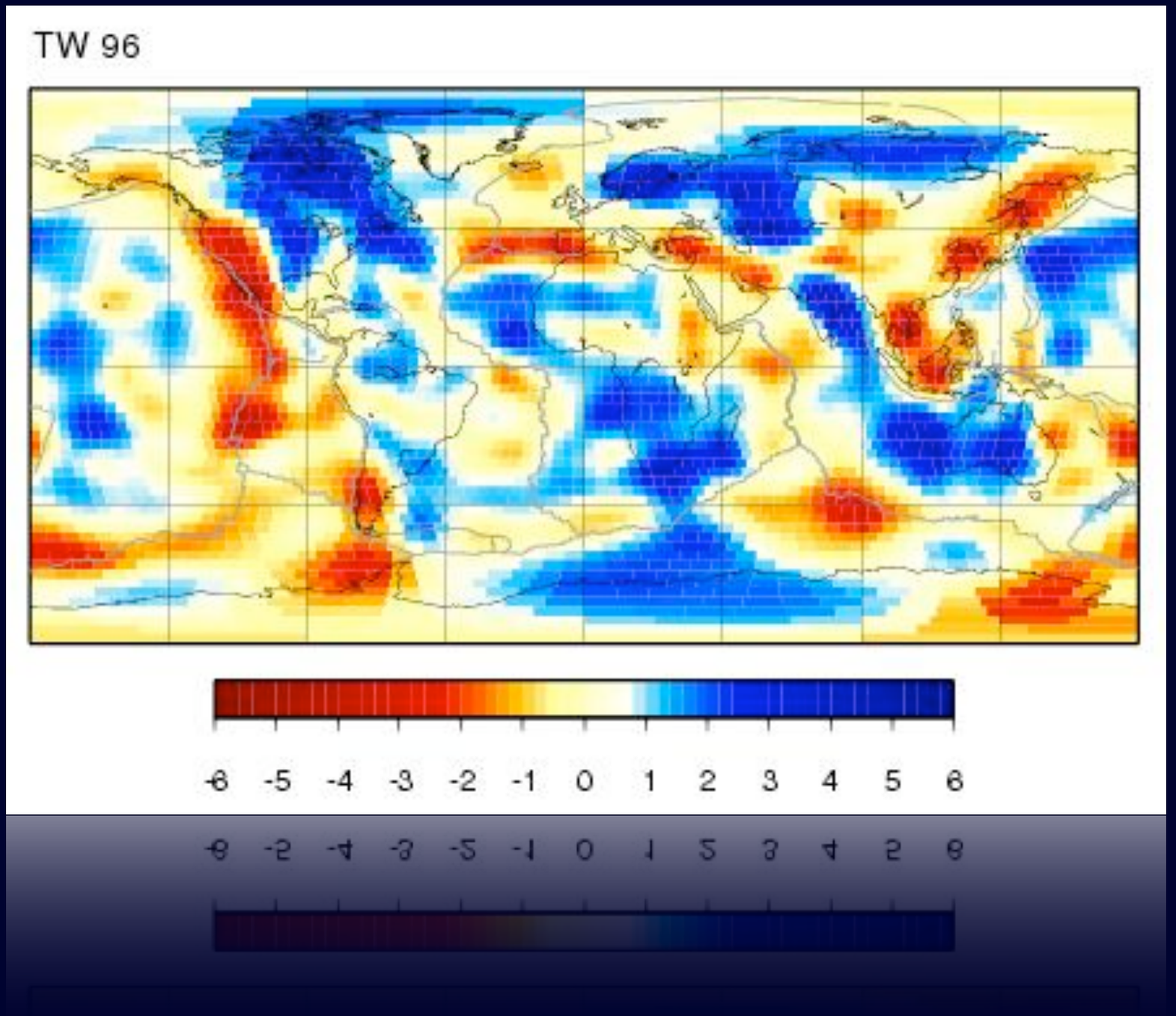

Phase velocity maps

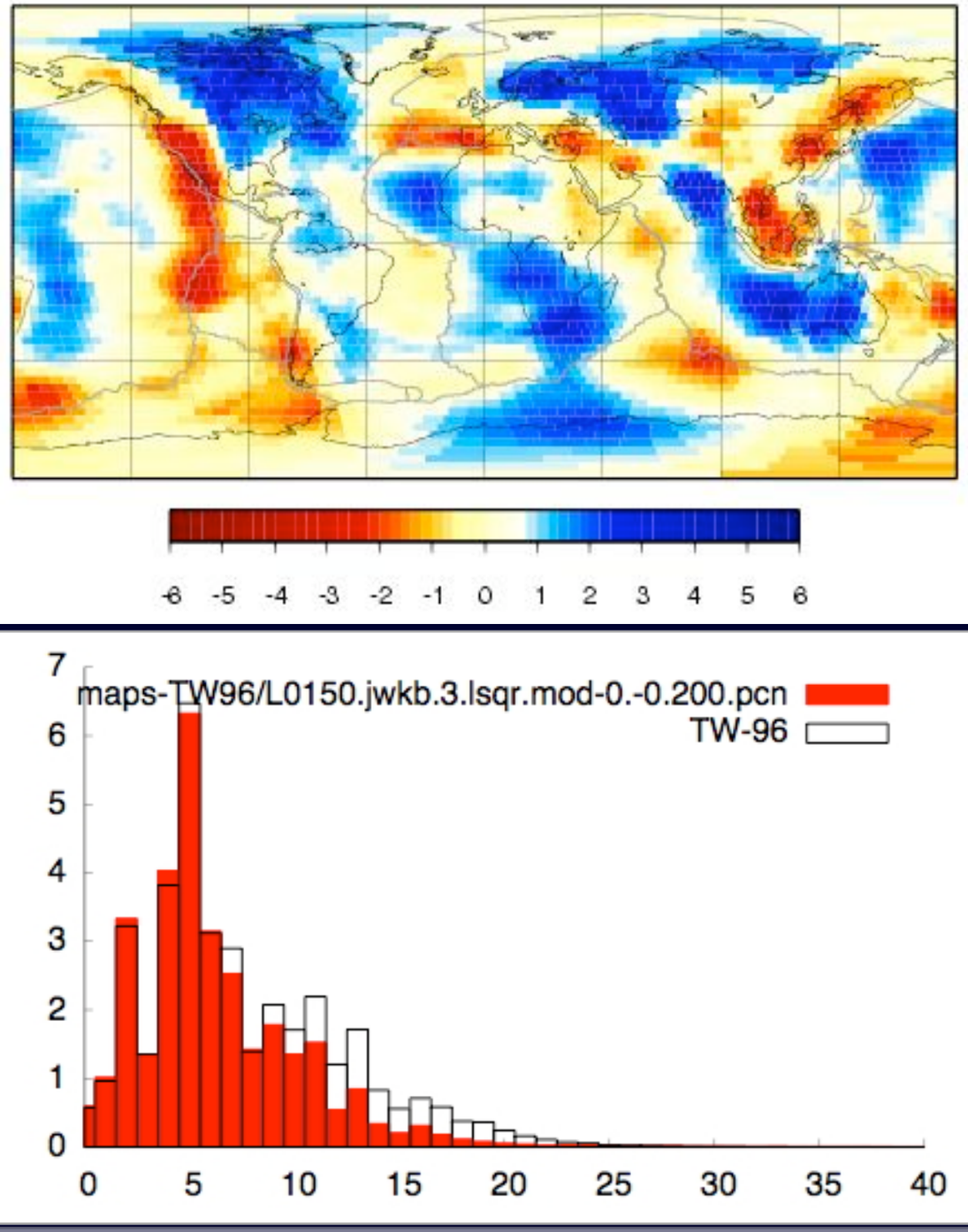

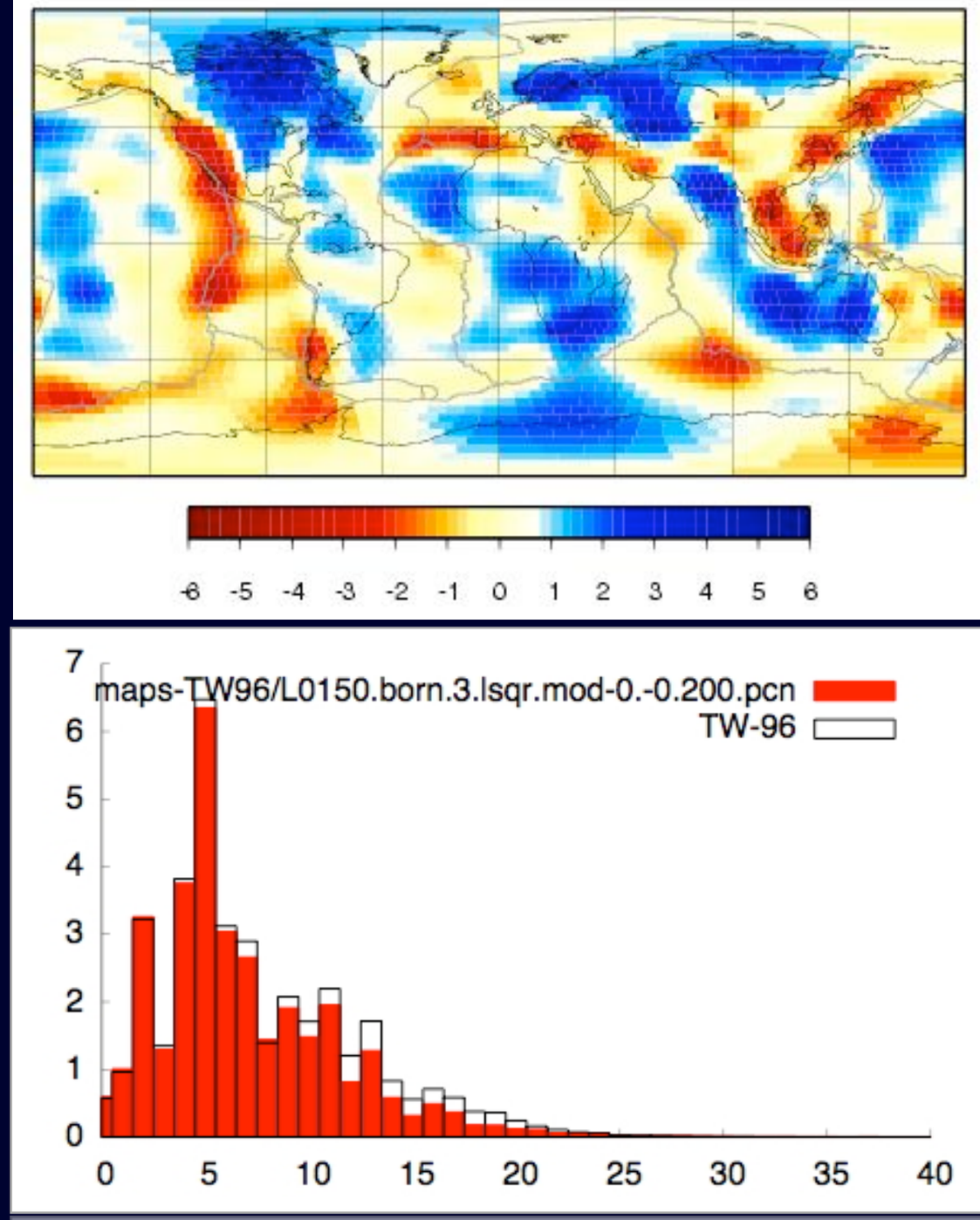

Daniel Peter | ETH Zurich